Scientific
Research
Publishing

Journal of Modern Physics

Journal Editorial Board

Table of Contents

Volume 10   Number 14   **December 2019**

Journal of Modern Physics (JMP)
Journal Information

SUBSCRIPTIONS

SERVICES

Advertisements

Advertisement Sales Department, E-mail: service@scirp.org

Reprints (minimum quantity 100 copies)

Reprints Co-ordinator, Scientific Research Publishing, Inc., USA.

E-mail: sub@scirp.org

COPYRIGHT

PRODUCTION INFORMATION

For manuscripts that have been accepted for publication, please contact:
E-mail: jmp@scirp.org

Scientific
Research
Publishing

The Modification of Special Relativity

Jian'an Wang

Department of Physics, Shenzhen University, Shenzhen, China
Email: wja@szu.edu.cn

Abstract

In this paper, the phenomenon of light velocity invariance is analyzed by using a new etheric view, and the physical mechanism of light velocity invariance is given, the principle of constancy of light velocity and the principle of special relativity are modified, and the Lorentz transformation is deduced by using these two modified principles. The relationship between mass and speed, the relationship between time and speed, and the relationship between length and speed are reanalyzed, and physical explanations different from the Special Relativity are given. Experiments for verification of the new theory are designed and presented. Experiment 1: Verify that the kinetic energy of a particle is only related to the speed of the particle relative to the ether, independent of the observer's motion. Experiment 2: Verify that magnetic field is produced by electric charge's motion relative to ether, and is independent of the observer. Experiment 3: Redoing the Michelson-Morley experiment on the space station to prove the existence of the ether. Experiment 4: Simulation of the generation and reversal of the Earth's magnetic field, thus proving that the magnetic field is generated by the relative motion of the electric charge to the ether. Experiment 5: Simulate the formation of the natural iron meteorites and show that the atom becomes smaller with the increase of the etheric density of the space. Experiment 6: Aberrations contrast experiment to prove that for the observers on Earth, according to the theory of this paper, stars have aberration but the light sources on Earth have no aberration; according to the theory of special relativity, there are aberrations for both the stars and the light sources on Earth.

1. Introduction

In the 19th century, with the development of the wave theory of light, "ether"

theory [1] became popular again. At that time, many physicists believed that there must exist an elastic material "ether" in space that could propagate light waves, and regarded "ether" as the absolutely static inertial system. To verify the existence of "ether" by experiments became the goal pursued by many scientists at that time. Since the Earth orbits the sun at a speed of 30 kilometers per second, it was thought that the Earth must encounter an "etheric wind" of 30 kilometers per second. In 1887 Michelson and Morley did the famous Michelson-Morley experiment [2] to measure the ether wind on Earth, but it turned out that ether wind does not exist and that the speed of light is the same in different directions on the surface of the Earth. In this historical context, Einstein abandoned the ether absolute stationary frame of reference and established the special relativity. In 1905 Einstein published the article "On Electrodynamics of Moving Bodies" [3] which is called "special relativity" by later generations. The starting point of this theory is two basic assumptions: the principle of special relativity and the principle of constancy of light velocity. The core equations of the theory are the Lorentz transformations [4]:

$$
\begin{cases}
x = \dfrac{x' + vt}{\sqrt{1 - (v/c)^2}} \\
y = y' \\
z = z' \\
t = \dfrac{t' + vx'/c^2}{\sqrt{1 - (v/c)^2}}
\end{cases}
$$

Special relativity predicted some new effects (relativistic effects) that Newton classical physics did not have, such as time dilation, length contraction, mass speed relation, mass energy relation and so on. Those relativistic effects have been verified by many relevant experiments, for example, the increase of the lifetime of the flying muon proves the correctness of the time dilation relativistic effect, the increase of the mass of the accelerated particles on the accelerator with the increase of speed proves the correctness of the relativistic effect of the relationship between mass and speed, and the explosion of atomic bomb proves the correctness of the relationship of special relativity between mass and energy. Today, special relativity is one of the foundations of modern physical theory.

The author believes that there is no end to science, and the spirit of science is to keep exploring. Although special relativity has achieved great success, it is by no means the end of physics. The core of special relativity is the principle of constancy of light velocity. The author believes that there should be a deep natural mystery behind the principle of constancy of light velocity, but in special relativity, the physical mechanism of this principle is not given. In addition, the principle of constancy of light velocity of special relativity is contradictory to people's daily experience and logic, and is incomprehensible. Besides, special relativity has no further physical explanations of its main conclusions, such as time dilation, length contraction and mass speed relation. In order to get the physical

mechanism of the principle of constancy of light velocity and discover the mystery behind it, the author started this research with great curiosity.

In this research, the first step needed is to get the physical mechanism of light velocity invariance so as to modify the principle of constancy of light velocity and the principle of special relativity. The second step needed is to derive the Lorentz transforms from the modified principle of constancy of light velocity and the modified principle of special relativity. The third step needed is to reinterpret the time dilation, the length contraction, the mass speed relation with the new Lorentz transforms. The final step is to design and present related experiments to verify the new theory.

2. On the Principle of Constancy of Light Velocity

2.1. The Physical Mechanism of Constancy of Light Velocity

The principle of constancy of light velocity can be expressed as "In any inertial frame, the propagation speed of light in vacuum is constant and does not change with the relative motion of the light source and the observer".

How do we understand this incomprehensible principle? The author holds that dialectical materialism is correct and that the world is made up of matter (including energy). One of the purposes of physical research is to understand the physical mechanism behind any hypothesis or mathematical formula of physics. The author believes that space and time are the properties of matter (including energy) and are not independent existence. Therefore, the frame of reference in physics must be made up of matter (including energy) rather than a purely mathematical concept.

Aristotle (384-322 BC), an ancient Greek philosopher of great knowledge, believed that vacuum does not exist at all, and that space is filled with continuous matter (ether) everywhere [1]. In the fourth century BC, two Chinese Song Yan and Yin Wen put forward the theory of "ultimate gas" believing that [1] the celestial bodies and all things in the world are composed of a kind of so-called "ultimate gas" substance. When the "ultimate gas" gathers it turns into tangible objects, and when the objects dissipate, they become "ultimate gas" and return to space. According to the mass and energy relation formula of special relativity [3], mass and energy can be converted into each other, so we can assume that the "ultimate gas" referred to by the two ancient Chinese philosophers is energy (ether).

From the energy conservation equation of Compton Scattering [5]:

$$\frac{hc}{\lambda} + m_0 c^2 = \frac{hc}{\lambda'} + \frac{m_0 c^2}{\sqrt{1 - (v/c)^2}}$$

in the formula, λ is the wavelength of incident light wave, m_0 is the static mass of electron, c is the speed of light in vacuum, v is the speed of the electron relative to the laboratory (Earth), λ' is the wavelength of outgoing light wave, and h is the Planck parameter. From the above formula, we can see that in

Compton Scattering experiment, when the photon collide with the electron, the total energy of the system (the photon and the electron) is calculated by using the electron as the frame of reference, that is to say, the electron is always regarded as static, and the speed of the photon relative to the electron is always at c (the speed of light in vacuum) regardless of the relative motion between the photon and the electron. But after the collision when the photon and the electron are separated, the total energy of the system (the photon and the electron) is calculated by using the laboratory (Earth) as the frame of reference, that is to say, the velocity of the electron is calculated by using the laboratory (Earth) as the frame of reference and the speed of the photon relative to the laboratory (Earth) is always at c (the speed of light in vacuum). From the Compton Scattering experiment, we can guess that the electron has an etheric layer that moves with it, and that the Earth also has an etheric layer that moves with it.

To sum up, we can assume that:

1) The cosmic space is full of ether (background energy), and ether is also the medium in which light waves travel.

2) All fields (gravitational field, electromagnetic field, strong interaction field and weak interaction field etc.) contain and compress ether (energy).

3) Each particle or object carries an etheric layer (sphere of influence) that surrounds and moves with it.

The following is a physical explanation of the principle of constancy of light velocity based on the above new etheric view: Because ether is full of space and the speed of the light wave relative to the ether medium is constant, so the speed of the light wave relative to the ether medium is independent of the motion of the light source. And because all fields contain and compress ether, any object or particle will attract and drag an etheric layer that surrounds it to move together. The thickness of the etheric layer dragged together is related to the total energy of the particle or object. In the etheric layer of an object or particle, the object or particle has the greatest influence, and the influence of other objects or particles can be ignored. For example, within the range of hundreds of kilometers above the surface of the Earth, the Earth (gravitational field) has the greatest influence, and the influence of the sun (gravitational field) and other planets (gravitational field) is negligible. Therefore, to study the motion of objects (such as cars, aircraft, satellites) in this range can be based on the etheric layer of the Earth as the absolute frame of reference. Usually the thickness of the etheric layer is of the same order of magnitude as the scale of the object. So when a photon approaches a particle or object, it will enter the etheric layer of the particle or object and adjust its speed to maintain the relative speed to the newly entered etheric layer at the constant speed of light c. So, no matter what velocity a particle or object moves at, the speed at which a photon moves relative to it when colliding with it or approaching it is constant at the constant speed of light c. This is the mystery of the constancy of light velocity.

In the Michelson-Morley experiment [2] the etheric wind was not detected because the Earth carries its own etheric layer with it, and the ether of the Earth

is almost completely stationary relative to the Earth's surface (the influence of the sun's ether is negligible on the Earth's surface). So light travels at the same speed relative to the Earth in any direction along the Earth's surface.

We can use the following case to better understand the physical mechanism of the principle of constancy of light velocity. Suppose a submarine moves together with a container filled with water, and a sound speed detector is installed in the container, then no matter how the submarine moves and no matter how the underwater sound source (like dolphin or whale) moves, the sound speed measured by the detector is constant. If we take the water as the ether, the sea as the universe, the container as the object, then we can very easily understand the principle of constancy of light velocity.

It can be seen that the constant velocity of light is actually a physical phenomenon in the universe, which is produced by the photon together with the object and the ether. The physical phenomenon of constant velocity of light can also be regarded as a proof of the existence of the ether and a proof that every particle or object drags a layer of ether to move together. The so-called constant velocity of light is actually that the photon's velocity relative to the ether remains constant, but its velocity relative to any fixed inertial system is variable. In a selected inertial system, the velocity of light varies as photons move from etheric system A to etheric system B, which is moving relative to etheric system A. For example, when we choose the solar etheric system as the frame of reference, then when a photon emits from the sun, it first moves at the speed of c in the etheric system of the sun, and then it goes into the etheric system of the Earth and moves at the speed of c in the etheric system of the Earth. Because the Earth has relative motion to the sun, the speed of the photon relative to the solar etheric system changes when the photon enters the etheric system of the Earth from the solar etheric system. So the physical phenomenon that the velocity of light is constant does not mean that the velocity of light relative to any inertia system remains constant in a vacuum, but that photons adjust their velocity when moving into the etheric layer of any object or particle so that the velocity relative to the etheric layer of the object or particle is always at the constant velocity of light c. In other words, any measurement of the collision velocity between a photon and an object will change the velocity of light so that the velocity of the photon relative to the etheric layer of the object is always adjusted to c the constant velocity of light, when the photon approaches the object and enters into the erthric layer of the object. Therefore, the principle of constancy of light velocity in special relativity is incorrect and needs to be corrected.

2.2. The Modification of the Principle of Constancy of Light Velocity

If we define the etheric layers that are dragged by different particles or objects and are moving with the particles or objects the different etheric systems, such as the etheric system of electron, the etheric system of nucleus, the etheric system of crystals, the etheric system of Earth, the etheric system of the sun, the etheric

system of galaxies, and define the space of the universe the etheric system of the universe, then "the propagation velocity of light in all etheric systems remains constant C (299,792,458 m/s), which has nothing to do with the motion of the light source and the motion of the etheric system" this is the modified principle of constancy of light velocity or called "principle of constancy of light velocity in ether".

3. On the Principle of Special Relativity

3.1. The Problem Exists in the Principle of Special Relativity

The principle of special relativity can be expressed as follows: the law of physics has the same form in any inertia system.

Here is one equation of the Maxwell equations in a vacuum [6]

$$\nabla \times \boldsymbol{B} = \mu_0 \boldsymbol{J} + \varepsilon_0 \mu_0 \frac{\partial \boldsymbol{E}}{\partial t}$$

In the above equation, $\boldsymbol{B}$ is the magnetic induction, $\boldsymbol{J}$ is the current density, ε_0 is the dielectric constant of the vacuum, μ_0 is the magnetic permeability of the vacuum, $\boldsymbol{E}$ is the electric field strength, and t is time. Since [7]

$$c = \frac{1}{\sqrt{\varepsilon_0 \mu_0}}$$

In the above formula c is the speed of light in vacuum. If the speed of light in vacuum cannot be maintained the same relative to different inertial frame of references, that is to say if the principle of constancy of light velocity is not true, then the mathematical form of the above Maxwell equation cannot be maintained the same in all inertial systems, in other words, the principle of special relativity is incorrect.

The status of various etheric systems (for example the etheric system of the Earth and etheric system of the Milky Way) is unequal due to the great differences in the quantity of energy contained in the etheric systems. For example, we can study the motion of the Earth with the sun as a reference frame, but we cannot study the motion of the sun with the Earth as a reference frame. We can study the motion of a car with the Earth as a frame of reference, but we can never study the motion of the Earth with the car as a frame of reference. Therefore, the inertia systems of equal status in special relativity do not exist in the real physical world.

In addition, the principle of special relativity is not true in the real physical world because it ignores the existence and influence of spatial background energy (ether), such as the influence of ether on the time, size and inertia mass of objects that move in the ether, as well as the influence of magnetic field, rotating electric field and electromagnetic wave on the charged body moving relative to it.

From the point of view of the new etheric view of this paper, the prolongation of time, the contraction of length and the increase of the inertia mass of a mov-

ing object are not the relative observational effects described in the special relativity, but the etheric effect, which is the absolute physical effect produced by the ether on the object when the object moves relative to the ether, and is independent of the motion state of the observer.

In summary, the principle of special relativity is incorrect and needs to be modified.

3.2. The Modification of the Principle of Special Relativity

If we define the etheric layers that are dragged by different particles or objects and are moving with the particles or objects the different etheric systems, such as the etheric system of electron, the etheric system of nucleus, the etheric system of crystals, the etheric system of Earth, the etheric system of the sun, the etheric system of galaxies; and define the space of the universe the etheric system of the universe, then the Maxwell equations can keep their mathematical forms unchanged in different etheric systems. Therefore, we can draw the conclusion that the form of any law of physics is the same in all kinds of etheric systems, which is the modified principle of special relativity, or called "the principle of relativity of etheric systems".

3.3. The Correct Selection of the Etheric System

Because the spatial scales of different etheric systems are very different (from the microcosm to the universe), the amount of energy (ether) contained in different etheric systems is also very different, different etheric systems are not equal. For example, it is impossible to equalize the etheric system of the Earth and the etheric system a car, because the Earth cannot move in the etheric system of the car, the physical laws of the Earth moving around the sun cannot exist in the etheric system of the car, but can exist in the etheric system of the sun. Therefore, when dealing with the kinematic dynamics of an automobile that moves relative to the Earth, we can only take the Earth etheric system as the reference frame, not the automobile etheric system as the reference frame, otherwise there will be problem of energy conservation.

All the etheric systems are the absolute frame of references, that are the working frameworks for scientific workers. It is very important to choose the proper etheric system when doing scientific research.

The physical world is very similar to human society in some aspects. Human society maintains order through laws, and the physical world maintains order through the laws of physics. For human society, the greater the power a government has the greater the influence. For physical world the more the energy (ether) a system has the greater the influence. The human society of a country is controlled by the national government, the state government, the city government, the township government and the village government etc. The universe is controlled by the cosmic etheric system, the galaxy group etheric system, the galaxy etheric system, the star etheric system, the planetary etheric system, the

crystal etheric system and the nuclear etheric system etc. Ether in the universe is similar as power in human society, the range and density of the ether distribution in universe is equal to the range of power and the influence in human society. For the human society, a normal individual can not affect the national machine's operation. For the universe, a car on the Earth can not affect the Earth's movement. For human society, the villagers are directly controlled by the village chief rather than the president of the country, and the village chief has far greater control over the villagers than the president. In the physical world, the electrons in the atom are directly bound by the nucleus (nuclear electrostatic field and ether contained in the electrostatic field), not the universe or the sun or the Earth. The influence of the nucleus to the electrons is far greater than the universe or the sun or the Earth. It can be seen that the principle of special relativity that all inertial systems are equal is not true, and the principle of general relativity that all non-inertial systems are equal is also untrue. Therefore, we must follow the following rules when choosing a frame of reference:

When we study the motion of galaxy clusters in the universe (or the motion of isolated objects far away from all galaxies), we must adopt the etheric system of the universe as the absolute reference system.

When we study the motion of galaxies in the galaxy cluster, we must adopt the etheric system of the galaxy cluster as the absolute reference system.

When we study the motion of stars in the galaxy, we must adopt the etheric system of the galaxy as the absolute reference system.

When we study the motion of the planets in the solar system, we must adopt the etheric system of the sun as the absolute reference system.

When we study the motion of the satellites around the planet, we must adopt the etheric system of the planet as the absolute reference system.

When we study the motion of the macroscopic objects on or near the Earth's surface, we must adopt the etheric system of the Earth as the absolute reference system.

When we study the motion of the free microscopic particles (such as cosmic rays entering the Earth's atmosphere) on or near the Earth's surface, we must adopt the etheric system of the Earth as the absolute reference system also.

When we study the motion of the particles accelerated by an cyclotron, we must adopt the etheric system formed by the magnetic field of the cyclotron as the absolute reference system.

When we study the motion of atoms or electrons in a crystal, we must adopt the etheric system formed by the crystal as the absolute reference system. For example when we study the motion of electrons in the wire, we must use the etheric system formed by the wire as the absolute reference system.

When we study the motion of the electrons bound by a nucleus, we must adopt the etheric system of the nucleus as the absolute reference system.

Therefore, in the Compton Scattering experiment [5], when the photon and the electron collide, the photon enters the etheric layer of the electron, the speed

and the energy of the electron and the photon must be calculated with the etheric layer of the electron as the absolute frame of reference. But, after the collision when the photon and electron are separated from each other, they enter the etheric layer of the Earth, respectively. At this time, the speed and energy of the electron and the photon must be calculated by using the etheric layer of the Earth as the absolute frame of reference.

For the human society, the residents of the fuzzy zone located on both sides of the border are often affected and bound by the two places. For the physical world the influence of both etheric systems must be taken into account in a space where the influence of both etheric systems cannot be ignored. For example, when studying the propagation of light in water flow of water pipes, the combined effects of Earth ether and water ether must be considered.

Because of the influence of background etheric system, the speed between the etheric layer dragged by rotating object and the surface of the rotating object will increase with the increase of the distance between etheric layer and the surface of the object, so it is necessary to make appropriate correction when choosing an etheric system for calculation. For example, when studying the motion of artificial satellites, it is necessary to take into account the influence of the fact that the farther away the satellite is from the Earth, the higher the speed of the etheric layer relative to the Earth, and make appropriate modifications to the calculation results.

In addition, among all the above etheric systems, only the cosmic etheric system is an isolated system, so all the conservation laws (such as energy conservation, momentum conservation, and angular momentum conservation, etc.) are strictly valid only in the cosmic etheric system.

4. On the Lorentz Transformation

4.1. The Derivation of Lorentz Transformation from the Modified Principle of Special Relativity and the Modified Principle of Constancy of Light Velocity

The lorentz coordinates and time transformations can be derived from the modified principle of special relativity and the modified principle of constancy of light velocity.

4.1.1. The Transformation Relationship between Space-Time Coordinates

If we assume that both time and space are uniform in a small etheric space, as shown in Figure 1, the transformation between space-time coordinates can be approximately linear. Let S and S' be two etheric systems, one large and one small, the small etheric system S' (for example, the Earth etheric system) is in the large etheric system S (for example, the solar etheric system) and is moving in a straight line with uniform speed v relative to S. For any event, the space-time coordinates of P in S system and S' system are (x, y, z, t) and (x', y', z', t') respectively. Since S' is moving along the x-axis with constant speed relative to S,
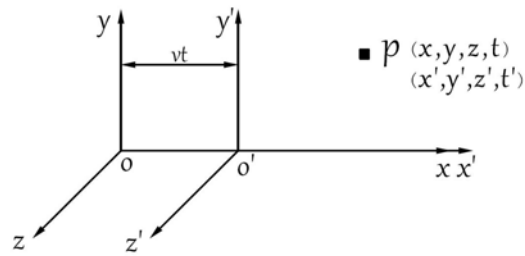
Figure 1. Transformation of space-time coordinates.

obviously $y' = y$, $z' = z$. The coordinates of the origin of S system observed in S system are: $x = 0$; and observed in S' system are: $x' = -vt'$ or $x' + vt' = 0$. So we have $x = x' + vt'$ 。 For any point in the space, we can set:

$$x = k(x' + vt') \tag{4.1}$$

In the above formula, k is a constant of proportionality. Similarly, we can get:

$$x' = k'(x - vt) = k'(x + (-v)t) \tag{4.2}$$

According to the "modified principle of special relativity" any law of physics in S system and S' system should be the same in the form, so the form of (4.1) and (4.2) should be the same (except positive and negative signs), so $k = k'$.

4.1.2. To Obtain the Constant k from the Modified Principle of Constancy of Light Velocity

Let S and S' be two etheric systems, one large and one small, the small etheric system S' (for example, the Earth etheric system) is in the large etheric system S (for example, the solar etheric system) and is moving in a straight line with uniform speed relative to S. Suppose a light signal travels along the x' axis from the origin in the S' system, then at any instant t', the coordinate of the point the signal reaches in the S' system is: $x' = ct'$, where c is the speed of light in ether (vacum). Suppose another light signal travels along the x axis from the origin in the S system, then at any instant t, the coordinate of the point the signal reaches in the S system is: $x = ct$, where c is the speed of light in ether (vacum). Suppose that at the instant in which the origin of the S system and the origin of S' system meet, one light signal travels along the x' (x) axis from the origin. Suppose that the S system disappear suddenly when the light signal start to travel from the origin, so the light travels in S' system, and we have $x' = ct'$. Suppose that S system is there but the S' system disappear suddenly when the light signal start to travel from the origin, so the light travels in S system, and we have $x = ct$. So we have:

$$xx' = c^2 tt' = k^2 (x - vt)(x' + vt') = k^2 (ct - vt)(ct' + vt') = k^2 tt'(c^2 - v^2) \tag{4.3}$$

From above equation we can get:

$$k = \frac{c}{\sqrt{c^2 - v^2}} = \frac{1}{\sqrt{1 - (v/c)^2}} \tag{4.4}$$

and then, we can get:

$$x' = \frac{x - vt}{\sqrt{1 - (v/c)^2}} \tag{4.5}$$

$$x = \frac{x' + vt'}{\sqrt{1 - (v/c)^2}} \tag{4.6}$$

By eliminating x' from the above two equations, we get:

$$t' = \frac{t - vx/c^2}{\sqrt{1 - (v/c)^2}} \tag{4.7}$$

By eliminating x, then we get:

$$t = \frac{t' + vx'/c^2}{\sqrt{1 - (v/c)^2}} \tag{4.8}$$

Based on the above results, the Lorentz transformations are obtained:

$$\begin{cases} x' = \dfrac{x - vt}{\sqrt{1 - (v/c)^2}} \\ y' = y \\ z' = z \\ t' = \dfrac{t - vx/c^2}{\sqrt{1 - (v/c)^2}} \end{cases} \tag{4.9}$$

and the Lorentz inverse transformations are obtained:

$$\begin{cases} x = \dfrac{x' + vt'}{\sqrt{1 - (v/c)^2}} \\ y = y' \\ z = z' \\ t = \dfrac{t' + vx'/c^2}{\sqrt{1 - (v/c)^2}} \end{cases} \tag{4.10}$$

It can be seen that the Lorentz transformations are the direct result of the modified principle of special relativity (*i.e.* the form of any law of physics is the same in all kinds of etheric systems) and the modified principle of constancy of light velocity (*i.e.* the propagation velocity of light in all etheric systems remains constant C (299,792,458 m/s), which has nothing to do with the motion of the light source and the motion of the etheric system).

4.2. Lorentz Velocity Transformations

4.2.1. The Derivation of Lorentz Velocity Transformations

Lorentz transformation is the relationship of the space-time coordinates of events between different etheric systems, and according to Lorentz coordinates transformations and Lorentz time transformation, Lorentz velocity transformations can be obtained. Let the velocity of an object in S system and S' system be (u_x, u_y, u_z) and (u'_x, u'_y, u'_z) respectively, according to Lorentz coordinates

transformations and time transformation, we can get:

$$dx' = \frac{dx - vdt}{\sqrt{1-(v/c)^2}} = \frac{(dx/dt - v)dt}{\sqrt{1-(v/c)^2}} = \frac{(u_x - v)dt}{\sqrt{1-(v/c)^2}}$$

$$dt' = \frac{dt - vdx/c^2}{\sqrt{1-(v/c)^2}} = \frac{dt(1-vu_x/c^2)}{\sqrt{1-(v/c)^2}}$$

so:

$$\frac{dx'}{dt'} = \frac{(u_x - v)dt}{\sqrt{1-(v/c)^2}} \left/ \frac{dt(1-vu_x/c^2)}{\sqrt{1-(v/c)^2}} \right.$$

that is:

$$u_x' = \frac{u_x - v}{1 - vu_x/c^2} \tag{4.11}$$

$y' = y$, $z' = z$, so $dy' = dy$, $dz' = dz$, then:

$$\frac{dy'}{dt'} = dy \left/ \frac{dt(1-vu_x/c^2)}{\sqrt{1-(v/c)^2}} \right.$$

that is:

$$u_y' = \frac{u_y\sqrt{1-(v/c)^2}}{1 - vu_x/c^2} \tag{4.12}$$

In the same way we can get:

$$u_z' = \frac{u_z\sqrt{1-(v/c)^2}}{1 - vu_x/c^2} \tag{4.13}$$

Therefore, we get the Lorentz velocity transformations:

$$\begin{cases} u_x' = \dfrac{u_x - v}{1 - vu_x/c^2} \\[3mm] u_y' = \dfrac{u_y\sqrt{1-(v/c)^2}}{1 - vu_x/c^2} \\[3mm] u_z' = \dfrac{u_z\sqrt{1-(v/c)^2}}{1 - vu_x/c^2} \end{cases} \tag{4.14}$$

and the inverse transformations:

$$\begin{cases} u_x = \dfrac{u_x' + v}{1 + vu_x'/c^2} \\[3mm] u_y = \dfrac{u_y'\sqrt{1-(v/c)^2}}{1 + vu_x'/c^2} \\[3mm] u_z = \dfrac{u_z'\sqrt{1-(v/c)^2}}{1 + vu_x'/c^2} \end{cases} \tag{4.15}$$

4.2.2. Discussions

1) When the velocities u and v are far less than c (the velocity of light), Lorentz velocity transformation (4.14) is transformed into Galileo velocity transformation:

$$u'_x = u_x - v$$

2) Using the Lorentz velocity transformation (4.15), it can be proved that the speed of light is c in any etheric system. Suppose that the speed of a light signal propagated along the x' direction measured by the observer in the S' system is c, and the speed of the light signal measured by the observer in the S system is:

$$u_x = \frac{c + v}{1 + vc/c^2} = c$$

That is to say, the speed of light in S system and S' system is the same.

4.3. The Physical Meaning and Proper Use of Lorentz Transformations

From the point of view of the new etheric view of this paper, the etheric system is unequal with any inertial or non-inertial system. Because any object that is moving in ether will produce associated physical effects (such as the changes in time, length, and inertial mass). Because only objects moving in ether can produce related physical effects, only the motion of objects in ether is physically meaningful. As an object moves from one etheric system to another etheric system that moves relative to the primary etheric system, the speed of the object relative to ether changes, The change of the speed of the object relative to ether will result in the change of the energy (etheric) density of the local space in which the object is located, resulting in the change of the local space and time. Therefore, the Lorentz transformations must be applied between the etheric system and any other etheric system that is moving uniformly in a straight line with respect to it (since there is no object in the universe that is really moving uniformly in a straight line, it can only be approximated). For example that a photon from a distant star outside the Milky Way galaxy reaches the Earth. The photon must first leave the etheric system of the star to enter the etheric system of the galaxy in which the star is located, and then enter the cosmic etheric system from the etheric system of the galaxy in which the star is located. And then from the cosmic etheric system to enter the Milky Way galaxy etheric system, from the Milky Way galaxy etheric system to enter the solar etheric system, and from the solar etheric system to enter the Earth etheric system. If we want to calculate exactly the velocity of the photon relative to the Earth to get a precise Aberration Angle, the Lorentz velocity transformation must be used to calculate the velocity of the photon to enter galaxy etheric system from the star etheric system, then to calculate the velocity of the photon to enter the cosmic etheric system from the galaxy etheric system, then to calculate the velocity of the photon to enter the Milky Way galaxy etheric system from the comic etheric system,

and then to calculate the velocity of the photon to enter the solar etheric system from Milky Way galaxy etheric system, and finally to calculate the velocity of the photon to enter the Earth etheric system from the solar etheric system. We cannot directly calculate the velocity of the photon relative to the Earth's etheric system by the lorentz transformation between the etheric system of the star that emits the photon and the Earth's etheric system. So Lorentz transformations are not appropriate for two etheric systems that are not directly related, nor is Lorentz transform suitable for any other two inertial systems that are not etheric systems. The transformation between any other two inertial systems that are not the etheric system (without considering the influence of the ether) is only suitable for the Galilean transformation. For example, assuming that the velocityies of particles A and B relative to the cosmic etheric frame of reference are v_a and v_b respectively according to the Lorentz transformation formula, the velocity of particle A relative to particle B should be calculated based on the Galileo transformation when the two particles are far apart, and should be the vector superposition of v_a and v_b. If both A and B particles are photons, the velocity of photon A relative to photon B should be $c + c$ (vector superposition) when the two photons are far away from each other. If two photons collide (either believing that photon A enter the etheric layer of photon B or that photon B enter the etheric layer of photon A), the Lorentz transform must be used to calculate the collision speed between the two photons that is always c (the constant speed of light).

From the point of view of special relativity, ether does not exist, all inertial systems have equal positions, and the Lorenz transform is suitable for the transformation between any two inertial systems.

So, it can be seen that Lorenz transformation has the above two different understandings and applications. From the point of view of the new etheric view of this paper, the inertial system in special relativity is a mathematical concept that does not exist in the physical world, and in the special relativity the understanding of the physical meaning of Lorenz transformation and the application of Lorenz transformation are wrong.

4.4. The Absoluteness of Simultaneity

According to the etheric theory of this paper, two simultaneous events in an etheric system occur simultaneously to any observer. For example, if a light pulse is emitted from the mid-point of a l_0 long capsule resting in the solar etheric system, the light signal will be received simultaneously by the capsule's head A and tail B to any observer, as shown in Figure 2. Because in this case according to the modified principle of constant speed of light of this paper, the speed of light traveling through the solar ether is constant c (299,792,458 m/s), independent of the observer (the result is the same whether observed by observers in the capsule stationary in the solar etheric system or from earth moving relative to the solar etheric system).
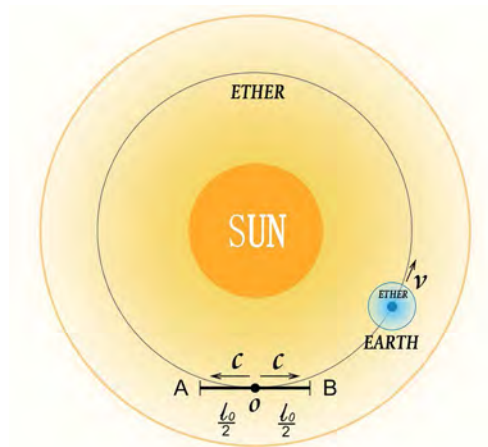
Figure 2. A light pulse is emitted from the mid-point of a l_0 long capsule resting in the solar etheric system, the light signal will be received simultaneously by the capsule's head A and tail B to any observer.

5. The Etheric Explanations for the Conclusions of Special Relativity

According to the new etheric view of this paper, the effect of speed on mass, the effect of speed on time and the effect of speed on length derived from the Lorentz transformation are not the relative observation effects between two different inertial systems, but the absolute real physical effects caused by ether when the object is moving in ether.

5.1. The Etheric Explanation of the Relation between Mass and Speed

5.1.1. Derivation of the Mass-Speed Relationship Formula

Suppose an object of stationary mass m_0 is placed stationary in the solar etheric system S and near earth orbit, as shown in **Figure 3**. When the earth is far away from the object, the object can be thought of as stationary in the solar ether.

When the earth moves to the position of the object and the object is then in the earth's ether, if the object is very close to the earth's surface, the object can be considered to be completely in the earth's ether. At this point, the object moves relative to the ether of the earth at the speed at which the earth revolves around the sun, and the mass of the object is the moving mass m, as shown in **Figure 4**.

We have the Lorentz time transformation formula (4.9):

$$t' = \frac{t - vx/c^2}{\sqrt{1 - (v/c)^2}}$$

and the Lorentz velocity transformation formula (4.15):

$$u_x = \frac{u_x' + v}{1 + vu_x'/c^2}$$

Since the object is stationary in the solar etheric system S, we have:
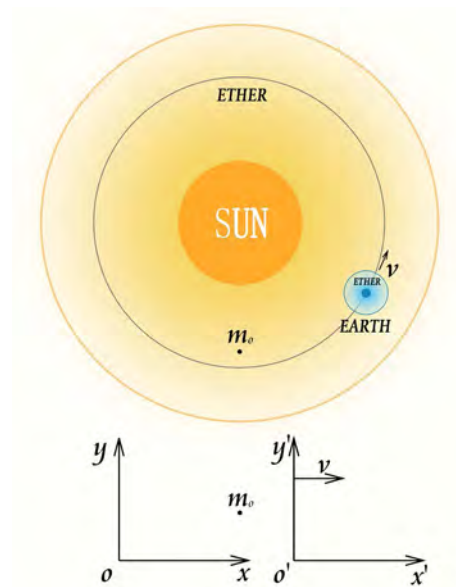
Figure 3. An object of stationary mass m_0 is placed stationary in the solar etheric system S and near earth orbit.
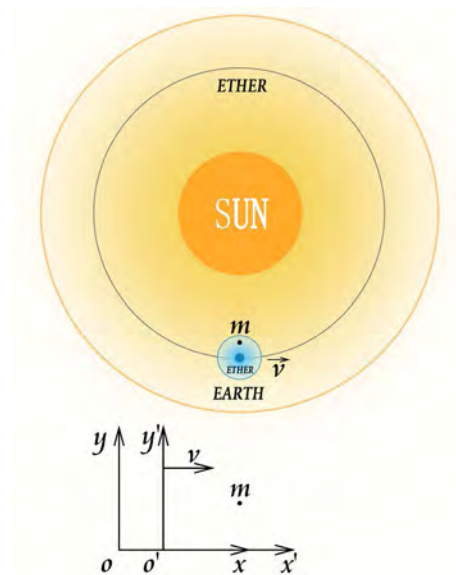
Figure 4. The object moves relative to the ether of the earth at the speed at which the earth revolves around the sun.

$$u_x = 0 \tag{5.1}$$

Bring Equation (5.1) into Equation (4.15), we get:

$$u'_x = -v \tag{5.2}$$

Since the object is at rest in S system, the mass of the object measured in S system is the object's static mass m_0. If F_x is the external force on the object along the x direction in S system, and F'_x is the external force on the object along the x' direction in S' system, then according to the "modified principle of special relativity" of this paper, we must have:

$$F_x = F'_x \tag{5.3}$$

Because if an object is not subjected to force and is stationary or moving in a straight line with a uniform speed in the S system, it should also be not subjected to force and be stationary or moving in a straight line with a uniform speed in the S' system, otherwise Newton's first law can't hold both in the S system and the S' system. Therefore, according to the modified principle of relativity in this paper that "any law of physics has the same form in all the etheric systems", Equation (5.3) must be true. And because:

$$F_x = \frac{\mathrm{d}p}{\mathrm{d}t} = \frac{\mathrm{d}(m_0 u_x)}{\mathrm{d}t} \tag{5.4}$$

$$F'_x = \frac{\mathrm{d}p'}{\mathrm{d}t'} = \frac{\mathrm{d}(m u'_x)}{\mathrm{d}t'} \tag{5.5}$$

From Equations (5.3), (5.4) and (5.5) we get:

$$\mathrm{d}(m u'_x) = \frac{m_0 \mathrm{d}u_x \mathrm{d}t'}{\mathrm{d}t} \tag{5.6}$$

Since the object is stationary in S system, $\mathrm{d}x = 0$. According to Equation (4.9), we have:

$$\mathrm{d}t' = \frac{\mathrm{d}t}{\sqrt{1 - (v/c)^2}} \tag{5.7}$$

Differential derivation of formula (4.15) we get:

$$\mathrm{d}u_x = \mathrm{d}\left(\frac{u'_x + v}{1 + v u'_x/c^2}\right) = \frac{(1 - v^2/c^2)\mathrm{d}u'_x}{(1 + v u'_x/c^2)^2} \tag{5.8}$$

Substitute Equation (5.1), (5.7) and (5.8) into Equation (5.6), and notice that $u'_x = -v$, we get:

$$\mathrm{d}(m u'_x) = m_0 \frac{\mathrm{d}u'_x}{\sqrt{\left(1 - \dfrac{v^2}{c^2}\right)^3}} \tag{5.9}$$

and:

$$\mathrm{d}(mv) = m_0 \frac{\mathrm{d}v}{\sqrt{\left(1 - \dfrac{v^2}{c^2}\right)^3}} \tag{5.10}$$

Integrate both sides of Equation (5.10), we get:

$$mv = \frac{m_0 v}{\sqrt{1 - \dfrac{v^2}{c^2}}} \tag{5.11}$$

that is:

$$m = \frac{m_0}{\sqrt{1 - \dfrac{v^2}{c^2}}} \tag{5.12}$$

5.1.2. The Physical Mechanism of the Mass-Speed Relationship

In the formula (5.12), v is the speed of the object relative to the ether when the object is moving in the ether, m_0 is the inertia mass of the object at rest relative to the ether, and m is the inertial mass of the object moving relative to the ether with speed v. So, when the speed of an object moving relative to the etheric system is fixed, the inertial mass of the object is the same no matter what reference frame is adopted for observation. For example, in the solar etheric system, the inertial mass (kinetic energy part) of the Earth is determined by the speed of the Earth relative to the solar etheric system (the etheric layer dragged together by the sun), and the results are the same whether the observer observes on Earth, on the moon or on Mars.

In the galactic etheric system, the inertial mass (kinetic energy part) of the Earth is determined by the speed of the Earth relative to the galactic etheric system, and the results are the same whether the observer observes on Earth, on the moon or on Mars.

In the etheric system of the universe, the inertial mass (kinetic energy part) of the Earth is determined by the speed of the Earth relative to the etheric system of the universe, and the results are the same whether the observer observes on Earth, on the moon or on Mars.

Because an object that moves in ether can contact more etheric particles (assuming that ether is made up of very tiny particles) in a unit time than an object that is at rest in the ether. Moreover, the faster the object moves, the more etheric particles are contacted per unit time, the more etheric particles are attracted and the higher the density of etheric particles is in the object. This is why the inertial mass of an object increases as it moves in the ether, and the faster the speed, the larger the inertial mass. It is also because the increase of the etheric density of space can lead to the slowness of time, so formula (5.12) is formed.

From the above discussions, we can get the conclusion that the higher the etheric density of the space, the greater the mass of the object, and that with the expansion of the universe, the etheric (energy) density of space is decreasing, so the mass of all objects and particles is decreasing.

5.2. The Etheric Explanation of the Relation between Time and Speed

5.2.1. Derivation of the Time-Speed Relationship Formula

Suppose an object is placed stationary near earth orbit in the solar etheric system S, as shown in **Figure 5**. When the earth is far away from the object, the object can be thought of as stationary in the solar ether. Assuming that in the S system there is a static clock and that two events (such as the birth and death of a bacterium) occur on the object one after another, and that the two events are recorded by the clock at t_1 and t_2 respectively, the time interval between the two events in the S system is as follows:

$$\Delta t = t_2 - t_1 = t_0 \tag{5.13}$$

In the above formula, t_0 is called the proper time.
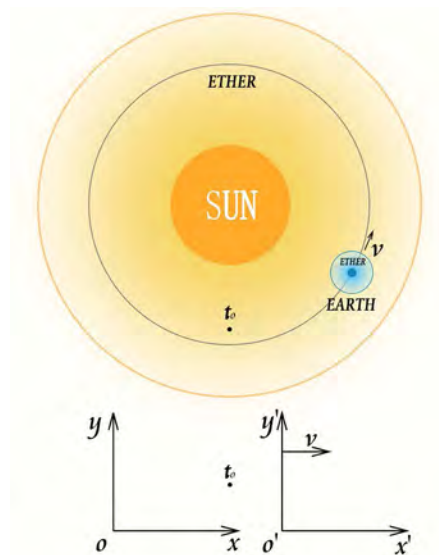
Figure 5. An object is placed stationary near earth orbit in the solar etheric system *S*, and two events occur on the object one after another. The time interval between the two events is t_0.

When the earth moves to the position of the object and the object is in the earth's ether, if the object is very close to the earth's surface, the object can be considered to be completely in the earth's ether. At this point, the object moves relative to the ether of the earth at the speed at which the earth revolves around the sun, as shown in **Figure 6**. Assuming that in the *S'* system there is also a static clock, and that the same two events (such as the birth and death of the same bacterium) occur on the object one after another and are recorded by this clock at t_1' and t_2' respectively, the time interval between the two events in the *S'* system is as follows:

$$\Delta t' = t_2' - t_1' = t \tag{5.14}$$

From Lorentz transformation (4.9) we have:

$$t_1' = \frac{t_1 - vx/c^2}{\sqrt{1 - (v/c)^2}} \tag{5.15}$$

$$t_2' = \frac{t_2 - vx/c^2}{\sqrt{1 - (v/c)^2}} \tag{5.16}$$

From Equations (5.13), (5.14), (5.15) and (5.16), we can get:

$$t = \frac{t_0}{\sqrt{1 - \dfrac{v^2}{c^2}}} \tag{5.17}$$

5.2.2. The Physical Mechanism of the Time-Speed Relationship

In formula (5.17) *v* is the speed of the object moving relative to the ether, and t_0 is the time interval between the two events when the object is at rest in ether, *t* is time interval between the two events when the object is moving relative to the ether with speed *v*.
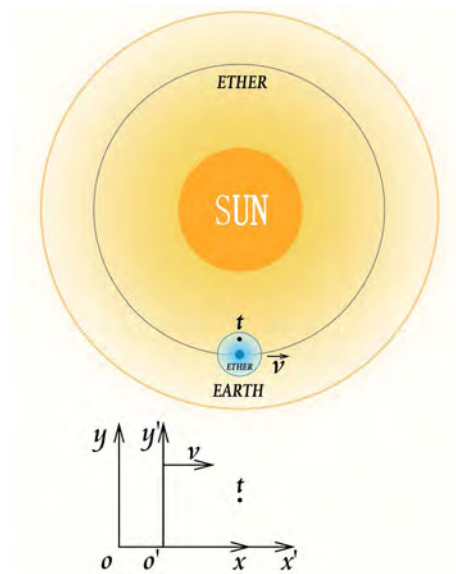
Figure 6. The object moves relative to the ether of the earth at the speed at which the earth revolves around the sun, and the same two events occur on the object. The time interval between the two events is *t*.

Because the etheric density in the space in an object will increase as the object moves in the ether, and the faster the speed, the greater the etheric density of the space in the object. The increase in the etheric density of the space in the object will slow down the time on the object. So, the speed effect of time is not the relative observation effect produced by the relative motion of the two inertial systems, but a real and absolute physical effect given by ether when the object moves in the ether (independent of the observer).

It can be seen from the formula (5.17) that with the decelerating expansion of the universe, the speed of all the objects relative to the universe etheric system decrease, or the inertial mass of all the objects decrease constantly, and the time on all the objects will continue to accelerate.

5.2.3. The Exploration for the Essence of Time

We know that the stronger the gravitational field is, the higher the density of the ether in the space of the gravitational field, and now we also know that the faster the object moves in ether, the higher the density of the ether in the space inside the object. So from the facts that time slows down with the gravitational field's increase, and slows down with the increase of the speed of the object relative to the ether, we can get the following conclusion: the time at a point in cosmic space during cosmic expansion (during which the ether flows from particles to cosmic space) slows down (speeds up) as the density of the ether at that point increases (decreases). Or, the product of the time and the density of ether at any point of the space is the same:

$$\rho t = b \tag{5.18}$$

In the formula, ρ is the etheric (energy) density of a point in the space, t is

the time at the same point, and *b* is a constant (the unit is Joule second/cubic meter). By formula (5.18), it can be seen that there is no meaning for the time in the case that the ether density is zero because the speed of time flow is infinite.

During cosmic contraction (during which the ether flows from space to particles), time at a point in space speeds up (slows down) as the density of the ether (energy) at that point increases (decreases). Or, the product of the time and the reciprocal of density of ether at any point of the space is the same.

It can be seen that time is the flow rate of ether from the object to the space during cosmic expansion or the flow rate of ether from the space to the object during cosmic contraction.

From the above discussions, we can also get the conclusions that the higher the etheric density of the space, the slower the time on the object, and that with the expansion of the universe, the etheric (energy) density of space is decreasing, the time is accelerating.

5.3. The Etheric Explanation of the Relation between Length and Speed

5.3.1. Derivation of the Length-Speed Relationship Formula

Let S and S' be two etheric systems, one large and one small, the small etheric system S' (for example, the Earth etheric system) is in the large etheric system S (for example, the solar etheric system) and is moving in a straight line with uniform speed relative to S. Suppose a thin rod is placed stationary along the direction of earth's motion in the position near the earth's orbit in the solar etheric system S, as shown in **Figure 7**. When the earth is far away from the rod, the rod can be regarded as stationary in the solar ether. At this time, for any observer, the coordinates of both ends of the rod, x_1 and x_2, are measured simultaneously (according to section 4.4, simultaneity is absolute), and the length of the measured rod is:

$$l_0 = x_2 - x_1 \tag{5.19}$$

In the formula, l_0 is the prober length.

When the earth moves to the position of the rod and the rod is in the earth's ether, if the rod is very close to the earth's surface, the rod can be considered to be completely in the earth's ether. At this point, the rod moves relative to the ether of the earth at the speed at which the earth revolves around the sun, as shown in **Figure 8**. At this time, for any observer, the coordinates of both ends of the rod, x_1' and x_2', are measured simultaneously (according to section 4.4, simultaneity is absolute), and the length of the measured rod is:

$$l = x_2' - x_1' \tag{5.20}$$

From Lorentz transformation (4.10) we have:

$$x_1 = \frac{x_1' + vt_1'}{\sqrt{1-(v/c)^2}} \tag{5.21}$$
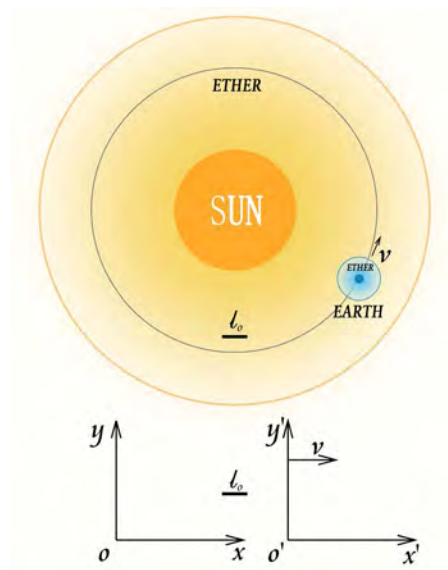
Figure 7. A thin rod is placed stationary along the direction of earth's motion in the position near the earth's orbit in the solar etheric system *S*.
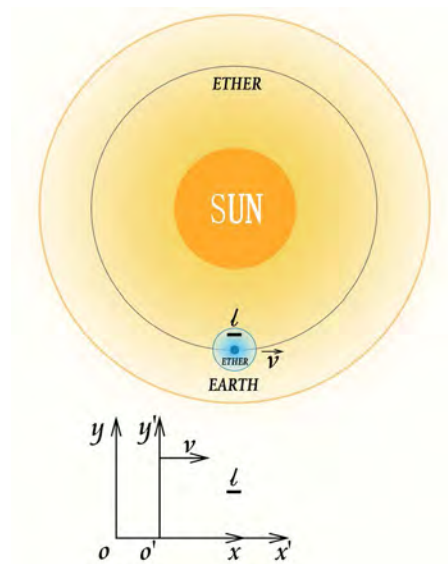
Figure 8. The rod moves relative to the ether of the earth at the speed at which the earth revolves around the sun.

$$x_2 = \frac{x_2' + vt_2'}{\sqrt{1 - (v/c)^2}} \tag{5.22}$$

In the formula $t_1' = t_2'$. Subtract the above two equations we get:

$$x_2 - x_1 = \frac{x_2' - x_1'}{\sqrt{1 - (v/c)^2}} \tag{5.23}$$

That is:

$$l = l_0 \sqrt{1 - \frac{v^2}{c^2}} \tag{5.24}$$

where v is the speed of the rod relative to the ether, and l_0 is the length when the rod is at rest in ether, l is the length when the rod is moving relative to the ether with speed v.

5.3.2. The Physical Mechanism of the Length-Speed Relationship

The speed effect of length is not the relative observation effect produced by the relative motion of the two inertial systems, but a real and absolute physical effect given by ether when the object moves in the ether (it has nothing to do with the observer).

The size of an object is determined by the average distance between the nucleuses of the object, and the average distance between the nucleuses is determined by the average size of the atoms composed of the object. The size of the atom is determined by the inertial mass of the electron and the coulomb force between the nucleus and the electron.

From the coulomb force formula between the electron and the nucleus [8]:

$$F_e = \frac{1}{4\pi\varepsilon_0} \frac{ne^2}{r_a^{\ 2}} \tag{5.25}$$

where F_e is the coulomb force between the electron and the nucleus, e is the electric charge of the electron, n is the number of proton of the nucleus, r_a is the distance between the electron and nucleus, ε_0 is the dielectric constant in vacuum. The formula of the inertial centrifugal force of the electron [9]:

$$F_I = \frac{mv_e^2}{r_a} \tag{5.26}$$

where F_I is the inertial centrifugal force of the electron orbiting the nucleus, and m is the inertial mass of the electron; v_e is the speed of the electron orbiting the nucleus. The formula of angular momentum conservation that the electron orbits the nucleus [10]

$$mv_e r_a = b = nh, \quad n = 1, 2, 3, \cdots \tag{5.27}$$

where b is invariant, h is planck constant. And the following equation:

$$F_e = F_I \tag{5.28}$$

We can get the radius of the electron orbiting the nucleus:

$$r_a = \frac{4\pi\varepsilon_0 b^2}{ne^2 m} \tag{5.29}$$

and the speed of electron orbiting the nucleus:

$$v_e = \frac{ne^2}{4\pi\varepsilon_0 b} \tag{5.30}$$

From (5.12) and (5.29) we can get:

$$r_a = \frac{4\pi\varepsilon_0 b^2}{ne^2 m_0} \sqrt{1 - \frac{v^2}{c^2}} = r_{a0}\sqrt{1 - \frac{v^2}{c^2}} \tag{5.31}$$

In the formula r_{a0} is the radius of the atoms that makes up the object as the

object is at rest relative to the ether, and v is the speed at which the object moves relative to the ether.

From formula (5.31) we can see that the faster the object moves relative to the ether, the greater the contraction of the atoms of the object, and the greater the contraction of the object. It can also be said that the faster the object moves relative to the ether, the higher the etheric density of the inner space of the object (because the kinetic energy of the object is greater), and the higher the etheric density of the inner space of the object, the more the object contracts.

By (5.31) we see that with the decelerating expansion of the universe, or as the object slows down along the direction of the universe expansion, the speed of the object relative to the cosmic etheric system decreases, the etheric density of the object decreases, the object expands.

From what has been discussed above, we can get the following conclusions: The higher the etheric density of space, the greater the contraction of the objects in space.

Corollary 1: Because the etheric (energy) density of space decreases with the decelerating expansion of the universe, all objects (stars, planets, molecules, atoms, etc.) in the universe expand as the universe expansion slows.

Corollary 2: Because the stronger the electric or magnetic field, the higher the density of the ether (energy) in space, the stronger the electric or magnetic field, the more shrinking the object in the electric or magnetic field.

5.3.3. The Exploration for the Essence of Space

As can be seen from section 5.2.3, time is meaningless in a vacuum. In addition, according to the discussions in the previous sections of this paper, all the laws of physics can hold only in the etheric system, so the vacuum is meaningless to physics. It follows that the space of physics is the space filled with ether, and that the essence of space is ether.

5.4. The Etheric Explanation of the Relation between Mass and Energy

According to the definition of momentum and the mass velocity relationship (5.12), we have:

$$p = \frac{m_0 v}{\sqrt{1 - v^2/c^2}} \tag{5.32}$$

Suppose a particle, under the action of a variable force, starts at rest and moves along the x-axis in one dimension. When the velocity of the particle is v, its kinetic energy is:

$$E_k = \int F_x \, \mathrm{d}x = \int \frac{\mathrm{d}p}{\mathrm{d}t} \mathrm{d}x = \int v \, \mathrm{d}p = pv - \int_0^v p \, \mathrm{d}v \tag{5.33}$$

From Equations (5.32) and (5.33) we get

$$E_k = mc^2 - m_0 c^2 \tag{5.34}$$

$$mc^2 = E_k + m_0 c^2 = E \tag{5.35}$$

That is:

$$E = mc^2 = \frac{m_0 c^2}{\sqrt{1 - v^2 / c^2}} \tag{5.36}$$

In formula (5.36), v is the speed of the object relative to the etheric system, mc^2 is the energy (ether content) of the object when the object moves relative to the etheric system with speed v, $m_0 c^2$ is the energy (ether content) of the object when the object is stationary relative to the etheric system. From formula (5.36) we see that the faster the object moves in the ether, the more the ether collected by the object (the higher the ether density of the object), and the greater the kinetic energy of the object.

6. Relevant Experimental Verifications

So far, all the experiments that have verified the correctness of special relativity (such as the experiments of the constancy of light velocity, the experiments of the relationship between time and speed, the experiments of the relationship between length and speed, the experiments of the relationship between mass and speed, the experiments of mass and energy formula or the explosion of atomic bombs, etc.) can also be explained by the theory of this paper. Therefore, these experiments have now proved that both theories are correct. Which of the two is the right one must be identified by additional experiments. The following are several additional experiments designed:

6.1. Experiment 1: Verify That the Kinetic Energy of a Particle Is Only Related to the Speed of the Particle Relative to the Ether, Independent of the Observer's Motion

Do the following particle collision experiments on cyclotron:

Collision experiment 1: Let two of the same particle A and B to move with a speed of $0.5C$ and $-0.5c$ relative to the laboratory frame of reference respectively and collide. Measure the collision energy produced by the collision.

Collision experiment 2: Two of the same particle A and B, let B be stationary relative to the laboratory frame of reference and A move with a speed of $(4/5)C$ relative to the laboratory frame of reference respectively, and let the two particles collide. Measure the collision energy produced by the collision. Comparing with the above two experiments, and it will be verified that the collision energy produced by two collision events is different. But if take B particle as the reference frame, then the collision energy of two collision events calculated according to the theory of Special Relativity is the same.

In collision experiment 1, the collision energy calculated with particle A or B as the reference frame is $\frac{5}{3} m_0 c^2$. It will be proved that the calculated result is not consistent with the experimental result.

In collision experiment 2, the collision energy calculated with the laboratory reference frame is $\frac{5}{3}m_0c^2$. It will be proved that the calculated result is consistent with the experimental result.

6.2. Experiment 2: Verify That Magnetic Field Is Produced by Electric Charge's Motion Relative to Ether, and Is Independent of the Observer

According to the theory of this paper, the Earth is dragging the ether to move together (the ether near the surface of the Earth is stationary relative to the surface of the Earth), and that the production of the magnetic field by the motion of the electric charge to ether is an absolutely real physical effect, and has nothing to do with the observer. The motion that the electric charged pole is stationary relative to the ether but the compass is moving relative to the pole is different from motion that the compass is stationary relative to the ether and the electric charged rod is moving relative to the compass, and will produce different physical effect. The former does not generate a magnetic field in space (the compass does not rotate), while the latter produces a magnetic field in space (the compass rotates).

Expected experimental results:

When the charged bar is stationary relative to the laboratory (etheric system of the Earth), no matter how the compass moves relative to the charged metal bar, the compass will not rotate.

When the charged bar moves relative to the laboratory (etheric system of the Earth) the compass rotates regardless of whether it is stationary or moving to the charged bar.

We can consider to put an electric charged rod and a compass on the table of a high-speed train (let charged rod and a compass close to each other), let the charged rod point to the direction of the high-speed train movement. When the train is moving and the compass is stationary relative to the charged rod, turn the compass to see if it will turn back or not. When the train is stationary and the compass is stationary relative to the charged rod, turn the compass to see if it will turn back or not.

Expected experimental results: When the high-speed train moves, there is magnetic field generated; when the high-speed train stops moving, there is no magnetic field generated.

This experiment will prove that the electric charge generates magnetic field when it moves relative to ether, and that the production of the magnetic field by the motion of the electric charge to "ether" is an absolutely real physical effect, and has nothing to do with the observer

6.3. Experiment 3: Redoing the Michelson-Morley Experiment on the Space Station

So far all measurements of the "etheric wind", such as the Michelson-Morley

experiment [3], have been carried out on the ground. According to the theory of this paper, the Earth drags ether to move together, and ether is stationary to the Earth's surface. Therefore, all the measurements of "etheric wind" done on the Earth's surface can't detect the "etheric wind". That the space station does not fall off is because of the centrifugal force created by the space station's motion relative to the ether of the Earth. So, there should be an "etheric wind" in the space station. In addition, as the etheric layers dragged by the wall of the space station and the experimental station are very thin, the light can be avoided to pass through these etheric layers during the experiment.

Prediction: The etheric wind will be detected if the Michelson-Morley experiment is done on the space station.

This experiment will prove that ether exists.

6.4. Experiment 4: Simulation of the Generation and Reversal of the Earth's Magnetic Field, Thus Proving That the Magnetic Field Is Generated by the Relative Motion of the Electric Charge to the Ether

Put a large spherical shell cover a small spherical shell of similar radius concentrically and charge the two spherical shells with equal but opposite static charges. Let the outer spherical shell rest, the inner spherical shell rotates, from the axis of rotation a magnetic field will emit out. Remove the outer shell and rotate the inner shell with the same speed, you will see that the magnetic field is much weaker. The experimental results show that the electrostatic field generated by the charged inner spherical shell gathers the ether, and the charged outer spherical shell rotates in the ether of the inner spherical shell, thus producing a magnetic field. The experiment will prove that the magnetic field is produced by the relative motion of the electric charge to the ether.

Let the outer spherical shell rotate and Let the rotating axis of the inner spherical shell periodically change 180 degrees relative to the rotating axis of the outer spherical shell in a short time. A reversal of the magnetic pole relative to the outer spherical shell occurs at each turn of 180 degrees. This experiment will reveal the physical mechanism of the generation and reversal of the Earth's magnetic field [11]

6.5. Experiment 5: Simulate the Formation of the Natural Iron Meteorites and Shows That the Atom Becomes Smaller with the Increase of the Etheric Density of the Space

Cool and crystallize the molten iron in strong magnetic field. Place this crystallized iron in an easily oxidized environment for antioxidant experiments.

Prediction: such iron is just as iron meteorites that is not easy to rust. Because the density of ether in strong magnetic field is very high, and the atom becomes smaller with the increase of etheric density in space, the density of iron condensed in strong magnetic field is higher than that of normal iron, which is not easy to react with oxygen molecule.

6.6. Experiment 6: Aberrations Contrast Experiment

Install an arm on the wall of a tall building at the high place, and Install a light source and suspend a heavy weight object on the arm respectively at a certain distance from wall of the building (such as 1.5 m and 1 m). Let the weight object be close to the ground. Install an observing instrument on the ground under the light source vertically to measure the aberration. If there is an aberration, the aberration angle (the angle between the observer and the vertical line of the suspended heavy object) produced by the position of the light source observed in the observing instrument is the same as that of the star. If there is no aberration, there is no aberration angle for the light source position seen by the observer (the observer is parallel to the vertical line of the weight suspended).

According to special relativity, since the constant velocity of light in vacuum is independent of the motion of the light source, the observation of the light source on top of a building and the observation of the stars should have the same aberration effect because both are caused by the movement of the Earth around the sun and the rotation of the Earth.

According to the theory of this paper, since the light source on the building and the observer are both in the Earth's etheric system, the photons emitted by the light source remain constant speed relative the Earth etheric system, while the observer is stationary relative to the Earth etheric system, so there should be no aberration effect. Because the light from a star must first enter the solar etheric system before it can enter the Earth's etheric system, and the Earth's etheric system has a relative motion with the sun's etheric system (caused by the movement of the Earth around the sun and the rotation of the Earth), there will be an aberration effect of the star for the observers on Earth.

The aberration angle ϕ can be calculated by the Lorentz velocity transformation (4.14) between the solar etheric system and the Earth etheric system:

$$\operatorname{tg}\phi = \frac{u'_y}{u'_x} = \frac{u_y}{\gamma(u_x - v)} = \frac{\sin\theta}{\gamma(\cos\theta - v/c)}$$

In the above formula, u'_y and u'_x are the vertical and horizontal velocity components of the photon in the Earth etheric system respectively, u_y and u_x are the vertical and horizontal velocity components of the photon in the solar etheric system respectively, v is the speed of the Earth's etheric system relative to the sun's etheric system, c is the speed of light in vacuum.

$$\gamma = 1 \Big/ \sqrt{1 - (v/c)^2}$$

In conclusion: for the observers on Earth, according to the theory of this paper, stars have aberration but the light sources on Earth have no aberration; according to the theory of special relativity, there are aberrations for both the stars and the light sources on Earth.

7. Conclusions

1) The cosmic space is filled with ether (energy), which forms the cosmic absolute static frame of reference and is named the cosmic etheric system.

2) Each particle or object carries an etheric layer (sphere of influence) that surrounds and moves with it. The etheric layer forms an absolute frame of reference and is named the particle or object etheric system.

3) Among all the etheric systems, only the cosmic etheric system is an isolated system, and all the conservation laws (such as energy conservation, momentum conservation, and angular momentum conservation, etc.) are strictly valid only in the cosmic etheric system.

4) The propagation speed of light in all etheric systems remains constant C (299,792,458 m/s), which has nothing to do with the motion of the light source and the motion of the etheric system.

5) The form of any law of physics is the same in all kinds of etheric systems.

6) The Lorentz transformation is only suitable for two related etheric systems (such as the Earth etheric system and the solar etheric system).

7) The effect of speed on mass, the effect of speed on time and the effect of speed on length derived from the Lorentz transformations are not the relative observation effects between two different inertial systems, but the absolute real physical effects caused by ether when the object is moving in ether.

8) The higher the etheric density of the space, the greater the mass of the object, the more the object contracts, and the slower the time on the object.

Conflicts of Interest

The author declares no conflicts of interest regarding the publication of this paper.

References

[1] Tan, S.H. (1987) *The Study of Dialectics of Nature*, No. 3, 7-17.

[2] Michelson, A.A., Pease, F.G. and Pearson, F. (1929) *Journal of the Optical Society of America*, **18**, 181-181.

[3] Einstein, A. (1905) *Annalen der Physik*, **17**, 891-921.

[4] Halliday, D., Resnick, R. and Walker, J. (2001) Fundamental of Physics. Chapter 38, Relativity, Sixth Edition, Wiley, New York, 932-933.

[5] Halliday, D., Resnick, R. and Walker, J. (2001) Fundamental of Physics. Sixth Edition, Wiley, New York, 960.

[6] Halliday, D., Resnick, R. and Walker, J. (2001) Fundamental of Physics. Sixth Edition, Wiley, New York, 762.

[7] Cutnell, J.D. and Johnson, K.W. (2001) Physics. Fifth Edition, Wiley, New York, 804.

[8] Halliday, D., Resnick, R. and Walker, J. (2001) Fundamental of Physics. Sixth Edition, Wiley, New York, 524.

[9] Cutnell, J.D. and Johnson, K.W. (2001) Physics. Fifth Edition, Wiley, New York, 134.

[10] Cutnell, J.D. and Johnson, K.W. (2001) Physics. Fifth Edition, Wiley, New York, 917-922.

[11] Jacobs, J. (1995) *Geophysical Journal International*, **121**, 574-575.

Cosmic Applications of Relative Energy between Quarks in Nucleons

F. C. Hoh

Retired, Uppsala, Sweden
Email: hoh@telia.com

Abstract

By taking into account the relative energy between the diquark and the quark in nucleons, the gravitational singularity in a black hole created from a collapsing neutron star can be removed; compatibility with quantum mechanics is restored. This black hole becomes a "black" neutron star. The negative relative energy identified as dark matter in the previous paper can account for the galaxy rotation curve. The positive relative energy identified as dark energy in the previous paper can explain the accelerating expansion of the universe. A possible scenario for cosmic ray generation is given.

Keywords

Gravitational Singularity, Relative Energy between Quarks, Scalar Strong Interaction Hadron Theory, "Weightless" Neutron, Black Neutron Star, Galaxy Rotation Curve, Accelerating Expansion of Universe, Cosmic Ray

1. Introduction

A neutron star with mass greater that the Tolman-Oppenheimer-Volkoff (TOV) limit $M_{TOV} \sim 3$ solar mass M_{SUN} becomes a black hole in which the star core collapses to a gravitational mass singularity in general relativity [[1] p172], [[2] black hole/§2.3]. The quark structure of the neutrons has been neglected. But in these dense stellar objects, gravitational forces are strong and their gradients large so that such a neglect cannot be carried out without appropriate justification. Further, such a singularity contradicts quantum mechanics.

Dark matter needed to account for many observation, e. g., the galaxy rotation curve, and the dark energy required to drive the rapidly expanding universe remain hypothetical as they cannot be observed.

Recently, it was shown [3] that the "hidden", unobservable relative energy between the diquark and quark in nucleons can interact with their ambient gra-

vitational potential and possibly play the roles of dark matter and dark energy in the universe. The underlying theory is the scalar strong interaction hadron theory SSI [4] [5].

In this paper, it is shown that, as a neutron on the surface of a neutron star with mass $\sim M_{TOV}$ falls toward the star center, not only gravitational energy is released, but a negative relative energy also emerges simultaneously. These two energies can cancel each other and prevent the collapse of the star and formation of a mass singularity. The negative relative energy generated in an expanding galaxy can play the role of dark matter and account for the galaxy rotation curve. The positive relative energy generated in outer regions of the universe can play the role of dark energy, leads to accelerating expansion of the universe and may eventually give rise to cosmic rays.

The relevant parts of SSI are outlined in Sections 2-5. Creation of negative relative energy applied to neutron star collapse is considered in Sections 6-7. In Section 8, such negative relative energy reinforces the existing gravitational potential in an expanding galaxy to account for the galaxy rotation curve qualitatively. The accelerating expansion of the universe by means of the positive relative energy created in the outer parts of the universe is qualitatively outlined in Section 9. Some scenarios of the outer regions of the universe including cosmic ray generation are shown in Section 10. The so-obtained scenario of the universe is summarized in Section 11.

2. Outline of Construction of Baryon Wave Equations in SSI [4] [5]

The starting point is the Dirac equations for three quarks A, B and C with masses m_A, m_B and m_C located at x_I, x_{II} and x_{III}, respectively. The quarks interact with each other via scalar strong potentials $V_{AB}(x_I)$, $V_{AC}(x_I)$, $\cdots$ in [[6] (2.1-3) or [4] [5] (9.1.1-3)]. These equations are in van der Waerden's spinor form which is manifestly Lorentz covariant contrary to the conventional bispinor Dirac equation which is not. For quark B, for instance, the equations read

$$\partial_{II}^{d\dot{e}}\chi_{B\dot{e}}(x_{II}) - i\left(V_{BC}(x_{II}) + V_{BA}(x_{II}) + V_{BG}(x_{II})\right)\psi_B^d(x_{II}) = im_B\psi_B^d(x_{II}) \quad (2.1.a)$$

$$\partial_{II\dot{e}f}\psi_B^f(x_{II}) - i\left(V_{BC}(x_{II}) + V_{BA}(x_{II}) + V_{BG}(x_{II})\right)\chi_{B\dot{e}}(x_{II}) = im_B\chi_{B\dot{e}}(x_{II}) \quad (2.1.b)$$

where $\partial_I = \partial/\partial x_I$, $\cdots$. The spinor indices run from 1 to 2 and the quark spinors χ_B and ψ_B are linear combinations of the four components in the conventional Dirac bispinor ψ according to [[4] [5] (C11)]. m_B is quark mass, about 2/3 of the proton mass [[4] [5] Table 5.2]. The scalar strong potentials V_{BA} and V_{BC} generated by quark A and C, respectively, are governed by [[6] (2.4) or [4] [5] (9.1.4)]. There is no gauge fields for electromagnetic interactions between the quarks. Here, the scalar gravitational potential V_{GB} from ambient matter and energy, neglected in the references, has been included.

To construct baryon wave functions, the three pairs of quark equations, one of them being (2.1), together with the cited strong potential equations, are multip-

lied together and the products of the quark spinors and those of the strong potentials are generalized to baryon wave functions and baryon potentials nonseparable in x_I, x_{II} and x_{III} according to [[4] [5] Sec. 9.2]. For ground state baryons, quark C at x_{III} has been merged into quark A at x_I to form a diquark at x_I. The nearly intractable three body problem is thus reduced to a manageable two body problem.

In [[4] [5] Sec. 9.3], each quark mass above has been generalized to a quark mass operator operatng on a flavour function in a fictitious, complex internal or flavour space z^p, where p runs from 1 to 6 representing the six quark flavours. The quark mass is recovered as eigenvalue of such an operator. The three flavour functions, one for each quark, are analogously multiplied together and generalized to a nonseparable baryon flavour function. The product of the three mass operators are similarly generalized to a nonseparable baryon mass operator in the flavour space and leads to a mass M_b [[4] [5] (9.3.19)] representing the quark mass contribution to the baryon mass.

The baryon flavour function can now be removed leaving behind the ground state baryon wave equation [[6] (2.9)], [[4] [5] (9.3.16)]

$$\partial_I^{a\dot{b}}\partial_I^{g\dot{h}}\partial_{II\,\dot{e}f}\chi^{\phantom{\{bh\}}f}_{\{\dot{b}\dot{h}\}}\left(x_I,x_{II}\right)=-i\left(M_b^3+\Phi_b\left(x_I,x_{II}\right)\right)\psi_{\dot{e}}^{\{ag\}}\left(x_I,x_{II}\right) \tag{2.2a}$$

$$\partial_{I\,\dot{b}c}\partial_{I\,\dot{h}k}\partial_{II}^{d\dot{e}}\psi_{\dot{e}}^{\{ck\}}\left(x_I,x_{II}\right)=-i\left(M_b^3+\Phi_b\left(x_I,x_{II}\right)\right)_{\{\dot{b}\dot{h}\}}^{d}\left(x_I,x_{II}\right) \tag{2.2b}$$

$$M_b=\left(m_A+m_B+m_C\right)\big/2 \tag{2.2c}$$

The interbaryon strong potential Φ_b is a triple product of three strong interaction quark potentials of the type of V_{BA} and V_{BC} in (2.1) and is governed by [[4] [5] (9.2.13b)]. The six component χ and ψ can be decomposed into a quartet or spin 3/2 part, which can be separated off, leaving behind a doublet or spin 1/2 part [[4] [5] (10.0.6)]:

$$\partial_I^{a\dot{b}}\partial_{II}^{f\dot{e}}\partial_I^{e\dot{f}}\chi_{0\dot{b}}\left(x_I,x_{II}\right)=-i2\left(M_b^3+\Phi_b\left(x_I,x_{II}\right)\right)\psi_0^a\left(x_I,x_{II}\right) \tag{2.3a}$$

$$\partial_{I\,\dot{b}c}\partial_{II\,\dot{e}h}\partial_{I\,\dot{h}e}\psi_0^c\left(x_I,x_{II}\right)=-i2\left(M_b^3+\Phi_b\left(x_I,x_{II}\right)\right)\chi_{0\dot{b}}\left(x_I,x_{II}\right) \tag{2.3b}$$

where χ_0 and ψ_0 the wave functions of the doublet baryons.

3. Laboratory and Relative Spaces

Since quarks cannot be observed, their coordinate spaces are converted into an observable laboratory space X^μ for the baryon and a relative space x between the diquark and the quark via the linear transformation given above [[7] (6.2)] or by [[6] (5.1)], [[4] [5] (3.1.3a)]

$$x^\mu=x_{II}^\mu-x_I^\mu,\qquad X^\mu=\left(1-a_m\right)x_I^\mu+a_m x_{II}^\mu \tag{3.1}$$

For observable particles, a_m is often determined by that X^μ is the center of mass of these particles. If these particles have equal mass, $a_m=1/2$. Such kind of determination cannot be done here because quarks are not observable individually. a_m has been taken to be an arbitrary real constant and represents a new

degree of freedom. The relative space $x = \left(x^0, \underline{x} \right)$ is "hidden" [[4] [5] (3.1.3)] and cannot be observed. If it were observable, then (3.1), with a given a_m, leads to that both the diquark at x_I and quark at x_{II} become observables, contrary to experience. This can also be seen directly in the first of (3.1) in which the right side members cannot be measured; hence x^μ is also "hidden", independent of a_m. It turns out that the bulk of hadron physics in SSI lies in such "hidden" spaces.

The baryon wave functions in (2.1) have been factorized into the form of [[4] [5] (10.1.1)],

$$\chi_{0\dot{b}} \left(x_I, x_{II} \right) = \chi_{0\dot{b}} \left(\underline{x} \right) \exp\left(-iK_\mu X^\mu + i\omega_K x^0 \right)$$
$$\psi_0^a \left(x_I, x_{II} \right) = \psi_0^a \left(\underline{x} \right) \exp\left(-iK_\mu X^\mu + i\omega_K x^0 \right)$$

(3.2)

$$K_\mu = \left(E_K, -\underline{K} \right) \quad \text{[[4] [5] (3.1.6)]} \quad = \quad (3.3)$$

where E_K is the energy of the baryon and $\underline{K}$ its momentum. x^0 is the relative time and $-\omega_K$ the associated relative energy in the "hidden" relative space and can also not be observed within SSI.

In spherical coordinates, $\underline{x} = \left(r, \theta, \phi \right)$ [[4] [5] (3.1.7b)], the doublet wave functions in (3.2) with total angular momentum $j = 1/2$ and orbital angular momentum $l = 0$ read [[4] [5] (10.2.3)]

$$\psi_0^1 \left(\underline{x} \right) = g_0 \left(r \right) Y_{00} \left(\theta, \phi \right) + if_0 \left(r \right) \sqrt{\frac{1}{3}} Y_{10} \left(\theta, \phi \right), \quad \psi_0^2 \left(\underline{x} \right) = if_0 \left(r \right) \sqrt{\frac{2}{3}} Y_{11} \left(\theta, \phi \right) \quad (3.4)$$

where the Y's are the usual spherical harmonics. $\chi_{0\dot{a}}$ is found by changing the signs of $f_0(r)$ in (3.4).

4. Radial Wave Equations in Relative Space, Solutions and Results

Consider baryons at rest, $\underline{K} = 0$. $a_m = 1/2$ is set as in the meson case [[4] (3.5.7)], [[5] (5.7.2)]. Similarly, the "hidden" relative energy $-\omega_0 = 0$ is also set following the meson case [[4] (3.5.6)], [[5] (5.7.1)]. Insertion of (3.1-4) into (2.3) using [[4] [5] (3.1.4)] leads to the radial wave equations [[6] (6.9)], [[4] [5] (10.2.12)]

$$\left[\frac{E_0^3}{8} + M_b^3 + \Phi_{bd} \left(r \right) + \frac{E_0}{2} \Delta_0 \right] g_0 \left(r \right) + \left(\frac{E_0^2}{4} + \Delta_0 \right) \left(\frac{\partial}{\partial r} + \frac{2}{r} \right) f_0 \left(r \right) = 0 \quad (4.1a)$$

$$\left[\frac{E_0^3}{8} - M_b^3 - \Phi_{bd} \left(r \right) + \frac{E_0}{2} \Delta_1 \right] f_0 \left(r \right) - \left(\frac{E_0^2}{4} + \Delta_1 \right) \frac{\partial}{\partial r} g_0 \left(r \right) = 0 \quad (4.1b)$$

where the subscript d denotes doublet and [[4] [5] (10.2.2a)] gives the diquark-quark strong interaction potential

$$\Phi_{bd} \left(r \right) = \frac{d_b}{r} + d_{b0} + d_{b1} r + d_{b2} r^2 + d_{b4} r^4 \quad (4.2)$$

here, the nonlinear potential $\Phi_{cd}(\underline{x})$ [[4] [5] (10.2.2)] vanishes for large normalization volume $\Omega_{cb} \to \infty$ in [[4] [5] (10.3.14)]. The d_b's are unknown integration constants.

The two coupled third order Equations (4.1) have been converted into six first

order equations [[4] (10.7.5)], [[5] (10.4.5)] which have six linearly independent solutions each associated with its own λ_+ values in [[4] [5] (10.2 8a)] found from the sixth order indicial equation [[5] (10.4.4)]. These eventually led to two free parameters $w_{(1)}$ and $w_{(2)}$ in [[4] [5] (11.1.1)]. It turned out that only $d_{b4} = 0$ led to results in near agreement with data [[5] §11.1.3]. Thus, there are four d_b and two w totalling six constants that can be varied to satisfy the six boundary conditions posed by the six first order system.

Due to the large number of unknown constants, (4.1-2) could not be solved as a conventional eigenvalue problem. A less ambitious approach has been adopted. The known mass of the neutron is used as input for the eigenvalue E_0 and the quark masses obtained from meson spectra given in [[4] [5] Table 5.2] are used as input for M_b according to (2.2c) where $m_A = m_C$ is the d quarks mass and m_B the u quark mass. The six first order equations [[4] (10.7.5)], [[5] (10.4.5)] have been solved on a computer. It turned out that given a d_{b2} value, the remaining five constants can be freely chosen such that $g_0(r)$ and $f_0(r)$ converge at large r. This is allowed since this takes place in the "hidden" relative space.

Here, the word "finite" on the first line of the second paragraph on [[5] p239] turned out to be incorrect in subsequent numerical calculations and should be changed to "infinite"; d_{b2} can be varied continuously to yield converging $g_0(r)$ and $f_0(r)$. One so-obtained neutron wave functions are plotted in [[4] Figure 12.1], [[5] Figure 11.1b] reproduced in **Figure 1**.

These wave functions have led to the nearly correct predictions of the neutron life and the electron asymmetry parameter A or the neutrino asymmetry parameter B [[5] Table 12.1] in its beta decay.

5. Relative Energy and Gravitation

If $a_m = 1/2$ and $-\omega_0 = 0$ used in (4.1) were not assumed, a derivative in (2.3) operated on (3.2) will, in terms of (3.1) [see [4] [5] (3.1.4)], be changed as follows

$$\partial_I^{a\dot{b}} = (1 - a_m)\partial_X^{a\dot{b}} - \partial^{a\dot{b}} = (1 - a_m)\left(-\delta^{a\dot{b}}\partial_{X0} - \underline{\sigma}^{a\dot{b}}\partial_{\underline{X}2}\right) + \delta^{a\dot{b}}\partial_0 + \underline{\sigma}^{a\dot{b}}\underline{\partial}$$
$$= \delta^{a\dot{b}}i\frac{1}{2}E_0 + \underline{\sigma}^{a\dot{b}}\underline{\partial} \rightarrow \delta^{a\dot{b}}i\left((1 - a_m)E_0 + \omega_0\right) + \underline{\sigma}^{a\dot{b}}\underline{\partial} \tag{5.1}$$

The expressions on both sides of the arrow will be equal if [[7] (6.6) or [4] [5] (3.1.10a)]

$$a_m = \frac{1}{2} + \frac{\omega_0}{E_0} \tag{5.2}$$

which keeps (4.1) invariant. The relative energy $-\omega_0$ is "hidden" with respect to strong and electromagnetic but not gravitational interactions [3]. This is indicated by V_{BG} in (2.1), which has been neglected in SSI because it is generally small next to the strong V_{BA}, V_{BC} there. In neutron stars and black holes, however, V_{BG} can be large and may not be neglected. Since a_m, hence also ω_0, can take on any real value, from $-\infty$ to $+\infty$, the relative energy can be important is astrophysics.
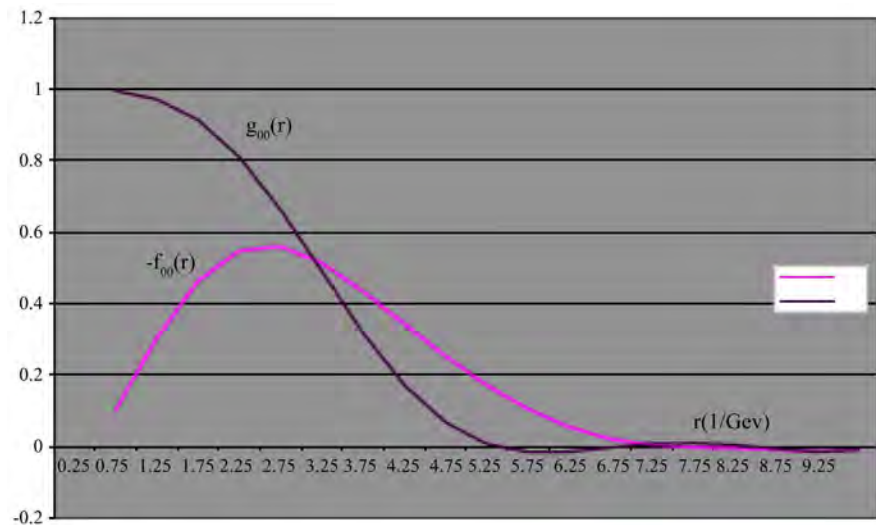
Figure 1. $g_{00}(r)$ and $f_{00}(r)$ are $g_0(r)$ and $f_0(r)$ in (4.1) normalized according to [[4] [5] (10.3.14)] for the $d_{b2} = -0.3202$ case in [[4] [5] Table 11.1] where the four d_b and two w constants are given. r is the diquark-quark distance. This wave function has been used to evaluate neutron decay parameters in [[5] §12.6.3].

In [3], $-\omega_0 > 0$ is identified as dark energy and $-\omega_0 < 0$ plays the role of dark matter. Both E_0 and ω_0 are observables with respect to gravitational forces. Lorentz invariance leads to that the associated baryon momentum $\underline{K}$ in (3.3) and the relative momentum represented by $\underline{\partial}$ in (5.1) are also observables. Thus, the conjugate variables $\underline{X}$, the coordinate of the baryon, and $\underline{x}$, the relative coordinate in (3.1), are also observables, remembering that $\underline{x}$ is still a "hidden" variable with respect to strong forces. By (3.1), both the diquark coordinate $\underline{x}_I$ and quark coordinate $\underline{x}_{II}$ are now observables with respect to gravitation indicated by V_{BG} in (2.1).

6. Neutron Star Collapse Scenario

Consider the following idealized scenario. A neutron star with a mass $M_{NS} = M_{NSa}$, a critical mass, such that the quantum degeneracy pressure of the neutrons and the strong neutron-neutron repulsion precisely balance off the gravitational pressure. Let an external neutron arrive at the surface of this star. The star now becomes too heavy and a gravitational collapse is anticipated to start. Conventionally, this collapse gives rise to a black hole and continues until the star ends up in a mass singularity at its center; the quark structure of the neutron is ignored. Actually, in neutron stars and black holes, the gravitational forces are strong and their gradients large that the diquark-quark structure of the neutron may need be taken into account. This scenario is illustrated in **Figure 2**.

In **Figure 2**, an external neutron arrives on the surface of the neutron star at position a on the right part of the figure. The interquark distance is $x_{II,a} - x_{I,a} = r_a \sim 4$ fm according to **Figure 1**. X_a lies in the middle corresponding to $a_m = 1/2$ in (3.1) and (4.1) and hence $\omega_0 = 0$ by (5.2). This neutron falls from X_a to X_b. To begin with, the three positions $x_{I,a}$, X_a and $x_{II,a}$ are simply
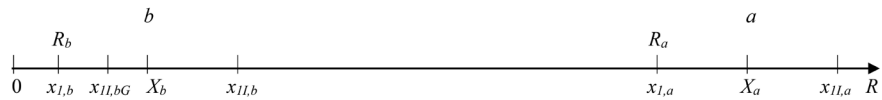
Figure 2. Illustration of the above idealized scenario. The horizontal line represents the radius R inside the neutron star. The center of the star is at $R = 0$. An external neutron arrives at X_a on the surface of this star at $R = R_a = x_{I,a}$ in position a and falls to X_b closer to the star center in position b. $x_{I,a}$ and $x_{II,a}$ are the positions of the diquark and quark of the arriving neutron, respectively. When this neutron has moved to X_b, the diquark and quark positions become at first $x_{I,b}$ and $x_{II,b}$, respectively; the diquark-quark distance is the same in both positions. Due to gravitational collapse, however, the neutron star becomes smaller at position X_b so that the diquark-quark distance in the arriving neutron is also reduced via the replacement of $x_{II,b}$ by $x_{II,bG}$. $R_b = x_{I,b}$ is radius of the collapsed star when the neutron has moved to X_b.

shifted to the left to become $x_{I,b}$, X_b and $x_{II,b}$, respectively. The diquark-quark distance $r_b = x_{II,b} - x_{I,b} = r_a$ remains unchanged. In the same fall, however, the neutron star radius at position b is reduced to $R_b < R_q$ due to gravitational collapse. The incoming neutron is thus similarly compressed to become smaller by a factor of R_b/R_a so that r_b is also reduced to a smaller value r_{bG} by the same factor;

$$r_b = x_{II,b} - x_{I,b} \rightarrow r_{bG} = x_{II,bG} - x_{I,b} = r_a \alpha, \qquad \alpha = R_b/R_a < 1 \qquad (6.1)$$

As was mentioned at the end of Section 5, gravity interacts directly with the quark at x_{II} in (2.1), hence also with that in Figure 2. Phenomenologically, it also interacts with the diquark at x_I in Figure 2. An equation of motion for the diquark on par with (2.1) for the quark has not been constructed. In an eventual such equation, the diquark mass is expected to be about twice the mass of the quark in (2.1) or at least greater than it. Assuming this, gravity will pull the diquark closer to the star center relative to the quark, as is indicated in Figure 2. Note that the quark and the diquark are point particles in quantum theory and hence cannot be "spaghettified" here. The radius R_b of the star at position b is taken to be $x_{I,b}$

If X_b were taken to be the star radius R_b at position b, then the diquark coordinate $x_{I,b}$ in Figure 2 would be negative at the star center $X_b = 0$, contrary to the requirement that a radius ≥ 0. Practically, X_b and R_b are of the magnitude km while their difference is of magnitude fm; both are nearly the same.

The radial wave Equations (4.1-2) hold for the arriving neutron in position a. At position b, (6.1) shows that the diquark-quark distance or radius r in (4.1) is reduced by a factor of α. Equations (4.1-2) remain invariant under the transformations $r \rightarrow r\alpha$, $E_0 \rightarrow E_0/\alpha$, $M_b \rightarrow M_b/\alpha$, $d_{b2} \rightarrow d_{b2}/\alpha^5$, $\cdots$. The neutron mass E_0 and the quark masses in M_b at position b are unchanged. So does also the confining constant $d_{b2} = -0.3202$ in Figure 1; this value is tied up by neutron decay [[5] §12.6.3]. The remaining three d_b and two w constants mentioned above Figure 1 can be varied to produce converging $g_0(ar)$ and $f_0(ar)$ analogous to the computations that led to Figure 1. These wave functions will obviously be much narrower than those in Figure 1 having an average width of

$ar_a \sim 4a$ fm.

7. Removal of Mass Singularity and "Black" Neutron Star

Application of (3.1), (5.2) and (6.1) to position b in **Figure 1** yields

$$a_m = \frac{1}{2} + \frac{\omega_0}{E_0} = 1 + \frac{X_b - x_{II,bG}}{x_{II,bG} - x_{I,b}} = \frac{1}{2}\frac{r_a}{r_{bG}} = \frac{R_a}{2R_b}, \quad -\frac{\omega_0}{E_0} = -\frac{R_a}{2}\left(\frac{1}{R_b} - \frac{1}{R_a}\right) \quad (7.1)$$

where $-\omega_0$ is the relative energy gained when the external neutron arriving at position a falls to position b. In this fall, the gravitational energy E_G released is given by

$$\frac{E_G}{E_0} = \frac{R_{Sa}}{2}\left(\frac{1}{R_b} - \frac{1}{R_a}\right), \qquad R_{Sa} = 2GM_{NSa} \quad (7.2)$$

where G is the gravitational constant and R_{Sa} is the Schwarzschild radius of this collapsing star with radius R_a in **Figure 1** These two energies cancel each other when the star's radius

$$R_a = R_{Sa} \quad (7.3)$$

i.e., when the neutron star in **Figure 1** with the critical mass M_{NSa} has a radius R_a equal to its Schwarzschild radius R_{Sa}. At the star center $R_b = 0$, both energies become infinite but these both singularities cancel; no net mass singularity is created when (7.3) holds. This is consistent with that SSI is a quantum theory not allowing such a singularity. Note that when approaching the star center and R_b becomes of the size of the neutron of a few fm. For $R_a \sim 10$ km; $a_m = R_a/2R_b$ is a huge number $\sim 10^{18}$.

In this case, the fall of this external neutron actually gains no energy because $E_G - \omega_0 = 0$ for all R_b. This neutron therefore remains at position a and becomes "weightless". The anticipated collapse of the neutron star does not start and no mass singularity is created.

The radius R_a of the initial neutron star has been estimated by equating gravitational pressure to the pressure of the degenerate neutrons [[1] p161]

$$R_a = 0.0026R_{Earth}\left(\frac{M_{SUN}}{M_{NSa}}\right)^{1/3} \quad (7.4)$$

which together with (7.2-3) yields $R_a = R_{Sa} = 10.8$ km and $M_{NSa} = 3.6M_{SUN}$. This mass is consistent with the similarly estimated maximum mass $4.3M_{SUN}$ [[1] p162] of a neutron star. It is of somewhat higher than $M_{TOV} \sim 3M_{SUN}$. cited in Section 1. However, estimates of M_{TOV} are uncertain and vary widely due to that the equations of state for extremely dense matter are not well known and to uncertain effects of neutron-neutron repulsion and of pressure in general relativity [[1] p162]. Thus, the so-estimated star mass may be used on equal footing with those in the literature.

A possible scenario is as follows. As additional neutrons arrive at the star surface, a thin shell of weightless neutrons is added to the star at first. Let the mass

of this shell be ΔM_{NSa}, the new Schwarzschild radius will be $R_{Sa\Delta} = (1+\Delta) R_{Sa}$ and the new star radius will be $R_{a\Delta} = (1+\Delta)^{1/3} R_a$, assuming that the neutron density in the shell is the same as that in the star.

Since $R_{Sa\Delta} > R_{a\Delta}$, a black hole is created. As a new neutron arrive at the new star surface with radius $R_{a\Delta}$, it will tend to fall inwards. This time, the gravitational energy (7.2) will slightly exceed the relative energy loss (7.1) and this new neutron tends to fall slowly. However, the pressure of the degenerate neutron gas in the shell is now unopposed by the weightless neutrons and this gas will therefore expand accompanied by a reduced density. If the expansion reaches a radius $> R_{Sa\Delta}$, the back hole is lost and this enlarged star will be a visible neutron star similar to the initial star in **Figure 2**. If the expansion stops just inside $R_{Sa\Delta}$, the created black hole persists and one arrives at a situation nearly the same as that on the right part of **Figure 2** with R_a replaced by $R_{a\Delta}$ and (7.3) holds. This process may be repeated and more shells are added. It can in principle lead to a super-massive black hole. How the neutrons, part of them "weightless", are distributed inside such a black hole is unknown and needs not be known, inasmuch as they are inside its Schwarzschild radius and cannot be observed any way; there is no conflict with observation.

In this scenario, the neutrons in such a black hole fill it up to its Schwarzschild radius. Such a black hole may more suitably be called a "black" neutron star. The absence of mass singularity here is consistent with the conjecture that an eventual future quantum gravity theory will not contain any singularity.

8. Galaxy Rotation Curve without Dark Matter

There is a large body of data that require the presence of dark matter. The first one is the galaxy rotation curve [[2] Dark Matter §3.1]. However, nothing is known about this hypothetical dark matter. In [3], this matter has been identified as the negative relative energy $-\omega_0 < 0$ between the diquark and quark in nucleon. Here, the role of the dark matter in accounting for this rotation curve will be played by this $-\omega_0$.

Consider again an idealized scenario as follows. A spiral galaxy with an appreciable part of its mass consisting of hydrogen gas was in its earlier stage of development. In that stage, this galaxy was smaller, denser and hotter according to the big bang model and the gravitational potential resisting such an expansion was insufficient. It therefore expanded. The situation is analogous to a violation of Jeans criterion for a gas cloud.

To illustrate the mechanism, let us turn off the gravity for a moment. Follow now the movement of a proton, denoted by c, in a hydrogen molecule. In this thermal expansion, this molecule will collide with other molecules, exchange energy and momentum with them and end up in a new position, labeled d, farther out from the galaxy center. In this journey, the forces involved are all Coulomb forces, between the proton and the orbiting electron and between the orbiting electrons in other molecules. The protons get dragged along; their quark

structure is not involved in the expansion.

The situation is illustrated in **Figure 3**.

In **Figure 3**, the coordinate of proton c is X_c which lies in the middle between the diquark at $x_{I,c}$ and quark at $x_{II,c}$. This corresponds to $a_m = 1/2$ and $\omega_0 = 0$ in (7.1) for a free baryon at rest, similar to those for the neutron in position a in **Figure 2**. In this thermal expansion, these three coordinates are simply shifted to the right with $X_c \rightarrow X_d$. The new $x_{I,c}$ and $x_{II,c}$ are on both sides of X_d with the same separation distance.

Turn now on gravity, the situation is reversed. Gravitational effects on electrons are negligible due to their small mass. Gravitational forces now act on this proton at X_d and try to pull it back together with other protons acted upon. However, they turn out to be too small to account for the galaxy rotation curve and prevent the escape of the outer stars. Here, such escapes are prevented by including the negative energies generated by differentiated gravitational pull on quarks and proton.

Just like the neutron star case mentioned below (6.1), gravity also acts directly on the quarks and tends to pull them towards the galaxy center, with the heavier diquark at $x_{I,d}$ closer to this center than does the lighter quark at $x_{II,d}$, as is shown in **Figure 3**. Here, the diquark-quark distance $x_{II,c} - x_{I,c} = x_{II,d} - x_{I,d} = r_a \approx 4$ fm as was mentioned below **Figure 2**. This distance is fixed by the strong inter-quark potential (4.2) and is unaffected by gravity here; the core collapse situation in position b of **Figure 2** is absent here.

Applying (3.1) the gravity pulled position d in **Figure 3** yields the relative energy $-\omega_0$ given by

Figure 3. Illustration of the expanding galaxy scenario. The horizontal line represents the radius R_g inside the galaxy. The center of the galaxy is at $R_g = 0$. A proton in position c is moved to position d in the expansion. X_c denotes the position of the proton at position c, $x_{I,c}$ that of the diquark in this proton, and $x_{II,c}$ that of the quark. In the expansion, this proton c moves from X_c to X_d in position d. When gravity is turned on, the quark coordinates become $x_{I,d}$ and $x_{II,d}$, respectively.
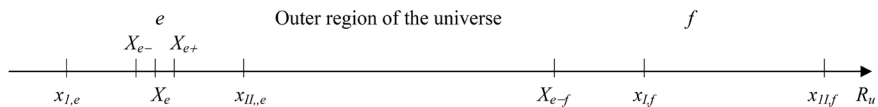

Figure 4. Illustration of the expanding universe scenario. The horizontal line represents the distance R_u from some unspecified inner region of the universe. X_e denotes the coordinate of a proton in a hydrogen molecule at position e, $x_{I,e}$ that of the diquark in this proton and $x_{II,e}$ that of the quark. X_e lies in the middle between them. A second hydrogen molecule containing a second proton with its diquark and quark at the same $x_{I,e}$ and $x_{II,e}$ is also present. The coordinate of this second proton may be X_{e-} or X_{e+} close to X_e. The second proton at X_{e-} will generate a positive relative energy that pushes its both quarks outwards. The coordinate of this proton lags behind. This process continues and this second proton arrives at position f with the coordinates $x_{I,f}$ and $x_{II,f}$ for the quarks and X_{e-f} for this second proton.

$$a_m = \frac{1}{2} + \frac{\omega_0}{E_0} = \frac{X_d - x_{I,d}}{x_{II,d} - x_{I,d}}, \quad -\frac{\omega_0}{E_0} = \frac{1}{2} - \frac{X_d - x_{I,d}}{r_a}, \quad r_a = x_{II,d} - x_{I,d} \approx 4\,\text{fm} \quad (8.1)$$

This energy has the same negative sign as the gravitational potential energy produced by matter inside X_d and hence reinforces it to become large enough to keep the outer stars of the galaxy from escaping. It is due to the lag of the "hidden" quark coordinates $x_{I,d}$, $x_{II,d}$ behind the observable proton coordinate X_d in **Figure 3**, caused by gravitational pull, in the expansion. This lag is caused by that the mass of the diquark and the quark is greater than the proton mass E_0 itself, as can be seen below (2.1) and (6.1); the unobservable quarks experience greater gravitational pull than does the proton containing them. The difference between these two masses is taken up by the strong, confining potential $\Phi_{bd}(r)$ of (4.2) in the "hidden", relative space.

The required energy is $-\omega_0 \approx -5.5 E_0$ per proton, when averaged over the whole universe, and is generated for "free" at "no cost". This $-\omega_0$ value leads to $a_m \approx 6$ ([3] §6.1) so that the "whole" size of this gravitationally polarized proton in **Figure 3** becomes $X_d - x_{I,d} \approx 24$ fm by (8.1). Further, the proton in a hydrogen atom moves in an orbit around the center of gravity of the electron-proton system. This orbit has a diameter ≈ 60 fm so that X_d is uncertain by this amount which is greater than the above 24 fm in **Figure 3**; there will be no observational difference.

This scenario, characterized by **Figure 3**, is also expected to have dominated in the earlier stages of the universe when it was smaller, hotter, denser, and fast expanding.

9. Accelerating Expansion of the Universe without Dark Energy

The observed accelerating expansion of the universe is currently considered to be due to assumed dark energy in the outer regions of the universe. This hypothetical energy may here be replaced by the positive relative energy $-\omega_0 > 0$ corresponding to $a_m < 1/2$ in (8.1).

As in Sections 6 and 8, consider the following idealized scenario. The expansion mechanism in Section 8 applied to a galaxy can analogously be used in some later stage of the development of the universe. In the outer part of the universe, its expansion leads to that the hydrogen gas density decreases and the gas temperature drops there. The expansion nearly comes to a halt. In this region, the gas is tenuous, cold and experiences very weak gravitational force.

Consider a proton in a hydrogen molecule of this gas. The configuration of this proton in position d of **Figure 3**, with the galaxy replaced by the universe, has now largely returned to its original form in position c of **Figure 3**. This proton is also similar to the neutron in position a of **Figure 2** with $a_m \approx 1/2$ and the pulling energy $-\omega_0 < 0$ approaching $-\omega_0 \approx 0$. The situation is illustrated in position e of **Figure 4**.

Let a second hydrogen molecule arrive at position e simultaneously. It con-

tains a second proton with its diquark and quark at the same $x_{I,e}$ and $x_{II,e}$. Due to differences in the paths of these both molecules before they reach position e, this second proton may end up at nearby $X_{e-} = X_e - \Delta\left(x_{II,e} - x_{I,e}\right)$ or $X_{e+} = X_e + \Delta\left(x_{II,e} - x_{1,e}\right)$ where $\Delta \ll 1$.

If its position is X_{e+}, then (8.1) yields a negative relative energy $-\omega_0 = -\Delta E_0 < 0$. Analogous to the situation below (8.1), this small energy tends to pull the quarks toward the left in **Figure 4** into the inner region of the universe. This tendency is countered by the slightly higher gas pressure inside X_e. No appreciable net movement of the quarks is expected; the situation is stable.

If its position is X_{e-}, then (8.1) yields a positive relative energy $-\omega_0 = -\Delta E_0 > 0$. Contrary to the above X_{e+} case, this small energy tends to push the quarks outward, towards the right part of **Figure 4**. This tendency is reinforced by the slightly higher gas pressure inside X_e; Δ increases and a_m decreases. The quarks move toward the outer region of the universe but the observable proton coordinate X_{e-} lags behind; this situation is opposite to that for X_{e+} above or to that in position d in **Figure 3** mentioned below (8.1). After some time, the unobservable quarks arrive at $x_{I,f}$ and $x_{II,f}$ in **Figure 4**. Application of (8.1) to the coordinates in position f indicates that a_m has decreased from $1/2 - \Delta$ at position e to <0 at position f so that the positive relative energy $-\omega_0$ by (8.1) has grown appreciably to $>E_0/2$. This new, larger positive relative energy further pushes the quarks outwards at a greater pace and tends to increase the lag of the proton coordinate X_{e-f} behind the quark coordinates $x_{I,f}$, $x_{II,f}$ in **Figure 4**. This by (8.1) generates still greater $-\omega_0 > 0$ which gives still greater pushing force on the quarks. This is an unstable, "run away" situation which can in principle continue forever. The driving relative energy is "free", "costs nothing" and is not conserved. If this mechanism is applied to all protons in the outer regions of the universe, an acceleratingly expanding universe emerges.

Current data show that dark energy exceeds the energy of ordinary matter by a factor of ≈ 14 when averaged over the universe. Identifying this energy with $-\omega_0$, (8.1) leads to $a_m = -13.5$ ([3] §6.1). This value and (8.1) give the "whole" size of this second proton at position f in **Figure 4** $x_{II,f} - X_{e-f} = 58$ fm which is close to but still within the error margin ≈ 60 fm for X_{e-f} mentioned at the end of Section 8. This margin is small relative to the size of hydrogen atom and does not alter its behavior as a hydrogen atom.

This scenario, characterized by **Figure 4**, also dominates in the later stages of the universe when it has become large.

10. Scenarios in the Outer Regions of the Uiniverse

10.1. Possible Plasma Creation

As the above "run way" situation continues, the "whole" size of this proton, $x_{II,f} - X_{e-f}$ in **Figure 4** or the proton-quark separation gets larger and eventually reaches 0.55Å, the radius of hydrogen atom. Since the observable proton coordinate X_{e-f} is located at the center of the atom, the quarks will in the same orbit

as the electron. These two objects may come to be close to each other and interact via some so far unspecified mechanism. Since the electron is much lighter than a quark, which has a mass of about 2/3 of the proton mass mentioned below (2.1), it will be assumed that the electron gets ejected, noting that the ionization energy of hydrogen atom is negligible relative to the energy scale involved here. This hydrogen atom becomes ionized.

The relative energy corresponding to this case is by (8.1) $-\omega_0 \approx 1.29 \times 10^{13}$ eV. In this scenario, hydrogen atoms in the expanding outer regions of the universe having this energy or greater turn into plasma.

10.2. Generation of Cosmic Rays

According to 10.1., the hydrogen gas in outer regions of the universe can expand until an average atom acquires an energy $\sim 1.29 \times 10^{13}$ eV, beyond which the atom becomes ionized. For atoms carrying higher energies, the gas becomes a tenuous plasma in intergalactic space. In this plasma, the protons continue to gain energy by the increasing $-\omega_0$ but the ejected electrons lag behind, inasmuch as gravity is absent in Dirac's equation for an electron in a Coulomb field. This leads to a proton current flowing radially outwards which in its turn generates transverse magnetic field. As there are inhomogeneities in gas distribution in this region, the magnetic field will also vary in space.

As the "run away" expansion in Section 9 continues, some protons become very energetic. The magnetic field will cause them to move perpendicular to their path and to the direction of the magnetic field. Some of these high energy protons may be moved by magnetic fields such that they return to the inner part of the universe. Such protons can be a source of cosmic rays with energy $> 10^{13}$ eV,

For a cosmic ray proton having a high energy of, say, 10^{20} eV, The "whole" size of this proton $x_{II,f} - X_{e-f}$ in Figure 4 given by (8.1) is still rather small, ~ 0.4 mm (unobservable), which is hardly detectable even if it were observable.

10.3. Diquark-Quark "Flip" and Magnetic Curtailment

In Figures 2-4, the diquark is closer to the center of the star, galaxy or universe; $x_I < x_{II}$. This is due to that the heavier diquark experiences a stronger pull towards the centers than does the lighter quark. This pulling force becomes very weak far out in the universe where the positive relative energy increases by the above run away instability pushing the quarks outwards with ever increasing proton energy and greater proton-quark separation or the "whole" size of the proton, $x_{II,f} - X_{e-f}$ in Figure 4.

This may in principle go on forever. This pushing force is stronger on the heavier diquark than that on the quark and may eventually push the diquark past the quark farther out and "flip" their positions from $x_{I,f} < x_{II,f}$ in Figure 4 to $x_I > x_{II}$ farther away. In this scenario, (8.1) shows that a_m, hence also $-\omega_0$, changes sign; the expansion force switches to contracting force. The expansion

will slow down and change to contraction. If such processes continue, an "oscillating" scenario of the outer regions of the universe may emerge.

But even before this scenario, another one may take place. The protons with energy > 10^{13} eV are part of a plasma with transverse magnetic field in §10.2. Some of them will eventually move in a direction perpendicular to the direction of R_u in Figure 4. In that motion, the acceleration mechanism in Section 9 is no longer active. In this scenario, infinite proton energy and infinite expansion of the universe's outer regions may be curtailed by the magnetic fields.

11. Summary-Scenario of the Universe

The present results lead to the following scenario for the universe.

1) The universe contains neither dark matter nor dark energy.

2) A heavy neutron star with mass = M_{TOV} and radius = its Schwarzschild radius does not collapse into a mass singularity and may be called a "black" neutron star. If every neutron star gets heavier, becomes a black hole and passes through this stage in its development, there will be no mass singularity in the universe, in agreement with that quantum mechanics does not allow such a singularity.

3) The run away instability in Section 9 provides a mechanism for an accelerating expansion of the universe. The driving positive relative energy is "free" and "costs nothing". The density and temperature of the universe will decrease with time. This scenario may in principle go on forever.

4) In outer parts of the universe, fast expanding hydrogen gas may turn into plasma and part of it may become cosmic rays. There may also exist a scenario in which the above free expansion can halt and eventually reverts to contraction.

The above results are derived phenomenologically by joining SSI to aspects of general relativity. A formal integration of these both theories is beyond reach; no quantum gravity theory exists presently.

Conflicts of Interest

The author declares no conflicts of interest regarding the publication of this paper.

References

[1] Ryan, S.G. and Norton, A.J. (2010) Stellar Evolution and Nucleosynthesis. Cambridge University Press, Cambridge.

[2] Wikipedia (2019). https://en.wikipedia.org/wiki/Main_Page

[3] Hoh, F.C. (2019) *Journal of Modern Physics*, **10**, 635.

[4] Hoh, F.C. (2011) Scalar Strong Interaction Hadron Theory. Nova Science Publishers, New York.

[5] Hoh, F.C. (2019) Scalar Strong Interaction Hadron Theory. II Nova Science Publishers, New York.

[6] Hoh, F.C. (1994) *International Journal of Theoretical Physics*, **33**, 2125.

[7] Hoh, F.C. (1993) *International Journal of Theoretical Physics*, **32**, 1111.

Scientific Research Publishing

The Performance of a Novel Latching-Type Electromagnetic Actuator for Single-Port Laparoscopic Surgery

Haochen Wang, Ali El Wahed*

Mechanical Engineering, University of Dundee, Dundee, UK
Email: *a.elwahed@dundee.ac.uk

Abstract

This paper reports on the performance evaluation of a novel latching-type electromagnetic actuator which is designed to be embedded at selected joints along single-port laparoscopic surgical instruments (SLS). The aim of this actuator is to allow these instruments to become articulated with a push of a button in order to provide the optimum angulation required during SLS operations. This new actuator is comprised of electromagnetic coil elements, soft magnetic frames and a permanent magnet. Unlike conventional electromagnetic actuators, latching-type electromagnetic actuators could maintain their positions at either end of the actuation stroke without any power application requirement. In the current design, magnetic attraction forces initiated between the permanent magnet and the magnetic frame are utilised to lock the position of the actuator whilst a certain angulation position of the actuator is achieved as a result of the magnetic repulsion forces established between the permanent magnet and the coil elements. The performance of the new actuator in terms of the output force, maximum angulation and patient's safety, was evaluated experimentally and the results were found to compare well with those acquired numerically using finite element methods. This actuator was seen to exhibit sufficient actuation forces and hence, it was capable of providing adaptable angulation characteristics for SLS tools. Finally, thermal evaluation of the actuator's operation was conducted, which was found to be within safety limits specified by clinicians.

1. Introduction

Single-port laparoscopic surgery (SLS), which utilises one major incision instead

of multiple incisions, has become increasingly popular in the health service in recent years. Compared with the conventional multi-port laparoscopic surgery, SLS has many advantages such as less postoperative pain, early return of gastrointestinal function, shorter length of hospital stay and fewer blood losses [1]. However, SLS suffers from several problems such as inadequate exposure of the surgical field, surgical instrument crowding and lack of internal maneuverability for surgical tools, which have impeded the advancement of the SLS technique [1] [2] [3]. In addition, concerns have been raised that these problems have increased the length of operative times, which may potentially increase the risk of SLS operations for patients [4]. In order to solve some of the above SLS problems, several attempts have been carried out, for example, to improve the flexibility of SLS surgical instruments using a robotic platform [5], to direct the SLS camera using external magnetic fields [6] and to use pre-bent surgical instruments [7]. However, the sophisticated robotic instruments add to the cost and complexity of the surgery, and the time of training [8] [9] [10]. In addition, most of the developed tools could not be used as universal tools since they have their own limitations, including insufficient angulation and deficient force or torque output [11]. Consequently, a more practical approach is now necessary to advance SLS procedures. In this activity, the authors have been engaged in the development of novel latching-type electromagnetic actuators that could be embedded along SLS tools with the aim to enhance their levels of stiffness and degrees-of-freedom.

The applications of electromagnetic actuators in medical devices have seen a surge in recent years [12] [13] [14] [15]. This is attributed mainly to their relatively low magnetic energy that is deemed safe for patients as well as their uncomplicated fabrication and after use sterilisation processes. However, in order to introduce the electromagnetic actuator technology into the optimisation of SLS instruments, some difficulties need to be addressed including the remarkable reduction of the force output with the miniaturisation of these actuators [15] [16]. In addition, the inevitable heat buildup caused by the continuous current feed to energise the magnetic circuit of these actuators has been found in certain medical applications as a problem since it breaches the patient's safety [17]. This problem was overcome in some applications using latching-type electromagnetic actuators, which utilise a permanent magnet to lock the position of the actuator instead of the magnetic energy generated by the continuous activation of the actuator's electromagnetic circuit [18]. However, these new generations of electromagnetic actuators, which incorporate springs to aid their actuation, were aimed for relatively large applications, such as the actuation of valves of internal combustion engines [18]. Therefore, in order to miniaturise the existing latching-type electromagnetic actuators and make them suitable for SLS applications, a comprehensive work is required to optimise their structure, material and excitation level.

This paper reports on the performance evaluation of a new miniaturised latching-type electromagnetic actuator which utilises a permanent magnet and

dual-coil design for position locking and actuation, respectively. This new actuator is proposed to be embedded along SLS surgical instruments, which can be squeezed through a standard tocar-port, to enable the tool's angulation that is required during SLS operations. Special SLS requirements such as the trocar-port size, central channel for passing a cable to control the end effector, force output level and angulation degree rather than just a linear stroke have all been considered in the design of the new actuator. In this study, the performance of the new actuator under various input conditions was assessed using numerical and experimental approaches. A thermal camera was also employed to evaluate the optimum duty cycle of the actuator operation, which ensures patients safety. Finally, the overall performance of the new actuator is discussed and compared with other competitive actuators.

2. Actuator Design and Optimisation

The new latching-type electromagnetic actuator, Figure 1, comprises of two electromagnetic coil elements, one at either end of its central chamber, a permanent magnet armature which could slide along the central chamber and a solid shell made from a soft magnetic material. This actuator was designed to be cylindrical in shape in order to match the shape of SLS trocar port. Also, a central channel was allowed in the design of the new actuator which spans its whole length to accommodate a guide wire that is used to control the end effector of the surgical instrument. In addition, an air gap feature was allowed in the magnetic circuit of the actuator with the aim to enhance the magnetic interaction between the coil elements and the permanent magnet. Furthermore, a solid titanium sliding element was added on the side of the actuator shell, which is linked to the side of the permanent magnet armature to transmit its linear actuation into a bending action using a swivelling element at the top of the actuator. Since the new actuator is proposed to be embedded along SLS tools, the above arrangement should enable the controlled angulation of these tools as necessary during SLS operations.
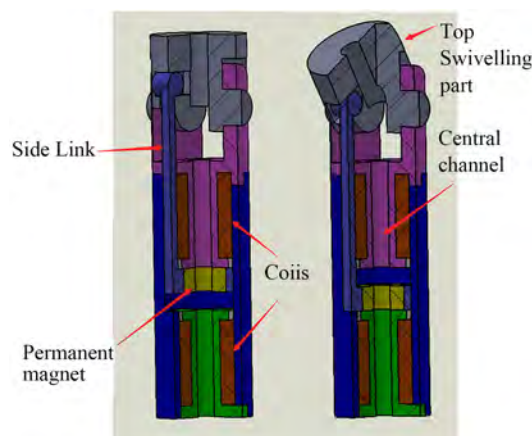

Figure 1. Cross-section views of the new actuator in its straight (left) and bending (right) positions.

The new actuator utilises the magnetic force established between the permanent magnet and the soft magnetic ends of the central chamber to maintain the position of the armature during the deactivated status of the actuator. When an actuation is required, the coil that is close to the permanent magnet is supplied with a short current pulse to generate an opposite magnetic field which is designed to neutralise and overcome the magnetic field of the permanent magnet. As a result, the permanent magnet is subjected to a repelling magnetic force which drives it towards the other end of the central chamber. Once the armature completes its full stroke and is in contact with the other chamber end, it again becomes firmly locked in its new position under the effect of the magnetic attraction forces with the chamber end while the coil is deactivated. Consequently, the transformation of the armature between the two locking positions should generate the required angulation of the actuator end, which is used in the current application to provide SLS tools with the necessary bending output.

In order to optimise the design of the new actuator, 3-D electromagnetic finite element analyses were carried out using Ansys Workbench software (Version 17.0) with its associated magnetostatic module. The actuator 3-D model was created using Solidworks CAD software (Version 2016) and subsequently exported into the Ansys Workbench environment. The components of the 3-D model were set up with their specific properties and then meshed with a maximum element length of 0.0002 m as shown in Figure 2. The permanent magnet armature was assumed to travel statically along its imaginary stroke between the two ends of the central chamber, whilst the total magnetic force acting on the permanent magnet and the corresponding coil-energising current were recorded as a function of the stroke path length.

The most important design factors that are expected to critically affect the overall performance of the developed actuator were identified, which included the size of the electromagnetic coils and their excitation level in addition to the size of actuator's outer shell, height of the actuation channel and the size and grade of the permanent magnet.

A step-by-step optimisation process of the above parameters was carried out, which is summarised in Figure 3. It was found that the size of the electromagnetic components and the excitation level of the coil elements are proportional to the output of the actuator before the magnetic saturation limit of the actuator material was reached. The systematic actuator optimisation process eventually made it possible for a balance between the size and the output of the actuator to be achieved. The main parameters of the optimised actuator are summarised in Table 1.

Using a conventional CNC machining facility, the new actuator was then manufactured. The machined magnetic parts were subsequently annealed in order to regain the original magnetic properties of the material and also to remove any carbon residue from the surface of the parts. Figure 4 shows the manufactured actuator.

A conservative model was developed to estimate the effects of the short current pulse on the temperature rise of the actuator, and the operating duty cycle. The heat generated by the coil, W subjected to a direct current pulse feed, which is equivalent to the power consumption of the coil element during one complete period of the duty cycle, was estimated using:
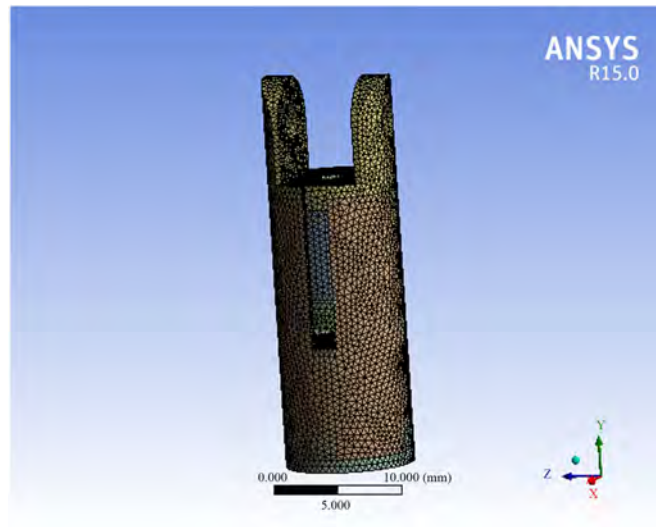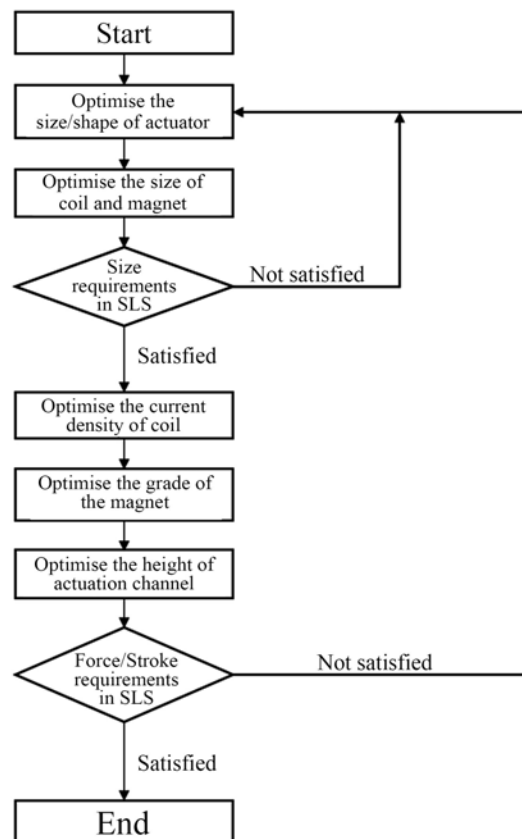

Figure 2. Mesh of the actuator model.

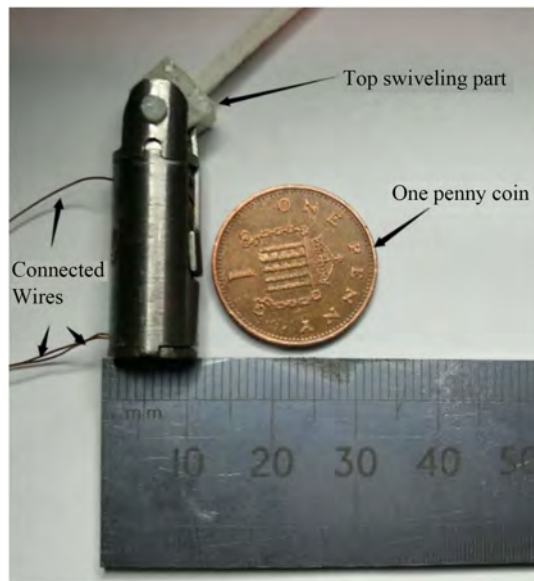**Figure 3.** Flowchart of the new actuator design optimisation procedure.

Figure 4. Prototype of new latching-type electromagnetic actuator shown next to a penny coin.

Table 1. Parameters of the optimised actuator.

COIL	
Coil Wire Diameter	0.29 mm
Number of Wire Turns per Coil	192
Applied Current	6.7 A
Coil Current Density	80,000 kA/m^2
Conducting Area	17.5 mm^2
PERMANENT MAGNET	
Inner Diameter	2 mm
Outer Diameter	8 mm
Thickness	2 mm
Grade	Neodymium N52
ACTUATOR	
Outer Diameter	10 mm
Height	31.6 mm
Central Channel Diameter	2 mm
Maximum Linear Stroke of Magnet	1.5 mm
Shell Material	MaxiMag Low-Carbon Magnetic Iron

$$W = I_{max}^2 R_1 t_1 \tag{1}$$

where t_1 is the current pulse width that is also the duration during which the circuit is open, I_{max} is the peak value of the direct short current pulse and R_1 is the maximum resistance of the electromagnetic coil at the peak temperature.

The temperature rise, ΔT of the coil element is given by [19]:

$$\Delta T = \frac{W}{\lambda S t_2} = \frac{I_{max}^2 R_1 t_1}{\lambda S t_2}$$

where λ is the heat dissipation coefficient, S is the surface area of the coil and t_2 is the heat dissipation (temperature decay) time which is the sum time of one duty cycle. The duty cycle, D is then approximated by the ratio t_1/t_2 [19], which is also given by:

$$D = \frac{t_1}{t_2} = \frac{\Delta T \lambda S}{I_{max}^2 R_1} \tag{2}$$

The relationship between the heat dissipation coefficient, λ and the temperature rise, ΔT could then be expressed by [19]:

$$\lambda = 0.039 \Delta T + 8.83 \tag{3}$$

By substituting Equation (3) into Equation (2), the optimum operating duty cycle under various operational conditions could then be estimated. The determination of the optimum operating duty cycle is essential in the current medical application since any operation that is more frequent than this duty cycle may result in an elevated coil temperature which could cause potential problems for the patients.

3. Experimental Arrangement

Various experimental protocols were designed to allow the systematic assessment of the performance of the new actuator, which included the least activation current tests, magnetic force tests and thermal tests aimed for the evaluation of the optimum working duty cycle of the actuator. The overall performance of the new actuator was then identified by analysing the results of the above tests under different conditions. A special circuit was designed to control the width of the short current pulse (between 0.1 s and 1 s), which is required for the excitation of the electromagnetic coils of the actuator. After several trials, it was found that the actuation performance of the actuator was not significantly affected when the current pulse width was varied along the above range, which indicates that the response time of the actuator is faster than 0.1 s as a result of the small linear stroke of the actuator. Hence, and aiming for a reduction in the temperature of the electromagnetic circuit of the actuator, the current pulse width, t_1 was fixed at 0.1 s in all subsequent experiments.

3.1. Least Activation Current Test Setup

In this study, the least activation current of the electromagnetic coil of the new actuator is defined as the minimum applied current that is required to generate a magnetic field capable of releasing the permanent magnet from a locking status, which should then be ready to move along the sliding central chamber with a further current supply. Under this current level, there should be a balance between the magnetic forces generated by the permanent magnet and the electro-

magnetic coil. In this test, ReaseJoy (Model QW-MS3010D) adjustable power source in addition to the current pulse width controlling circuit were used to energise the electromagnetic coil of the actuator whilst an Agilent Technologies (Model U3401A) digital multi-meter was used to record the peak value of the applied current. In this arrangement, the flat end of the shell of the actuator was connected to a solid horizontal platform while the permanent magnet armature was allowed to be attracted and attached to the upper end of the central chamber. Also, the permanent magnet was disconnected from the solid sliding link of the actuator in order to reduce any friction between the permanent magnet and the actuator shell. The applied pulse current was then gradually increased in steps of 0.1 A until the permanent magnet becomes detached from the central chamber upper end, which then drops towards the other end of the chamber with further current increase. Therefore, the peak current, which was recorded when the permanent magnet armature becomes detached from the upper end of the central chamber, was considered as the least activation current of the electromagnetic coil element.

In order to confirm the validity of this test, the procedure was repeated several times when the gap between the permanent magnet and the upper end of the central chamber was gradually increased using PTFE layers with specific thicknesses. The measured least activation current results were also compared with the numerical current results that were obtained from finite element simulations which will be detailed in Section 4.1.

3.2. Magnetic Force Test Setup

Magnetic force tests were conducted using a Tinius Olsen tensile machine, model H5KS. The shell of the actuator was vertically aligned and fixed to the upper 10N load cell of the machine whilst a non-magnetic metallic rod, which was supported by the platform of the machine, was routed through the central channel of the actuator and bonded to the permanent magnet. As a result, the position of the permanent magnet along the central sliding chamber could be controlled through precision axial input displacements that were supplied by the tensile machine and the corresponding total magnetic force acting on the permanent magnet was measured by the load cell of the machine. Figure 5 shows this experimental arrangement.

In this test, the ReaseJoy power supply as well as the current pulse width controlling circuit were used to energise the actuator, and the total magnetic force on the permanent magnet was measured for various positions along the actuation stroke for the two cases when the coil was activated and deactivated. The results of this test were compared with the numerical results that were obtained from the same finite element method which will be detailed in Section 4.1.

3.3. Thermal Test Setup

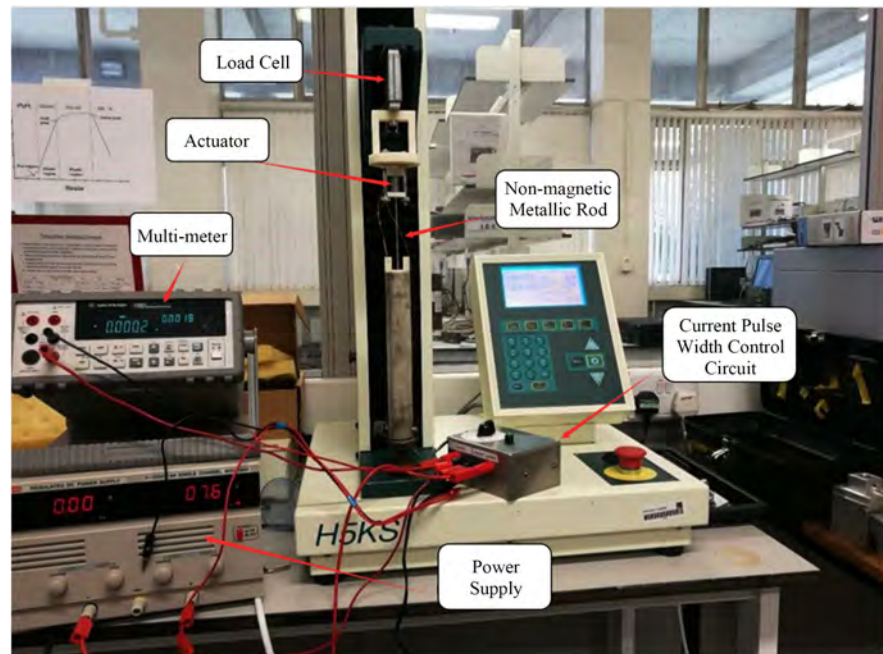A Micro-Epsilon infrared thermal camera, model thermoIMAGER TIM 160 was

Figure 5. Magnetic force test setup.

employed to evaluate the thermal performance of the new actuator. The camera was placed in front of the actuator which was energised using the same circuit that was detailed in Section 3.1. In order to analyse the effect of the current excitation on the thermal load of the actuator, the coil element was supplied with a continuous current of 6.7 A until the thermal camera recorded a maximum temperature of 50˚C in the detection area (nearby the upper coil position) of the actuator after which the current supply was stopped and the actuator was allowed to cool down naturally while the camera was still recording. The ambient temperature during these experimental investigations was maintained at 27˚C. Thermal analysis has also been conducted using Ansys Workbench software which will be detailed in Section 4.3. The thermal test results were used to evaluate a proper working duty cycle of the actuator that maintains the safety of patients during the operation of this actuator in SLS environments within tolerable levels.

4. Results and Discussion

In order to maintain consistency in this investigation, it was decided to allow the permanent magnet to start its stroke from the top-end of the central chamber in all the tests reported in this section.

An ISO-Tech oscillator, model IDS 8062, was employed to measure the rise time of the pulse current excitation of the actuator's electromagnetic coil. It was found that the average rise time is under 2 μs for pulse current excitations up to 6.7 A, which is negligible compared with the pulse current width that is around 100,000 μs (0.1 s). Therefore, the effect of the rise time of the applied pulse current on the results was not taken further into account in the subsequent tests.

4.1. Least Activation Current

The least activation current was measured for various gap thicknesses between the permanent magnet and the upper end of the central chamber, which were created by the addition of PTFE layers and the results are shown in Figure 6. The thickness of this gap was increased gradually up to a total thickness of 0.75 mm which represents half of the complete linear actuation stroke.

Also, a finite element analysis (FEA) using Ansys software was carried out to estimate comparable least activation current values which are also presented in Figure 6. This FEA model utilised the Ansys "Edge-Based" analysis method and a 3-D 20-node element, type "Solid 236", which is capable of modelling electromagnetic problems. In addition, a boundary, which was represented by a spherical air ball of 0.04 m diameter and subjected to a magnetic flux parallel condition of 0 mV, was allowed to encircle the actuator model. Moreover, material properties such as the B-H curve of the MaxiMag steel [20] as well as the coercive force and the residual induction of the permanent magnet [21] were subsequently specified in the FEA environment. Finally, the upper coil element was chosen as the source conductor in these FEA analyses. The least activation current values were then estimated using the Ansys FEA model following the same procedure that was applied to measure them experimentally. In particular, the supplied current to the upper coil element was gradually increased until the total force estimated on the permanent magnet armature was approximately zero ± 0.01 N. This current was then recorded as the least activation current which should enable the permanent magnet to detach itself from the upper end of the central chamber and subsequently slides towards the other end of the chamber with further current increase.

It can be seen, Figure 6 that for a zero gap, a current of about 3.3 A was required to energise the upper end coil element of the actuator in order to generate the required magnetic field that was sufficient to neutralise the permanent magnet field effect which initially permitted the locking status. However, when a gap of about 0.75 mm thick was allowed between the permanent magnet and the upper end of the central chamber, zero magnetic force was estimated on the permanent magnet without any current application as the magnet was exactly in the middle between the two ends of the central chamber and hence, the attraction forces established between the permanent magnet and the two ends balanced each other. Furthermore, it can be noted from Figure 6 that the numerical and experimental results are in a good agreement, indicating the validity of the employed Ansys finite element modelling technique.

4.2. Actuator Magnetic Force

Systematic testing of the new actuator was carried out and it was apparent that the optimum operation of the actuator was achieved when the current density of the electromagnetic coil element was approximately 80,000 kA/m^2, which corresponds to an applied current of about 6.7 A. The total magnetic force acting on

the permanent magnet armature was recorded along the linear actuation stroke for the two cases when the coil was deactivated and activated. In addition, these forces were determined using the Ansys finite element method that was detailed in Section 4.1. Figure 7 shows a comparison between the simulated and experimental total forces.

It can be seen that the magnetic force acting on the permanent magnet when it is in contact with one of the ends of the sliding chamber (locking status) was around 6.8 N whilst a magnetic force of about 2.5 N was required to start its actuation. These forces in association with the 5 mm offset that was allowed between the hinge of the side sliding link and the hinge of the top swivelling component enabled the new actuator to produce a torque output of about 34 mN.m.
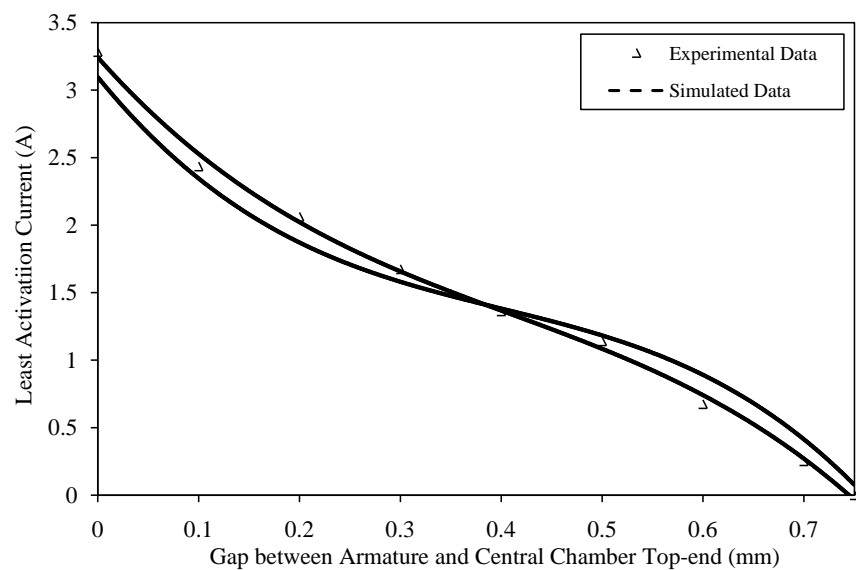

Figure 6. Least activation current versus gap between central chamber upper end and permanent magnet.
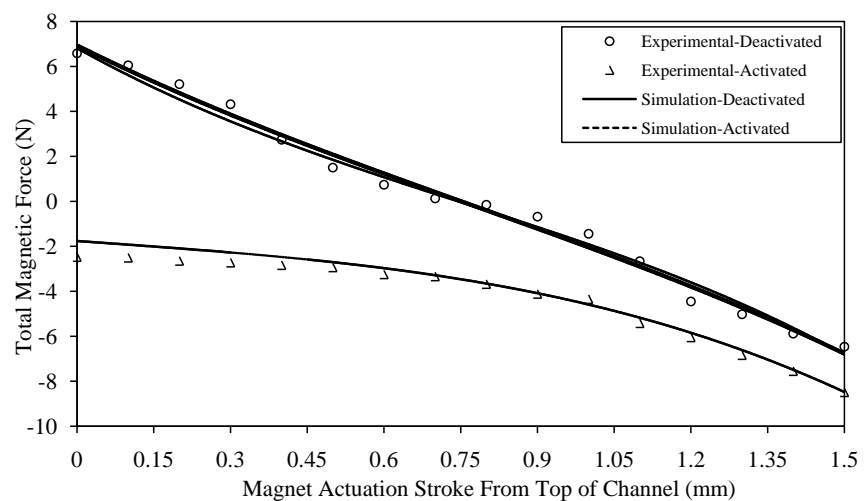

Figure 7. Total magnetic force on the permanent magnet along the actuation stroke.

4.3. Actuator Thermal Performance

The thermal assessment of the new actuator was carried out, as detailed in Section 3.3, under a maximum current excitation of 6.7 A which is the current under which the optimum actuator performance was achieved. The results of this test are shown in Figure 8 where the temperature growth and decay are seen to follow certain paths over a period of about 200 s. The 50˚C maximum temperature target represents the maximum safe temperature that is allowed in SLS operations without causing damages to human tissues [22].

The duty cycle of the coil was then obtained using Equation (2) for which certain parameters were required including the coil surface area, maximum applied current and the temperature rise from the ambient level to the 50˚C target together with the heat dissipation coefficient and the coil resistance. The first three parameters were substituted into the above equation as S = 358.032 mm^2, I_{max} = 6.7 A and ΔT = 23˚C, respectively. The heat dissipation coefficient, λ was estimated using Equation (3) which was found to be 9.727 whilst the electrical resistance of the coil element, R_1 was measured immediately after the temperature began to drop from the 50˚C level using a multi-meter and it was found to be approximately 1.6 Ohm. Accordingly, the duty cycle was estimated as 1.115 × 10^{-3}. This means that a heat dissipation time, t_2 would be around 89.7s with the assumption of t_1 as 0.1 s. As a result, the surgeon could actuate each single actuator about 4 times in every 3 minutes without breaching the safe heat generation level, which is a normal practice in most SLS operations.

4.4. Summary of Actuator Performance

The estimated overall performance of the new actuator is summarised in Table 2, which is benchmarked against the performance of other actuators already reported in the literature for SLS applications. According to this table, the torque and force output of the new actuator were found to be adequate to generate the bending required by SLS tools. This was achieved when the new miniature size actuator was energised by a low voltage feed in comparison with the relatively large actuators (reported in Table 2), which employed large power units and complex power transmission (see for example, the fluidic actuator requirements, including the need for fluid tank).

Important design parameters such as the length, total diameter and weight of the new latching-type electromagnetic actuator, which are 31.6 mm, 10 mm and 23 grams, respectively should permit its application to optimise the function of SLS tools. In addition, the 30˚ bending angle which is produced by the new actuator should enhance SLS tools articulation and adaptation to various SLS operation conditions. This articulation ability should be increased further if 3 to 4 new actuators are embedded at joints along the shaft of SLS tools, which should permit at least 6 degrees-of-freedom and 90˚ to 120˚ angulations in total. Furthermore, the results of the thermal tests have shown that considering conventional SLS surgical protocols, the new actuator is safe enough for operations in

SLS environments. Finally, a conventional SLS tool was modified to enable its articulation and facilitate multi-degrees-of-freedom motions when three proto-types of the new electromagnetic actuator, which could be individually controlled, were embedded in tandem (back to front) along its shaft, as shown in Figure 9. In future work, the reliability and practical performance of the developed articulated SLS tool with its associated electromagnetic actuators would be the subject of an intensive programme of clinical trials.
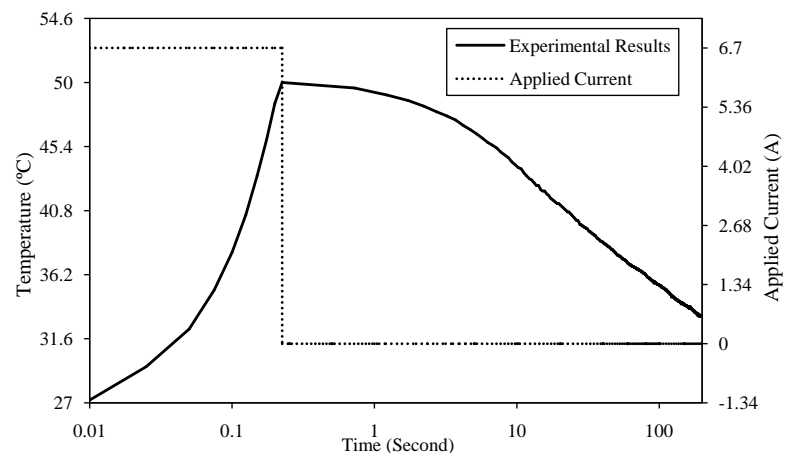

Figure 8. Temperature variation versus time for the new actuator under 6.7 A excitation.
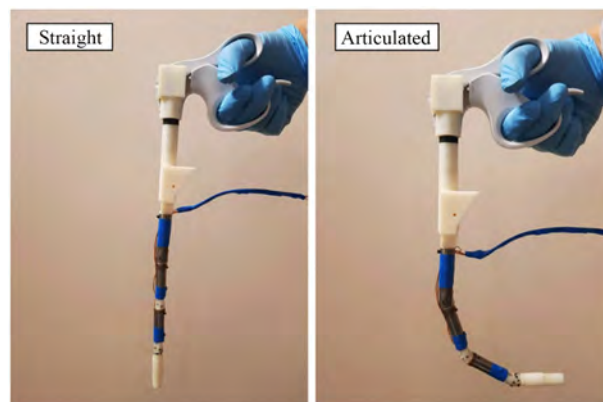

Figure 9. An SLS instrument prototype incorporating three new latching-type electromagnetic actuators (shown in its straight and articulated position).

Table 2. Performance of different actuators proposed for SLS applications.

Actuator Type	Total Length (mm)	Outer Diameter (mm)	Torque Output (mN.m)	Bending Angle
Tendon Drive Actuator [23]	35	12.5	5.7 - 17.5	45˚
Double-Screw Drive Actuator [24]	50	30	High	45˚
Pneumatic Drive Actuator [25]	50	35	N/A	120˚
Fluidic Drive Actuator [26]	78.4	9.6	26.39	125˚
New Latching-Type Electromagnetic Actuator	31.6	10	34	30˚

5. Conclusions

This paper reports on a new latching-type electromagnetic actuator that is developed for applications in single-port laparoscopic surgery (SLS). Various experiments were conducted with the aim to evaluate the performance of the new electromagnetic actuator. The actuator performance was benchmarked against that obtained using finite element modelling techniques which were executed using Ansys Workbench software and the agreement between the two sets of results was found to be good. In particular, the employed finite element model was capable of predicting the actuator's least activation current, total magnetic force and thermal behaviour under various input conditions. This indicated that the developed finite element techniques would be suitable to design other electromagnetic-type actuators that could be developed for various engineering applications.

The performance of the developed new actuator was found to satisfy current requirements in SLS operation. In particular, the size and weight together with the torque and bending outputs of the new actuator were found to exceed those offered by several other actuators that were also aimed for SLS applications.

Acknowledgements

Ethical Approval

Not required.

Conflicts of Interest

The authors declare no conflicts of interest regarding the publication of this paper.

References

[1] Bulut, O. (2016) *Annals of Laparoscopic and Endoscopic Surgery*, **1**, 38. https://doi.org/10.21037/ales.2016.11.20

[2] Fader, A. and Escobar, P. (2009) *Gynecologic Oncology*, **114**, 157-161. https://doi.org/10.1016/j.ygyno.2009.05.020

[3] Stolzenburg, J., Kallidonis, P., Hellawell, G., Do, M., Haefner, T., Dietel, A. and Liatsikos, E. (2009) *European Urology*, **56**, 644-650. https://doi.org/10.1016/j.eururo.2009.06.022

[4] Choi, B., Lee, K. and Lee, S. (2014) *Journal of Laparoendoscopic & Advanced Surgical Techniques*, **24**, 333-338. https://doi.org/10.1089/lap.2013.0497

[5] Ramirez, D., Maurice, M. and Kaouk, J. (2016) *Urology*, **95**, 5-10. https://doi.org/10.1016/j.urology.2016.05.013

[6] Park, S., Bergs, R., Eberhart, R., Baker, L., Fernandez, R. and Cadeddu, J. (2007) *Annals of Surgery*, **245**, 379-384. https://doi.org/10.1097/01.sla.0000232518.01447.c7

[7] Stolzenburg, J., Kallidonis, P., Oh, M., Nabi, G., Do, M., Haefner, T., Dietel, A., Till,

H., Sakellaropoulos, G. and Liatsikos, E. (2010) *Journal of Endourology*, **24**, 239-245. https://doi.org/10.1089/end.2009.0296

[8] Akshay, K. and Sameer, R. (2016) *IOSR Journal of Dental and Medical Sciences*, **15**, 112-115. https://doi.org/10.9790/0853-15071112115

[9] Goel, A. (2012) *Surgical Science*, **3**, 503-505. https://doi.org/10.4236/ss.2012.310100

[10] Le, H., Do, T. and Phee, S. (2016) *Sensors and Actuators A: Physical*, **247**, 323-354. https://doi.org/10.1016/j.sna.2016.06.010

[11] Vitiello, V., Lee, S., Cundy, T. and Yang, G. (2013) *IEEE Reviews in Biomedical Engineering*, **6**, 111-126. https://doi.org/10.1109/RBME.2012.2236311

[12] De Cristofaro, S., Stefanini, C., Pak, N., Susilo, E., Carrozza, M. and Dario, P. (2010) *Sensors and Actuators A: Physical*, **161**, 234-244. https://doi.org/10.1016/j.sna.2010.04.028

[13] Lo, H. and Xie, S. (2012) *Medical Engineering & Physics*, **34**, 261-268. https://doi.org/10.1016/j.medengphy.2011.10.004

[14] Sliker, L., Ciuti, G. and Rentschler, M. (2015) *Expert Review of Medical Devices*, **12**, 737-752. https://doi.org/10.1586/17434440.2015.1080120

[15] Jeong, S., Choi, H., Go, G., Lee, C., Lim, K., Sim, D., Jeong, M., Ko, S., Park, J. and Park, S. (2016) *Medical Engineering & Physics*, **38**, 403-410. https://doi.org/10.1016/j.medengphy.2016.01.001

[16] Ravaud, R., Lemarquand, G., Babic, S., Lemarquand, V. and Akyel, C. (2010) *IEEE Transactions on Magnetics*, **46**, 3585-3590. https://doi.org/10.1109/TMAG.2010.2049026

[17] Kumar, A., Attaluri, A., Mallipudi, R., Cornejo, C., Bordelon, D., Armour, M., Morua, K., Deweese, T.L. and Ivkov, R. (2013) *International Journal of Hyperthermia*, **29**, 106-120. https://doi.org/10.3109/02656736.2013.764023

[18] Kim, J. and Chang, J. (2007) *IEEE Transactions on Magnetics*, **43**, 1849-1852. https://doi.org/10.1109/TMAG.2006.892289

[19] Lee, H., Ahn, J. and Kim, H. (2016) D*Applied Sciences*, **6**, 288. https://doi.org/10.3390/app6100288

[20] Tennant Metallurgical Group Ltd., Chesterfield, United Kingdom (2014) Electromagnetic Test on Cast 80626. http://www.tenmet.co.uk

[21] Amazing Magnets, LLC, 5437 E La Palma Ave, Anaheim (2015) Magnet Grade Chart. https://www.amazingmagnets.com/magnetgrades.aspx

[22] Yarmolenko, P., Moon, E., Landon, C., Manzoor, A., Hochman, D., Viglianti, B. and Dewhirst, M. (2011) *International Journal of Hyperthermia*, **27**, 320-343. https://doi.org/10.3109/02656736.2010.534527

[23] Newton, R.C., Noonan, D.P., Vitiello, V., Clark, J., Payne, C.J., Shang, J., Sodergren, M., Darzi, A. and Yang, G.Z. (2012) *Surgical Endoscopy*, **26**, 2532-2540. https://doi.org/10.1007/s00464-012-2228-1

[24] Kobayashi, Y., Tomono, Y., Sekiguchi, Y., Watanabe, H., Toyoda, K., Konishi, K., Tomikawa, M., Ieiri, S., Tanoue, K., Hashizume, M. and Fujie, M. (2010) *The International Journal of Medical Robotics and Computer Assisted Surgery*, **6**, 454-464. https://doi.org/10.1002/rcs.355

[25] Cianchetti, M., Ranzani, T., Gerboni, G., Nanayakkara, T., Althoefer, K., Dasgupta, P. and Menciassi, A. (2014) *Soft Robot*, **1**, 122-131. https://doi.org/10.1089/soro.2014.0001

[26] Chang, B., Chew, A., Naghshineh, N. and Menon, C. (2012) *Smart Materials and Structures*, **21**, Article ID: 045008. https://doi.org/10.1088/0964-1726/21/4/045008

Light Induced Gravity Phonons

Philipp Kornreich[1,2]

[1]1090 Wien, Austria
[2]King of Prussia, PA, USA
 Email: pkornrei@syr.edu

Abstract

Einstein theorized that a mass travels towards another mass, not because it is attracted by a force acting across a distance, but because it travels through space and time that is warped by masses and energy. Einstein postulated that this space-time fabric can have wave-like modes which have been measured by the LIGO experiment. A consistent model of the generation of space-time-fabric-modes by a light Photon is derived for slight space-time deformations. Each Photon generates a shower of very small amplitude space-time fabric modes. Each mode can have a number of energy quanta. The probability of a Photon generating a shower of space-time modes is much larger than the probability of all the space-time modes collecting and generating a Photon. Therefore, this process has a **unique Arrow of Time**. Similar to the energy quanta of displacement modes in an elastic medium which is called Phonons, the energy quanta of the space-time fabric modes are called gravity Phonons. Both are tensor waves. Gravity Phonons have spin angular momentum of 2 and propagate with the speed of light. At every step of these calculations, equations derived from the General Relativity Theory by scientists and verified by Astronomical observations or experiments are employed.

Note

In the whole paper numbers such {8} in curly brackets denote equation numbers in the literature.

1. Introduction

Einstein [1] theorized in 1916 that a test mass travels towards a mass not because it is attracted by a force that acts across a distance between masses, but because

the test mass travels through space and time that is warped by mass and energy. **In this paper, the Interaction of a light Photon with a space-time fabric that has been deformed by a non-rotating Earth-like mass is described. The derivation is only for a slightly curved space-time fabric.**

A light Photon will not interact to first order with flat space-time, the ordinary four-dimensional Minkowski space. The Earth-like mass is used to remove this symmetry and facilitate the interaction of the Photon with warped space-time.

Einstein also postulated the existence of wave modes in the space-time fabric. This has been verified by the Laser Interferometer Gravity-Wave Observatory LIGO experiment [2]. The interaction of a Photon with warped space-time fabric generates space-time modes, which can have any number of energy quanta, called gravity Phonons. The energy quanta of displacement modes in an elastic medium are called Phonons. Because of the similarity of the interaction of light and Phonons, to the interaction of light and the space-time modes, the space-time mode energy quanta are called **gravity Phonons**. The gravity Phonons valid for slight deformation of the space-time fabric only, are different from Gravitons which presumably are valid for all values of gravity. In this paper, the gravity Phonons have an energy of 0.59893 atto eV and a wavelength of 1.7298 A. U. These small values are expected since the derivation is based on astronomical observations and experiments.

In this paper, equations derived from the General Relativity Theory (GRT) and verified by astronomical observations or experiments are employed at every step of the calculations.

Professor Paul Sutter of Ohio State University and Chief Scientist of the COSI Science Center [3] asks "Why Can't Quantum Mechanics Explain Gravity?" Quantized models exist for the other three forces, the Electromagnetic Force, the Weak Nuclear Force, and the Strong Nuclear Force. In this paper, a quantized formulation of Einstein's [1] space-time fabric modes is presented for slightly curved space-time fabric. Thus, now there exists quantized models for **all four forces**, a Gravity Force for slightly curved space-time fabric only, the Electromagnetic Force, the Weak Nuclear Force and the Strong Nuclear Force of the standard model of Physics.

This discussion involves **space-time** which permeates all space at all times, a **light electromagnetic wave**, and a large non-rotating **mass**. The mass used has the same value as the mass of the Earth. The derivation is in four steps:

FIRST, to model the affect of the slightly warped space-time on an electromagnetic wave, Einstein's description [1] of the deflection of a light wave by the curvature of space-time due to a mass is used. This has been verified by observing the deflection of a light beam passing close to the Sun by F. W. Dyson *et al.* [4].

SECOND, the affect of the energy of the light wave on the curvature of space-time is described by Einstein's equation [5]. In Einstein's equation, the Einstein tensor describes the curvature of space-time, and the affect of the energy of the light wave is described by the electromagnetic stress tensor [5] [6]. The affect of the energy of the light wave on the curvature of space-time is predicted

1675

by the GRT. The GRT has been proven correct in all its tests. Therefore, the affect of the energy of the light wave on the curvature of space-time, predicted by the GRT, must also be correct.

THIRD, a Taylor series expansion to second order of the time dilation equation is used for the derivation of the frequency ω of the light wave in the presence of gravity as a function of the frequency ω_E of the light wave in the absence of gravity and the space-time mode frequency ω_G. The gravitational blue shift of the frequency, in this case, of gamma rays emitted by iron ^{57}Fe samples mounted a vertical elevation of 22.5 m apart has been measured by R. V. Pond and J. L. Sinder [7].

In the **FOURTH** step, Quantum Electrodynamics [8] is used to formulate a Hamiltonian from the above described frequency relationship in second quantized form.

A momentum vector diagram illustrating the affect of the curvature of space-time on a light wave, and the affect of the energy of the light wave on the curvature of the space-time fabric to within a constant for slightly curved space-time fabric only, as shown in **Figure 2** is derived. The values of the change of the light wave momentum and momentum of the light wave generated space-time fabric modes are functions of the deflection angle of the light wave.

This derivation is not valid in the vicinity of large masses such as Black Holes and Neutron Stars. It is also not applicable to the Early Universe, where the mass density was much larger than it is now, and the affect of gravity was larger.

The space-time fabric, described by the second rank metric tensor has a similarity to an elastic fabric, described by the fourth rank elastic constant tensor. The metric tensor that describes the curvature of the space-time fabric is itself a function of the coordinate components of space-time. The elastic **constant** tensor is constant. The elastic fabric mode energy quanta are called Phonons. The electromagnetic field mode and space-time mode interactions are similar to the quantized electromagnetic field and acoustic mode interaction [9]. Because of this similarity the energy quanta of the space-time fabric modes are called "**gravity Phonons**".

The gravity Phonons are massless Bosons, that propagate with the speed of light. Light Photons are derived from a vector model, the Maxwell Electromagnetic Theory, and have a spin angular momentum of 1. The gravity Phonons are derived from a tensor model, the GRT, and have a spin angular momentum of 2. The space-time deformation caused by the mass acts as a cavity to determine the frequency of the space-time fabric modes.

Before Ludwig Boltzmann [10] in 1896, continuous wave theories were used to formulate Statistical Thermodynamic models of acoustic and electromagnetic modes. But none of these formulations agreed with observations. First Boltzmann [10] and later Bose [11] used a discrete model of Statistical Thermodynamic employing quantized energy and obtained results in agreement with observations that are used until today. The most used formulas are the Boltzmann Entropy and the Bose-Einstein distribution function. In most of the Universe, except in

the vicinity of Black holes or Neutron stars, the space-time fabric is only slightly deformed.

Therefore, the gravity Phonons derived here can be used for the calculations of statistical Thermodynamic properties of the space-time fabric such as its average energy, entropy, pressure, and temperature (2.72503˚K). The thermal energy of 0.2340247 meV of the Cosmic Background Radiation is much larger than the energy of a gravity Phonon of 0.59893 atto eV calculated here. The calculations of the Statistical Thermodynamic models are deferred to future publications.

A. D. Sakharov [12] of the Sovietski Academii Nauk (Soviet Academy of Science) and later H. E. Puthoff [13] postulated that gravity is not a basic force. It is a consequence of the electromagnetic force, where the electromagnetic force is generated by a Zero Point Fluctuation of the vacuum. The electromagnetic force can also be generated by a Zitterbewegung, Jitter Motion in German, of particles. However, we are not concerned with the basic phenomena that generate electromagnetic waves. But, like Sakharov and Puthoff, we are concerned with the contribution to the deformation of the space-time fabric by the energy of an electromagnetic wave.

Each light Photon generates **a shower of identical space-time modes**, see Figure 1. Each space-time mode can have any number of energy quanta, called gravity Phonons. Quantum Mechanics is a probabilistic model of Nature. The probability of generating a space-time mode shower is much larger than the probability of all the gravity Phonons collecting and generating a Photon. The entropy of the shower of gravity Phonons is much larger than the entropy of the electromagnetic wave that created the gravity Phonon shower. Therefore, this process has a **unique Arrow of Time**.

This Arrow of time is consistent with Arthur Stanley Eddington's [14] concept of the Arrow of Time. Another explanation for the discussion of the Arrow of Time, are in References [15] [16] and [17]. Stephen Hawking [18] discusses the Arrow of Time in "*The Beginning of Time*" based on the way the Universe developed. This is very different from the Arrow of Time of the gravity Phonons. The gravity Phonons model developed here is also not valid for the beginning of the Universe discussed by Hawking.

The reciprocal relationship between electromagnetic wave modes and gravity is similar to the reciprocal interaction between sound waves and gravity discussed by Nicolis and Penco [19] in "*Mutual Interaction of Photons, Rotons, and Gravity*" and A. Esposito [20] *et al.* in "*Gravitational Mass Carried by Sound Waves*". Instead of a reduction of the symmetry of the space-time fabric, they use a non-linear sound wave effect. The model described in this paper does not have to resort to Plank time or Plank length, or other exotic parameters.

An interesting approach to the interaction of Electromagnetic fields and deformations of the space-time fabric is discussed by Gerald E. Marsh [21] in "*Electromagnetic and Gravity Waves: The Third Dimension*". He uses the Lorenz force and the second-order equation of geodesic deviation followed by the
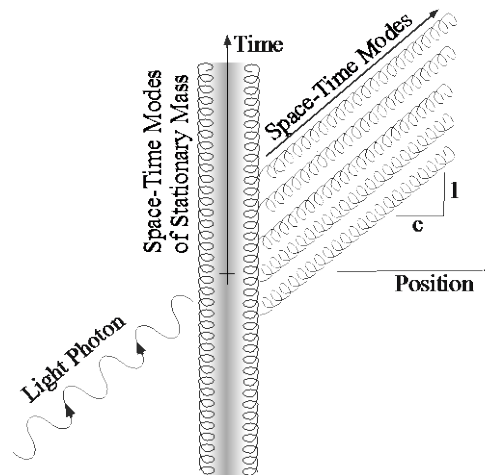
Figure 1. The annihilation of a light Photon generates **a shower of identical space-time modes**. Each space-time mode can have any number of energy quanta called **gravity Phonons**. A stationary Mass causes a distortion of the space-time fabric, which facilitates the interaction of the photon and the space-time modes. The distortion of space-time by the mass can also be expressed in terms of standing space-time waves. Also, both the light Photon and gravity Phonons propagate with the velocity of light. This derivation is for slightly curved space-time fabric only fields only.

introduction of a local inertial frame. In this paper, we also use a second-order expansion approach in our derivations.

Bryce C. DeWitt attempts to derive a Quantum theory of gravity from the GRT starting with a General Relativistic Lagrangian. His derivation is intended to be applicable for all gravity values. He wrote 3 papers [22] [23] [24] but he was unable to produce a Quantum Mechanical model of gravity in a form that has useful applications.

The model derived in my paper corresponds approximately to DeWitt's limit Hamiltonian H_∞ appearing in equation {4.9} on page 1119 of Quantum Theory of Gravity I. DeWitt is using the full tensor formulation of the GRT for his derivation. I use contractions with time-like unit vectors of the tensors in the GRT which results in a scalar formulation of the GRT. The contraction leaves only functions that were verified by astronomical observations or experiments because most of the tests that validated the GRT were based on calculations that reduced parameters of the GRT to scalars. This results in a description that is similar to an Empirical description of physical observations. Since my derivation is from equations validated by real physical observations and experiments it supersedes any difficulties that occur in the full quantization of the GRT.

Carlo Rovelli [25] in his paper "*Notes for a Brief History of Quantum Gravity*" describes in detail the history of formulizing Quantum gravity in the time period from 1930 to 2001. Rovelli describes three main approaches to the formulation of Quantum Gravity.

The FIRST attempt was to formulate a quantum field theory of the fluctuations of the metric on a classical flat Minkowski space. Even though Van Nieu-

wenhuizen, and others, found firm evidence of a non-renormalizability model, a search for an extension of the GRT using a renormalizable perturbation expansion was started. A high order derivative theory and supergravity theory converged successfully to string theory.

The SECOND was an attempt to construct a quantum theory in which the Hilbert space carries a representation of the operators corresponding to the full metric, or some functions of the metric, without a background metric to be fixed. The formal equations of the quantum theory were successfully formulated with loop quantum gravity.

The THIRD was an attempt to use some version of Feynman's functional integral quantization to define the theory. This is somewhat similar to the approach used in this paper.

The paper "*Potential Origin of a Quantitive Equivalence between Gravity and Light*" by Michael A. Persinger [26] is even more speculative. It invokes a mass of the Photon and the mass of the universe to calculate the pressure of Photons in the Universe.

The research described above and in references [21] through [27] are attempts to formulate a quantized gravity mode model that is generally applicable. The Quantized space-time fabric modes derived in this manuscript, are based only on an interaction of an electromagnetic wave and a weak gravitational field. It does not require renormalization and is not based on String Theory or Loop Quantum Gravity [25] [28]. The model of space-time fabric quantization described in Chapter V of this paper is used for the calculation of the gravity Phonon generation rate by Solar radiation.

2. Reciprocal Interaction of Space-Time Modes and a Light Wave

NOTE: This derivation is only valid for slightly curved space-time fabric.

The effect of the curvature of the space-time fabric on a light wave is to deflect it as Einstein [1] described. To describe the affect of the energy of the light wave on the curvature of space-time, Einstein's equation is used. In Einstein's equation, the Einstein tensor describes the curvature of space-time, and the affect of the light wave energy is described by the electromagnetic stress tensor.

The deflection of a light wave by the curvature of space-time due to the Solar mass is calculated in Einstein's Chapter "*On the Influence of Gravitation on the Propagation of Light*" in section § 4 "*Bending of Light-Rays in the Gravitational Field*" on page 108 and page 168, equation {74}. The deflection angle [1] $\theta_\odot$ is:

$$\text{a) } \theta_\odot = \frac{2M_\odot G}{c^2 R_\odot} \quad \text{b) } \theta_\odot = \frac{r_{\odot ss}}{R_\odot} \quad \text{c) } \frac{r_{\odot ss}}{R_\odot} \equiv \textbf{Schwarzschild ratio} \tag{1}$$

Here $M_\odot$ is the solar mass, $R_\odot = 6.957 \times 10^8 \, \text{m}$ is the radius of the Sun and $r_{\odot ss} = 2954.030552 \, \text{m}$ is its Schwarzschild [29] radius. G is Newton's gravitational constant.

$$r_{\odot ss} = \frac{2M_\odot G}{c^2} \tag{2}$$

For the Sun the Schwarzschild ratio $\dfrac{r_{\odot ss}}{R_{\odot}} = 4.246127 \times 10^{-6}$ and the deflection angle $\theta_{\odot} = 0.8758266$ arc seconds. It was first measured by F. W. Dyson, A. S. Eddington, and C. Davidson [4] in 1919. Subsequent measurements have confirmed the value of the deflection angle. For the Earth $r_{ss} = 8.869518$ mm is the Schwarzschild radius and R = 6.378 × 10^6 m is the radius. For the Earth, the Schwarzschild ratio $\dfrac{r_{ss}}{R} = 1.390642 \times 10^{-9}$. The deflection angle of a light beam θ = 0.286841 marc seconds which corresponds to slightly curved space-time.

The wave vector $\dfrac{\omega_E}{c}$ of the light wave in the absence of gravity, the wave vector $\dfrac{\omega}{c}$ of the light wave subject to gravity, and change in the wave vector Δk of the light wave due to the deflection by gravity form the large triangle in **Figure 2**. Similar to equation 1b, this deflection angle θ is approximately equal to the Schwarzschild ratio $\dfrac{r_{ss}}{R}$.

$$a)\ \sin\theta = \frac{c\Delta k}{\omega_E} \quad b)\ \theta \approx \frac{c\Delta k}{\omega_E} \quad c)\ \frac{r_{ss}}{R} \approx \frac{c\Delta k}{\omega_E} \quad d)\ \Delta k \approx \frac{r_{ss}\omega_E}{cR} \tag{3}$$

Dadhigh Naresh [6] writes in "*Subtle is the Gravity*" Section 5, that since energy and mass are equivalent in the GRT, the energy of the light wave also contributes to the curvature of the space-time fabric. The affect of the light electromagnetic wave on the curvature of space-time can be calculated from Einstein's equation [5]. To date, all astronomical observations and experimental measurements have verified the accuracy of the GRT. The affect of the energy of the light wave on the curvature of space-time is very small. I could not find any astronomical observation or experimental measurements of this affect. However, since the affect is predicted by the GRT which has been proven correct in all its tests, the affect of the energy of the light wave on the curvature of space-time must also be valid.

$$a)\ \frac{c^4}{8\pi G}E_{\mu\nu} = T_{\mu\nu} \quad \text{where} \quad b)\ E_{\mu\tau} = R_{\mu\tau} - \frac{1}{2}g_{\mu\tau}R \tag{4}$$
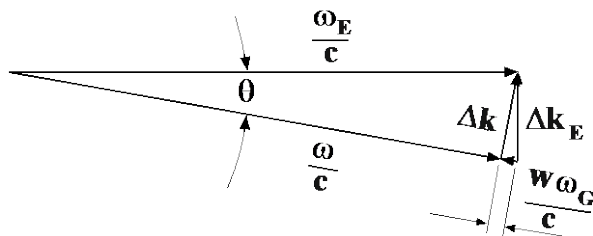

Figure 2. Derived here are wave vector triangles, which express the conservation of momentum. The large right triangle describes the affect of the curvature of space-time on the light wave, and the small right triangle describes the affect of the energy of the light wave on the curvature of space-time to within a constant w.

$E_{\mu\nu}$ is the Einstein tensor derived from the Ricci tensor $R_{\mu\nu}$. $T_{\mu\tau}$ is the electromagnetic part of the stress-energy tensor. Here $g_{\mu\tau}$ is the metric tensor. The Ricci tensor is derived by a contraction over the indices ρ and σ of the Riemann-Christoffel tensor $B^{\rho}_{\mu\sigma\tau}$. The curvature of space-time is described by the Riemann-Christoffel tensor. Equation (4) is a tensor equation. It can be reduced to a scalar equation for slightly curved space-time fabric only by contracting Equation (4) with a time like unit vector with components u^{μ}.

$$a)\ \frac{c^4}{8\pi G}\left[R_{\mu\tau}u^{\mu}u^{\tau}-\frac{1}{2}g_{\mu\tau}u^{\mu}u^{\tau}R\right]=T_{\mu\tau}u^{\mu}u^{\tau}$$

$$b)\ -\frac{c^4}{8\pi G}R_{tt}\approx T_{tt} \tag{5}$$

$$c)\ \frac{c^4}{8\pi G}\text{Curvature}=\text{Electromagnetic energy density function}$$

Summation over repeated Greek indices is implied. No summation over the Latin indices t is implied. E_{tt} and T_{tt} are the tt components of the Einstein tensor and Stress Energy tensor. Here the T_{tt} component of the Stress Energy tensor is equal to the electromagnetic energy density function. The timelike unit vector u^{μ} is:

$$u^{\mu}=\begin{bmatrix}-1 & 0 & 0 & 0\end{bmatrix} \tag{6}$$

The development of Einstein's equation resulting in Equation (5b) is described in detail by Lee Loveridge in "*Physical and Geometric Interpretations of the Riemann Tensor, Ricci Tensor and Scalar Curvature*", Reference 5. Loveridge gives an excellent description of the derivation of the Einstein equation from the concept of curvature of space-time, the Riemann-Christoffel Tensor, and the Ricci Tensor. Loveridge uses the sum over the coordinates of a large number of point particles in the vicinity of the original point particle under consideration. Summing over a large number of particles is equivalent to the contraction of the Riemann-Christoffel tensor to form the Ricci tensor. Instead of describing the motion of a single point particle one has now to describe the motion of a volume δV of all the point particles in the vicinity of the original point particle. From Loveridge's [5] equation {7} one can express the left side of Equation (5b), in the form of second time derivatives of the volume δV in a three-dimensional space.

$$-\frac{c^4}{4\pi G}\left[\frac{1}{V_0}\frac{D^2\delta V}{c^2 dt^2}-\frac{1}{V_0}\frac{D^2\delta V_{\text{Mass only}}}{c^2 dt^2}\right]=Q(t) \tag{7}$$

where $Q(t)$ is the electromagnetic energy density function. Loveridge also derives Newton's laws from the Einstein equation, Equation (4). The electromagnetic energy density function $Q(t)$ in the real world is a function of space and time. A constant and uniform electromagnetic energy density would result in a constant, uniform and therefore, isotropic space-time fabric deformation. But the electromagnetic field does not interact with an isotropic space-time fabric. $Q(t)$ can be expressed as a Fourier Integral.

$$-\frac{c^4}{4\pi G}\left[\frac{1}{V_o}\frac{D^2\delta V}{c^2 dt^2}-\frac{1}{V_0}\frac{D^2\delta V_{\text{Mass only}}}{c^2 dt^2}\right]=\int_{-\infty}^{\infty}d\psi\,\frac{\hbar\Delta k(\psi)c}{V_o}q(\psi)\exp(j\psi t) \quad (8)$$

where $j=\sqrt{-1}$. Here $q(\psi)$ is a dimensionless Fourier Integral of the electromagnetic energy density function and ψ is a frequency. A detailed derivation of the electromagnetic stress tensor and its contraction is derived in **Appendix A**. Equation (A4b) is used in the argument of the Fourier integral on the right sides of Equations (8). Expressing the incremental volume δV also as Fourier integrals.

a) For curved space-time $\delta V=\int_{-\infty}^{\infty}d\psi V(t)\exp(j\psi t)$

b) For curved space-time due to mass only $\delta V_{\text{Mass only}}=\int_{-\infty}^{\infty}d\psi V_o\exp(j\psi t)$ $\quad(9)$

where $V(t)$ is a very slow varying function of time. By substituting Equations (9) into Equation (8).

$$-\frac{c^2}{4\pi G}\left[\frac{D^2}{dt^2}\int_{-\infty}^{\infty}\frac{V(t)}{V_o}\exp(j\psi t)d\psi-\frac{D^2}{dt^2}\int_{-\infty}^{\infty}\exp(j\psi t)d\psi\right]$$
$$=\int_{-\infty}^{\infty}d\psi\,\frac{\hbar\Delta k(\psi)c}{V_o}q(\psi)\exp(j\psi t) \quad (10)$$

Performing first, the differentiation of the terms in the square bracket of Equation (10). The volume amplitude $V(t)$ in the first Fourier Integral in the square bracket of Equation (10) is a very slow varying function of time compared to the oscillation. Therefore, it is treated as a constant in the Fourier Integral. Taking the inverse Fourier Integral:

$$\frac{c^2}{4\pi G}\left[-\frac{\ddot{V}}{V_o}-2j\frac{\omega_G\dot{V}}{V_o}+\frac{\omega_G^2 V}{V_o}-\omega_G^2\right]=\frac{\hbar\Delta k(\omega_G)c}{V_o}q(\omega_G) \quad (11)$$

where ω_G is an oscillating frequency of a Fourier component of the incremental volume δV. Therefore, ω_G is also an oscillating frequency of the space-time fabric modes. Since the volume $V(t)$ is a very slow varying function of time, the first term in the square bracket of Equation (11) has been neglected. The Volume V in the third term in the square bracket of Equation (11) was approximated by V_o. Collecting the remaining terms of Equation (11).

$$-j\frac{c^2\omega_G}{2\pi G}\frac{\dot{V}}{V_o}=\frac{\hbar\Delta k(\omega_G)c}{V_o}q(\omega_G) \quad (12)$$

Assuming the volume V has also a harmonic time dependence. Therefore, one can approximate the first time derivative $\dot{V}$ of V in Equation (12) by:

$$\dot{V}\equiv j\frac{2\pi G\hbar q}{c^2}w\frac{R}{r_{ss}} \quad (13)$$

where $\frac{2\pi G\hbar}{c}\frac{R}{r_{ss}}=1.060763\times10^{-43}\ \text{m}^3/\text{second}$ and where the dimensionless constant w will have to be evaluated from observations. Substituting Equation (13) into Equation (12).

$$\Delta k = w \frac{R \omega_G}{r_{ss} c} \tag{14}$$

The disturbance of the space-time fabric with wave vector $\frac{\omega_G}{c}$ propagates in the opposed direction to the deflected wave, see **Figure 2**. The smaller triangle of **Figure 2** is illustrated by Equation (14), describes the affect of the energy of the light wave on the curvature of space-time to within a constant w. The large triangle of **Figure 2** describes the affect of the curvature of space-time on the light wave. By substituting Equation (14) into Equation (3d) one obtains for the ratio of the oscillating frequency ω_G of the space-time fabric mode and the frequency ω_E of the light in the absence of gravity.

$$a) \ \frac{\omega_G}{c} \frac{wR}{r_{ss}} \approx \frac{r_{ss} \omega_E}{cR} \qquad b) \ \frac{\omega_G}{\omega_E} \approx \frac{r_{ss}^2}{wR^2} \tag{15}$$

For the Earth $\frac{r_{ss}^2}{R^2} = 1.938138404 \times 10^{-18}$ is as expected, a very small number.

Equations (3) and (14) describe the reciprocal relationship of the light wave and the space-time fabric. Equation (15b) describes the combined affect of the space-time curvature acting on the light wave and the energy of the light wave acting on the space-time curvature.

3. The Relationship between the Frequency of the Light Wave Subject to Gravity, the Frequency of the Light Wave Not Subject to Gravity and the Frequency of the Space-Time Modes

The electromagnetic energy density is employed for deriving a Hamiltonian of the electromagnetic mode and space-time fabric modes in second quantized form. The electromagnetic energy density has a quadratic form in the components $F_{\mu\nu}$ of the electromagnetic field tensor. Therefore, in order to derive the Hamiltonian, a quadratic form of a function of the small Schwarzschild ratio $\frac{r_{ss}}{R}$ is obtained from a Taylor series expansion of the gravitational time dilation [1] equation.

The other General Relativistic affect used, is that clocks run slower when closer to the center of gravity of a mass than at larger distances from the mass [1] [7]. Clocks use oscillators, such as pendulums or vibrating crystals as the timing elements. Thus, the frequency of an oscillator is lower when closer to the center of gravity of a mass. The oscillating frequency of the light wave behaves like the oscillating frequency of the clock oscillators. This affect has been experimentally verified by measuring the gravitational blue shift of the frequency of gamma rays emitted by iron ^{57}Fe by R. V. Pond and J. L. Sinder [7].

This change of frequency can be calculated from the time dilation. The time dilation was calculated by Einstein [1] in the chapter "*The Foundation of the GRT*" section §22 "*Behavior of Rods and Clocks in the Static Gravitational Field.*

Bending of Light Rays. Motion of the Perihelion of a Planetary Orbit." on page 160 using g_{44} from equation {70}. This equation for g_{44} is also the Schwarzschild metric [30] or Schwarzschild solution. The frequency ω of a light wave in a gravitational field as a function of the frequency ω_E of the light wave in the absence of the gravitational field ϕ can be derived from the time dilation [1].

a) $\omega = \dfrac{\omega_E}{\sqrt{1 - \dfrac{2\phi}{c^2}}}$ form ref. [31] b) $\phi = -\dfrac{MG}{R}$ resulting in c) $\omega \approx \dfrac{\omega_E}{\sqrt{1 + \dfrac{r_{ss}}{R}}}$ (16)

Equation (16c) can also be calculated from the dilation of the oscillating period of a harmonic oscillator derived in "*Relativistic Harmonic Oscillator*" by Kirk T. McDonald [32] of the Joseph Henry Laboratory, of Princeton University. He calculated the time deletion of the period of oscillation of a mass and a spring oscillator in a gravitational field. When one reverses the approximation used to derive Professor McDonald's equations {8} and {12} in his paper [32] one obtains Equation (16c). Another reference for the gravitational time dilation from which one can derive the function of the frequency ω in a gravitational field, as a function of the frequency ω_E of the light wave far from the mass in the absence of the gravitational field is given in "*Gravitational Time Dilation*" in Wikipedia [33]. Expanding Equation (16c) to second order in a Taylor series in the small parameter $\dfrac{r_{ss}}{R}$ to obtain a quadratic equation.

$$\omega \approx \omega_E \left(1 - \frac{r_{ss}}{2R} + \frac{3r_{ss}^2}{8R^2} + \cdots \right) \tag{17}$$

This is the quadratic form of the function of the small Schwarzschild ratio $\dfrac{r_{ss}}{R}$ discussed above.

The smaller the distance R, the closer the light wave is to the center of gravity of a mass, and the stronger is the affect of gravity acting on the light wave. The smaller the distance R, the lower the oscillating frequency ω of the light wave. The light frequency is "Red Shifted". Recall that in stronger gravity, clocks run slower, and the light wave oscillates slower.

Here $\dfrac{r_{ss}}{R}$ represents the distortion of the curvature of the space-time fabric by the mass which facilitates the interaction of the light wave and the space-time fabric.

Substituting Equation (15b) into Equation (17) one obtains for the frequency ω of the light wave near the surface of an Earth like mass:

$$
\begin{aligned}
\text{a)} \quad & \omega \approx \omega_E - \frac{\sqrt{w\omega_E\omega_G}}{2} + \frac{3w\omega_G}{8} + \cdots \\
\text{b)} \quad & \omega \approx \left(\sqrt{\omega_E} - \frac{\sqrt{w\omega_G}}{4} \right)^2 + \frac{5w\omega_G}{16}
\end{aligned}
\tag{18}
$$

Putting the last term $\dfrac{5w\omega_G}{16}$ of Equation (18b) temporarily aside, multiplying

the remaining equation by $\hbar$ -Plank's constant divided by 2π, and taking the square root.

$$\sqrt{\hbar\omega} \approx \sqrt{\hbar\omega_E} - \frac{\sqrt{\hbar w\omega_G}}{4} \qquad (19)$$

The constant w in Equations (18) and (19) will have to be evaluated from observations.

4. Formulation of the Second Quantized Form of the Space-Time Modes

Next, a second quantized Hamiltonian is derived from the square root of the energy $\hbar\omega$ of the light wave in the presence of gravity of Equation (19), as a function of:

the square root of the energy $\hbar\omega_E$ of the light wave in the absence of gravity,

the energy $\frac{\hbar w\omega_G}{16}$ of the space-time fabric modes,

and the energy term $\frac{5w\hbar\omega_G}{16}$ that was set aside in Equation (18).

The Quantum Electrodynamics models described in "*Quantum Electronics*" by Amnon Yariv [34] in the section on "*Plane Wave Quantization*" equations {5.6.15} on page 98 are employed for the electric field vector operator $\mathbf{E}(\omega)$ and the magnetic flux density pseudo vector operator $\mathbf{B}(\omega)$ as functions of the light frequency in the presence of gravity. These operators are also described in reference [35] equations {2.12}, {2.13}, and {2.52}; and also in reference [36].

$$\text{a) } \mathbf{E}(\omega) = j\hat{\mathbf{a}}_E S(\mathbf{r}) \sqrt{\frac{\hbar\omega}{2V\varepsilon_o}} \left(a e^{-jkz} - a^\dagger e^{jkz} \right)$$

$$\text{and b) } \mathbf{B}(\omega) = \hat{\mathbf{a}}_B S(\mathbf{r}) \sqrt{\frac{\hbar\omega\mu_o}{2V}} \left(a e^{-jkz} + a^\dagger e^{jkz} \right) \qquad (20)$$

where ε_o is the dielectric constant of free space, μ_o is the permeability of free space, $\hat{\mathbf{a}}_x$ is a unit vector. $S(\mathbf{r})$ is a normalized description of the space-time distribution of the electromagnetic field modes and V is the volume occupied by the light Photons. By substituting Equation (19) for $\sqrt{\hbar\omega}$ into Equations (20).

$$\text{a) } \mathbf{E}(\omega) = j\hat{\mathbf{a}}_E \sqrt{\frac{\hbar}{2V\varepsilon_o}} \left[S_E(\mathbf{r}) \sqrt{\omega_E} \left(a e^{-jkz} - a^\dagger e^{jkz} \right) - S_G(\mathbf{r}) \frac{\sqrt{w\omega_G}}{4} \left(b e^{-jqz} - b^\dagger e^{jqz} \right) \right]$$

$$\text{b) } \mathbf{B}(\omega) = \hat{\mathbf{a}}_B \sqrt{\frac{\hbar\mu_o}{2V}} \left[S_E(\mathbf{r}) \sqrt{\omega_E} \left(a e^{-jkz} + a^\dagger e^{jkz} \right) - S_G(\mathbf{r}) \frac{\sqrt{w\omega_G}}{4} \left(b e^{-jqz} + b^\dagger e^{jqz} \right) \right]$$

$$(21)$$

where the form factors S_E and S_G are normalized.

$$\text{a) } 1 = \frac{1}{V} \int_{Volume} S_E S_E^* dv \qquad \text{b) } 1 = \frac{1}{V} \int_{Volume} S_G S_G^* dv \qquad (22)$$

The form factors S_E and S_G are calculated by using post-Newtonian Maxwell equations and the boundary conditions.

Photon mode operators $\boldsymbol{a}$ and $\boldsymbol{a}^\dagger$ are associated with the square root $\sqrt{\hbar\omega_E}$ of the energy $\hbar\omega_G$, and gravity Phonon mode operators $\boldsymbol{b}$ and $\boldsymbol{b}^\dagger$ are associated with the square root $\dfrac{\sqrt{w\hbar\omega_G}}{4}$ of the energy $\dfrac{w\hbar\omega_G}{16}$. The space-time energy quanta, gravity Phonons form a Hilbert space. The Photons also form a Hilbert space. The state raising and state lowering operators on these Hilbert spaces are defined as:

$\boldsymbol{a}^\dagger$ is the light Photon number state raising operator;

$\boldsymbol{a}$ is the light Photon number state lowering operator;

$\boldsymbol{b}^\dagger$ is the gravity Phonon number state raising operator;

$\boldsymbol{b}$ is the gravity Phonon number state lowering operator.

The state raising and state lowering operators, which operate on the light Photon and gravity.

Phonon number state wave functions $|n\rangle$ and $|m\rangle$, are given below. Where $n = 0,1,2,3,4,\cdots$, $m = 0,1,2,3,4,\cdots$

$$
\begin{aligned}
&\text{a) } \boldsymbol{a}^\dagger|n\rangle = \sqrt{n+1}\,|n+1\rangle &\qquad &\text{e) } \boldsymbol{b}^\dagger|m\rangle = \sqrt{m+1}\,|m+1\rangle \\
&\text{b) } \boldsymbol{a}|n\rangle = \sqrt{n}\,|n-1\rangle &\qquad &\text{f) } \boldsymbol{b}|m\rangle = \sqrt{m}\,|m-1\rangle \\
&\text{c) } \boldsymbol{a}|0\rangle = 0 &\qquad &\text{g) } \boldsymbol{b}|0\rangle = 0 \\
&\text{d) } \langle n|k\rangle = \delta_{nk} &\qquad &\text{h) } \langle m|\ell\rangle = \delta_{m\ell}
\end{aligned}
\tag{23}
$$

The light Photon operators $\boldsymbol{a}$ and $\boldsymbol{a}^\dagger$ commute with the gravity Phonon operators. $\boldsymbol{b}$ and $\boldsymbol{b}^\dagger$ The commutation relation for the light Photon operators $\boldsymbol{a}$ and $\boldsymbol{a}^\dagger$ as well as the commutation relation for the gravity Phonon operators $\boldsymbol{b}$ and $\boldsymbol{b}^\dagger$ are:

$$
\text{a) } \boldsymbol{a}\boldsymbol{a}^\dagger - \boldsymbol{a}^\dagger\boldsymbol{a} = 1 \qquad \text{b) } \boldsymbol{b}\boldsymbol{b}^\dagger - \boldsymbol{b}^\dagger\boldsymbol{b} = 1
\tag{24}
$$

The electromagnetic energy density u is described by John David Jackson [37] in "*Classical Electrodynamics*", Chapter 6, section 6.7 equation {6.106} on page 259, and by L. D. Landau and E. M. Lifshitz [38] in "*The Classical Theory of Fields*" equations {31.1} and {31.5} on page 76. The total electromagnetic energy U is:

$$
\begin{aligned}
&\text{a) } U = \frac{1}{2}\int_{\text{Volume}}\left(\frac{2}{\mu_o}F_{0\beta}F^{\beta 0} - \frac{1}{2\mu_o}F_{\mu\alpha}F^{\alpha\mu}\right)dv \\
&\text{b) } U = \frac{1}{2}\int_{\text{Volume}}\left(E_\alpha E_\alpha \varepsilon_o + \frac{B_\alpha B_\alpha}{\mu_o}\right)dv
\end{aligned}
\tag{25}
$$

where MKS units were used. The electromagnetic field tensor with components $F^{\alpha\beta}$ is described by Jackson [37] in equation {11.137} on page 556, and by Landau and Lifshitz [38] equation {23.5} on page 61, and also in equations {5} and {6} of Reference [39]. Substituting equations 21 into equation 25b, similar to the derivation of the Hamiltonian of equation {5.6-10} by Yariv [34], to obtain the total Hamiltonian **H** operator. The derivation of the Hamiltonian operator **H** is performed in **Appendix B**.

Substituting Equations (24) into Equation (B3) of **Appendix B** for $\boldsymbol{a}\boldsymbol{a}^\dagger$ and

$bb^\dagger$, adding the term $\dfrac{5w\hbar\omega_G}{16}$ of Equation (18b), back in, and performing the integration using Equations (22).

$$\mathbf{H} = \hbar\omega_E\left[a^\dagger a + \frac{1}{2}\right]$$
$$-\frac{1}{V_{Int.}}\int_{Int.Vol.} dv\, \frac{S_G S_E^* + S_E S_G^*}{2}\frac{\hbar\sqrt{w\omega_E\omega_G}}{2}\left[b^\dagger a e^{-j(k-q)z} + ba^\dagger e^{j(k-q)z}\right] \quad (26)$$
$$+\frac{w\hbar\omega_G}{8}\left[b^\dagger b + 3\right]$$

Equation (26) represents the three terms of Equations (17) and (18a). Equation (26) contains three sub Hamiltonian operators, an Electromagnetic wave Hamiltonian operator $\mathbf{H}_E$, an Interaction Hamiltonian operator $\mathbf{H}_{Int}$, and a gravity wave Hamiltonian operator $\mathbf{H}_G$:

$$\boxed{\begin{aligned}
&a)\ \mathbf{H}_E = \hbar\omega_E\left[a^\dagger a + \frac{1}{2}\right]\\[2mm]
&b)\ \mathbf{H}_{Int} = \frac{-1}{V_{Int.}}\int_{Int.Vol} dv\, \frac{S_G S_E^* + S_E S_G^*}{2}\hbar\omega_G\left[\left(N_G b^\dagger\right)a e^{-j(k-q)z} + \left(N_G b\right)a^\dagger e^{j(k-q)z}\right]\\[2mm]
&c)\ \mathbf{H}_G = \frac{w\hbar\omega_G}{8}\left[b^\dagger b + 3\right]
\end{aligned}}$$
$$(27)$$

Equation (27b) implies that each Photon interacts with N_G fold degenerate space-time fabric modes. Each of these space-time fabric modes can have any number m of energy quanta, gravity Phonons. The number N_G is derived from the term $\dfrac{\sqrt{w\omega_G\omega_E}}{2}$ in Equations (18a) divided by ω_G and Equation (15b).

$$a)\ \frac{\sqrt{w\omega_G\omega_E}}{2w\omega_G} = \frac{1}{2}\sqrt{\frac{\omega_E}{w\omega_G}} \qquad b)\ \frac{1}{2}\sqrt{\frac{\omega_E}{w\omega_G}} = \frac{R}{2r_{ss}} \qquad c)\ N_G \approx \frac{\sqrt{w}R}{2r_{ss}} \quad (28)$$

For an Earth-like mass $N_G = 1.79773024 \times 10^8$. The quantity $S_G S_E^* + S_E S_G^*$ is always real. The two operators in the Interaction Hamiltonian operator $\mathbf{H}_{Int}$ of Equation (27b) describe the reciprocal actions of the electromagnetic and gravity waves. The terms in the Interaction Hamiltonian operator $\mathbf{H}_{Int}$ define; either that a light Photon is annihilated and N_G identical gravity Phonon modes are created in a forward traveling wave $e^{-j(k-q)z}$, or N_G gravity Phonons spontaneously assemble and are annihilated, and a light Photon is created in a reverse traveling wave $e^{j(k-q)z}$. Therefore, each light Photon generates **a shower of** N_G **identical space-time modes**, see Figure 1. Each space-time mode can have any number of energy quanta, gravity Phonons.

The Interaction of the electromagnetic wave and gravity wave are restricted to the volume where both are present. This is the Interaction volume V_{Int}.

Quantum mechanics is a probabilistic model of Nature. The probability that a light Photon is annihilated and N_G gravity Phonons are created, is much larger than the probability that all N_G gravity Phonons will spontaneously assem-

ble and create a light photon. **This process exhibits a unique Arrow of Time** [15] [17]. From Equation (27c) the gravity Phonon ground state is:

$$\langle 0|\mathbf{H}_G|0\rangle = \frac{3w}{8}\hbar\omega_G \tag{29}$$

The total energy and momentum before and after the interaction must also be conserved.

$$\hbar\omega = \hbar\omega_E - N_G\hbar\omega_G + \frac{3w}{8}\hbar\omega_G \tag{30}$$

where ω of Equation (18) is the frequency in the presence of gravity. Substituting Equation (15b) for ω_G into Equation (30).

$$\hbar\omega = \hbar\omega_E\left(1 - \frac{r_{ss}}{2R} + \frac{3r_{ss}^2}{8R^2}\right) \tag{31}$$

Equation (31) is in agreement with Equation (17).

5. Calculation of the Gravity Phonon Generation Rate

Fermi's Golden Rule is employed to calculate the average rate $\dfrac{1}{\tau(\omega_E)}$ at which the light from the Sun generates gravity Phonon modes with frequency ω_G. Fermi's Golden Rule was derived by Enrico Fermi [40] using time dependent perturbation theory in "*Nuclear Physics*", and described in "*Quantum Mechanics*" by Eugene Merzbacher [41] Chapter 19 equation {19.99}.

$$\frac{1}{\tau(\omega_E)} = \frac{2\pi}{\hbar}\rho(\omega_E)\left|\langle 1|\langle N_{Sun}-1|\mathbf{H}_{Int}|N_{Sun}\rangle|0\rangle\right|^2 \tag{32}$$

Here $\langle 1|\langle N_{Sun}-1|\mathbf{H}_{Int}|N_{Sun}\rangle|0\rangle$ is an interaction matrix element, where $|N_{Sun}\rangle$ is the Photon number state wave function for N_{Sun} Solar radiation generated light Photons, and $|0\rangle$ is the initial gravity Phonon number state wave function. Here $\rho(\omega_E)$ is the density of states per unit Photon energy $\hbar\omega_E$ per unit volume.

$$\text{a) } \rho(\omega_E) = \frac{1}{V}\frac{dn}{d(\hbar\omega_E)}f(\hbar\omega_E) \qquad \text{b) } \rho(\omega_E) = \frac{\omega_E^2}{2\pi^2\hbar c^3}\frac{1}{\exp\left(\dfrac{\hbar\omega_E}{kT}\right)-1} \tag{33}$$

The Bose-Einstein distribution function [11] is included with the density of states. The Interaction Hamiltonian of Equation (27b) includes the integral over the interaction volume. Substituting Equation (27b) and Equation (33b) into Equation (32) to obtain the gravity Phonon generation rate $\dfrac{1}{\tau(\omega)}$. The term in Equation (27b) that annihilates N_G gravity Phonons and generates a light Photon is neglected. The gravity Phonon Generation Rate is:

$$\frac{1}{\tau(\omega_E)} = \frac{V_{Int}\omega_E^2\omega_G^2 N_G^2 N_{Sun}}{\pi c^3\left[\exp\left(\dfrac{\hbar\omega_E}{kT_{Sun}}\right)-1\right]} \tag{34}$$

The following data is used:

ω_E = 3.755898 × 10^{15} radians per second, the frequency at the peak of the black body radiation curve for a solar temperature T_{Sun} of 5778°K.

ω_G = 0.0072634797 radians per second calculated from Equation (15b), corresponding to a gravity wave wavelength of 2.593318 × 10^{11} m or 1.733526 A.U.

N_G = 3.591514389 × 10^8 calculated from Equations (28c).

The top of the Earth atmosphere receives a Solar radiation energy density of 1361 W/m^2. This results in a Photon density N_{Sun} = 1.144981 × 10^{13} Photons/m^3.

Setting the value of the constant w equal to 1. By substituting the numerical values into equation 34 one obtains:

$$\frac{1}{\tau(\omega_E)} = 9.143898 \times 10^{28}\, \text{m}^{-3} \cdot \text{sec}^{-1} \quad \text{and} \quad \tau(\omega_E) = 1.093626 \times 10^{-29}\, \text{sec} \cdot \text{m}^3 \,.$$ By

comparison, the Plank time $t_p = \sqrt{\dfrac{\hbar G}{c^5}} \approx 5.391159 \times 10^{-44}\, \text{sec}$.

6. Conclusions

Einstein [1] theorized in 1916 that a test mass travels towards a mass not because it is attracted by a force that acts across a distance, but because the test mass travels through space and time that is warped by mass and energy. A light Photon will not interact to first order with flat space-time, the ordinary four-dimensional Minkowski space. The Earth-like mass is used to remove this symmetry and facilitate the interaction of the Photon with warped space-time. **In this paper, the Interaction of a light Photon with a space-time fabric that has been deformed by this non-rotating Earth-like mass is described. The derivation is only for a slightly curved space-time fabric.**

Einstein also postulated the existence of wave modes in the space-time fabric. This has been verified by the LIGO experiment [2]. The interaction of a Photon with the space-time fabric generates space-time modes. Each space-time mode can have any number of energy quanta, called **gravity Phonons**. Gravity Phonons are tensor waves, they are Bosons, they have a spin angular momentum of 2, and propagate with the speed of light. In this example, the space-time quanta have an energy of 0.59893 atto eV and a wavelength of 1.7298 A.U.

Slightly curved space-time fabric implies that the escape velocity of a test mass from the surface of a mass under consideration is much less than the velocity of light. It also implies that the space-time fabric mode caused by the mass can expand with the velocity of light to a size that is much larger than the mass.

The curvature of space-time deflects an electromagnetic wave. The energy of the electromagnetic wave also contributes to the curvature of space-time. Thus, there is a reciprocal relationship between an electromagnetic wave mode and space-time fabric modes. Second quantization is employed to formulate the space-time fabric energy quanta. Each mode can have any number of energy quanta called **gravity Phonons**. The Phonon number state wave functions form a Hilbert space. The gravity Phonons propagate with the speed of light and are

massless Bosons. Since the gravity **Phonons are tensor waves**, they have spin angular momentum 2. The shape of the deformation of space-time and the Photon frequency ω_E determine the space-time fabric mode frequency ω_G.

As of this date, 29 October 2019, there now exists quantized models for all four forces, a Gravity Force for slightly deformed space-time fabric, the Electromagnetic Force, the Weak Nuclear Force and the Strong Nuclear Force of the standard model of Physics. The gravity Phonons can, among other applications, be used to calculate the Statistical Thermodynamic quantities of the space-time fabric such as its average energy, entropy, pressure, and temperature (2.72503˚K), etc. The space-time mode quanta have only an energy of 0.59893 atto eV and the thermal energy of the Cosmic Background Radiation (CBR) in the Universe at a temperature of 2.72503˚K has a thermal energy of 0.23482478 meV. Therefore, the ratio of the space-time mode quanta energy of equation 29 to the thermal energy of the CBR is only 2.55054×10^{-15}. Thus, the Ideal Gas Law should hold for the Universe modeled as a gas, with the galaxies as molecules.

It should be possible to verify this model by observations since its derivation is based on astronomical observations and experiments.

Each gravity Phonon has an energy of only 0.6 atto eV. The annihilation of a light Photon generates a shower of 36,000,000 identical space-time modes. Each space-time mode can have any number of energy quanta gravity Phonons. This interaction has two forms. The Photon can generate 36,000,000 space-time modes, or the 36,000,000 space-time modes can assemble and create a Photon. Quantum Mechanics is a probabilistic model of Nature. The probability of a Photon generating a large number of gravity Phonons is much larger than the probability of a large number of gravity space-time modes assembling and form a Photon. Therefore, this process exhibits a **Unique Arrow of Time**. That is, the **Unique Arrow of Time** is a consequence of a large number of gravity Phonons necessary to create a light Photon because gravity is such a weak force.

A quantized model of space-time modes and their properties for slightly curved space-time fabric only has been derived in this paper.

Acknowledgements

Conflicts of Interest

The author declares no conflicts of interest regarding the publication of this paper.

References

[1] Einstein, A., Lorentz, H.A., Weyl, H. and Minkowski, H. (1952) The Principles of

Relativity. Dover Publishing Co., Mineola.

[2] Abbott, B.P., *et al.* (2016) Observation of Gravitational Waves from a Binary Black Hole Merger. *Physical Review Letters*, **116**, Article ID: 06112. https://doi.org/10.1103/PhysRevLett.116.061102

[3] Sutter, P. (2016) Why Can't Quantum Mechanics Explain Gravity.

[4] Dyson, F.W., Eddington, A.S. and Davidson, C. (1920) A Determination of the Deflection of Light by the Sun's Gravitational Field, from Observations Made at the Total Eclipse of May 29, 1919. *Philosophical Transactions of the Royal Society of London. Series A, Containing Papers of a Mathematical or Physical Character*, **220**, 291-333. https://doi.org/10.1098/rsta.1920.0009

[5] Loveridge, L.C. (2004) Physical and Geometric Interpretations of the Riemann Tensor, Ricci Tensor and Scalar Curvature.

[6] Dadhigh, N. (2001) Subtle Is the Gravity. 21*th Conference of India Association for General Relativity*, Nagpur, 30 January 2001.

[7] Pond, R.V. and Sinder, J.L. (1964) Affect of Gravity on Nuclear Resonance. *Physical Review Letters*, **13**, 539-540. https://doi.org/10.1103/PhysRevLett.13.539

[8] https://www.physik.hu-berlin.de/de/nano/lehre/copy_of_quantenoptik09/Chapter2

[9] Li, E.B., *et al.* (2014) Photonic Aharonov-Bohm Affect in Photon-Phonon Interactions. *Nature Communications*, **5**, Article No. 3225. https://doi.org/10.1038/ncomms4225

[10] Boltzmann, L. (1896) Vorlesungen über Gastheorie, Vol. I. J.A. Barth, Leipzig. Boltzmann, L. (1898) Vorlesungen über Gastheorie, Vol. II. J.A. Barth, Leipzig.

[11] Bose (1924) Plancks Gesetz und Lichtquantenhypothese. *Zeitschrift für Physik*, **26**, 178-181. (In German) https://doi.org/10.1007/BF01327326

[12] Sakharov, A.D. (1968) Docladi Academii Nauk. *Soviet Physics—Doklady*, **12**, 1040.

[13] Puthoff, H.E. (1989) Gravity as a Zero-Point-Fluctuation Force. *Physical Review A*, **39**, 2333-2342. https://doi.org/10.1103/PhysRevA.39.2333

[14] Eddington, A.S. (1928) The Nature of the Physical World. The Gifford Lecture 1927, MacMillan Company, New York.

[15] Coveney, P. and Highfield, R. (1991) The Arrow of Time.

[16] Hawking, S. (2008) A Brief History of Time. Bantam Books, New York, London.

[17] Kornreich, P. (2008) Mathematical Models of Information and Stochastic Systems. CRC Press Taylor and Francis Group, Boca Raton, 289.

[18] Hawking, S. (1996) The Beginning of Time. http://www.hawking.org.uk/the-beginning-of-time.html

[19] Nicolis, A. and Penco, R. (2018) Mutual Interaction of Photons, Rotons, and Gravity. *Physical Review B*, **97**, Article ID: 134516. https://doi.org/10.1103/PhysRevB.97.134516

[20] Esposito, A.K. and Rafael Nicolis, A. (2019) Gravitational Mass Carried by Sound Waves. *Physical Review Letters*, **122**, Article ID: 084501. https://doi.org/10.1103/PhysRevLett.122.084501

[21] Marsh, G.E. (2011) Electromagnetic and Gravity Waves: The Third Dimension. Argon National Laboratory, Chicago.

[22] DeWitt, B.C. (1967) Quantum Theory of Gravity. I. The Canonical Theory. *Physical Review*, **160**, 1113-1147. https://doi.org/10.1103/PhysRev.160.1113

[23] DeWitt, B.C. (1967) Quantum Theory of Gravity. II. The Manifestly Covariant

Theory. *Physical Review*, **162**, 1195-1239. https://doi.org/10.1103/PhysRev.162.1195

[24] DeWitt, B.C. (1967) Quantum Theory of Gravity. III. Applications of the Covariant Theory. *Physical Review*, **162**, 1239-1256. https://doi.org/10.1103/PhysRev.162.1239

[25] Rovelli, C. (2001) Notes for a Brief History of Quantum Gravity. https://doi.org/10.1142/9789812777386_0059

[26] Persinger, M.A. (2012) Potential Origin of a Quantitative Equivalence between Gravity and Light. *The Open Astronomical Journal*, **5**, 41-43. https://doi.org/10.2174/1874381101205010041

[27] Hamada, Y., Noumi, T. and Shiu, G. (2019) Weak Gravity Conjecture from Unitarity and Causality. *Physical Review Letters*, **123**, Article ID: 051601. https://doi.org/10.1103/PhysRevLett.123.051601

[28] Thiemann, T. (2002) Lecture on Loop Quantum Gravity. MPI f. Gravitationsphysik, Albert Einstein Institute, Am Mühlenberg 1, 14476, Glm near Potsdam, Germany. Preprint AEI-2002-087.

[29] Schwarzschild, K. (1916) Über das Gravitationsfeld eines Massenpunktes nach der Einsteinschen Theorie. Sitzungsberichte der Deutschen Akademie der Wissenschaften zu Berlin, Klasse fur Mathematik, Physik, und Technik, 189.

[30] Eddington, A.S. (1924) Mathematical Theory of Relativity. Cambridge UP 1922, 2nd Edition, 85-93.

[31] Beig, R., Crusciel, P.T., Hilweg, C., Kornreich, P. and Walther, P. (2018) Weakly Gravitating Isotropic Waveguides. *Classical and Quantum Gravity*, **35**, Article ID: 244001. https://doi.org/10.1088/1361-6382/aae873

[32] McDonald, K.T. (2013) Relativistic Harmonic Oscillator. Joseph Henry Laboratory, Princeton University, Princeton.

[33] Gravitational Time Dilation. Wikipedia. http://en.wikipedia.org/wiki/gravitational_time_dilation#Outside__a_non_rotating sphere

[34] Yariv, A. (1989) Quantum Electronics. 3rd Edition, John Wiley & Sons, Hoboken, 98.

[35] D'Auria, R. and Trigiante, M (2015) Quantization of the Electromagnetic Field. Chapter 2, Springer, Berlin.

[36] Bialynicki-Birula, I. and Bialynicka-Birula, Z. Polish Academy of Science, Warsaw, Poland "Quantum Theory of the Electromagnetic Field". http://www.cft.edu.pl/nbrula/publ/QED.pdf

[37] Jackson, J.D. (2018) Classical Electrodynamics. Third Edition, Wiley India Pvt. Ltd., New Delhi.

[38] Landau, L.D. and Lifshitz, E.M. (1975) The Classical Theory of Fields. Fourth Revised English Edition, Volume 2 of the Course of Theoretical Physics, Pergamon Press Ltd., Oxford.

[39] Dos Santos, W.C. (2016) Introduction to Einstein-Maxwell Equations and Rainich Conditions.

[40] Fermi, E. (1950) Nuclear Physics. University of Chicago Press, Chicago.

[41] Merzbacher, E. (1998) Quantum Mechanics. 3rd Edition, John Wiley and Sons, Hoboken.

Appendix A

The electromagnetic field tensor described here is only valid for gravity-free space. However, since small terms describing slightly curved space-time fabric are employed with this field tensor, and any slightly curved space-time fabric affects included in the field tensor would result in a second order affect, which is neglected. The contravariant Electromagnetic field tensor with components $F^{\mu\nu}$ and the covariant Electromagnetic field tensor with components $F_{\mu\nu}$ are:

$$a)\ F^{\mu\nu} = \begin{bmatrix} 0 & -\dfrac{E_1}{c} & -\dfrac{E_2}{c} & -\dfrac{E_3}{c} \\ \dfrac{E_1}{c} & 0 & -B_3 & B_2 \\ \dfrac{E_2}{c} & B_3 & 0 & -B_1 \\ \dfrac{E_3}{c} & -B_2 & B_1 & 0 \end{bmatrix} \quad b)\ F_{\mu\nu} = \begin{bmatrix} 0 & \dfrac{E_1}{c} & \dfrac{E_2}{c} & \dfrac{E_3}{c} \\ -\dfrac{E_1}{c} & 0 & -B_3 & B_2 \\ -\dfrac{E_2}{c} & B_3 & 0 & -B_1 \\ -\dfrac{E_3}{c} & -B_2 & B_1 & 0 \end{bmatrix} \tag{A1}$$

The electromagnetic stress tensor with components $T_{\mu\nu}$ is a function of the electromagnetic field tensor $F_{\mu\nu}$.

$$T_{\mu\nu} = \frac{1}{\mu_o}\left[F_\mu{}^\alpha F_{\alpha\nu} - \frac{1}{4}\delta_{\eta\nu} \mathrm{Tr}\left(F_\mu{}^\alpha F_{\alpha\nu} \right) \right] \tag{A2}$$

Substituting Equations (A1) into Equation (A2)

$$T_{\mu\nu} = \frac{1}{\mu_o}\left\{ \begin{bmatrix} \dfrac{E_1^2+E_2^2+E_3^2}{c^2} & -\dfrac{E_2B_3-E_3B_2}{c} & \dfrac{E_1B_3-E_3B_1}{c} & -\dfrac{E_1B_2-E_2B_1}{c} \\ \dfrac{E_2B_3-E_3B_2}{c} & \dfrac{E_1^2}{c^2}-B_3^2-B_2^2 & \dfrac{E_1E_2}{c^2}+B_1B_2 & \dfrac{E_1E_3}{c^2}+B_1B_3 \\ -\dfrac{E_1B_3-E_3B_1}{c} & \dfrac{E_1E_2}{c^2}-B_1B_2 & \dfrac{E_2^2}{c^2}-B_3^2-B_1^2 & \dfrac{E_3E_2}{c^2}+B_3B_2 \\ \dfrac{E_1B_2-E_2B_1}{c} & \dfrac{E_1E_3}{c^2}-B_1B_3 & \dfrac{E_3E_2}{c^2}-B_3B_2 & \dfrac{E_3^2}{c^2}-B_2^2-B_1^2 \end{bmatrix} \right.$$

$$\left. -\frac{1}{2}\left[\frac{E_1^2+E_2^2+E_3^2}{c^2} - B_1^2 - B_2^2 - B_3^2 \right] \begin{bmatrix} 1 & 0 & 0 & 0 \\ 0 & 1 & 0 & 0 \\ 0 & 0 & 1 & 0 \\ 0 & 0 & 0 & 1 \end{bmatrix} \right\} \tag{A3}$$

Contracting the electromagnetic stress tensor $T_{\mu\nu}$ of Equation (A3) with time-like unit vectors $\begin{bmatrix} -1 & 0 & 0 & 0 \end{bmatrix}$ with components u^μ to obtain the energy density.

$$a)\ T_{\mu\nu}u^\mu u^\nu = \frac{1}{2}\left[\varepsilon_o E_a E_a + \frac{B_a B_a}{\mu_0} \right],\ a=1,2,3 \quad b)\ T_{\mu\nu}u^\mu u^\nu \approx \frac{\hbar \Delta k c}{V_o} \tag{A4}$$

where the time-like unit vector u^μ is given by Equation (6). For the special case when the cross product of the electric field vector and the magnetic flux density

pseudo vector are equal to zero:

$$\mathbf{E} \times \mathbf{B} = 0 \tag{A5}$$

The electromagnetic stress tensor takes the form:

$$
T_{\mu\nu} = \frac{1}{\mu_o} \left\{
\begin{bmatrix}
\dfrac{E_1^2 + E_2^2 + E_3^2}{c^2} & 0 & 0 & 0 \\[2mm]
0 & \dfrac{E_1^2}{c^2} - B_3^2 - B_2^2 & \dfrac{E_1 E_2}{c^2} + B_1 B_2 & \dfrac{E_1 E_3}{c^2} + B_1 B_3 \\[2mm]
0 & \dfrac{E_1 E_2}{c^2} - B_1 B_2 & \dfrac{E_2^2}{c^2} - B_3^2 - B_1^2 & \dfrac{E_3 E_2}{c^2} + B_3 B_2 \\[2mm]
0 & \dfrac{E_1 E_3}{c^2} - B_1 B_3 & \dfrac{E_3 E_2}{c^2} - B_3 B_2 & \dfrac{E_3^2}{c^2} - B_2^2 - B_1^2
\end{bmatrix}
\right.
$$

$$
\left.
- \frac{1}{2} \left[\frac{E_1^2 + E_2^2 + E_3^2}{c^2} - B_1^2 - B_2^2 - B_3^2 \right]
\begin{bmatrix}
1 & 0 & 0 & 0 \\
0 & 1 & 0 & 0 \\
0 & 0 & 1 & 0 \\
0 & 0 & 0 & 1
\end{bmatrix}
\right\} \tag{A6}
$$

Appendix B

Substituting Equations (21) into Equation (25b) to obtain the total Hamiltonian **H** operator.

$$
\begin{aligned}
\mathbf{H} = \int_{\text{Vol.}} dv \Bigg\{ \frac{-\hbar}{4V} &\left[S_E(\mathbf{r})\sqrt{\omega_E}\left(a e^{-jkz} - a^\dagger e^{jkz}\right) - S_G(\mathbf{r})\frac{\sqrt{\omega_G}}{4}\left(b e^{-jqz} - b^\dagger e^{jqz}\right) \right] \\
\times &\left[S_E^*(\mathbf{r})\sqrt{\omega_E}\left(a e^{-jkz} - a^\dagger e^{jkz}\right) - S_G^*(\mathbf{r})\frac{\sqrt{\omega_G}}{4}\left(b e^{-jqz} - b^\dagger e^{jqz}\right) \right] \\
+ \frac{\hbar}{4V} &\left[S_E(\mathbf{r})\sqrt{\omega_E}\left(a e^{-jkz} + a^\dagger e^{jkz}\right) - S_G(\mathbf{r})\frac{\sqrt{\omega_G}}{4}\left(b e^{-jqz} + b^\dagger e^{jqz}\right) \right] \\
\times &\left[S_E^*(\mathbf{r})\sqrt{\omega_E}\left(a e^{-jkz} + a^\dagger e^{jkz}\right) - S_G^*(\mathbf{r})\frac{\sqrt{\omega_G}}{4}\left(b e^{-jqz} + b^\dagger e^{jqz}\right) \right] \Bigg\}
\end{aligned}
\tag{B1}
$$

Multiplying out Equation (B1)

$$
\begin{aligned}
\mathbf{H} = \frac{1}{V}\int_{\text{Vol.}} dv\, \frac{\hbar}{4}\Bigg\{ & S_E S_E^* \omega_E \left[-aa e^{-j2kz} + a^\dagger a + aa^\dagger - a^\dagger a^\dagger e^{j2kz} \right] \\
&+ S_G S_E^* \frac{\sqrt{\omega_E \omega_G}}{4}\left[ba e^{-j(k+q)z} - b^\dagger a e^{-j(k-q)z} - ba^\dagger e^{j(k-q)z} + b^\dagger a^\dagger e^{j(k+q)z} \right] \\
&+ S_E S_G^* \frac{\sqrt{\omega_E \omega_G}}{4}\left[ab e^{-j(k+q)z} - a^\dagger b e^{j(k-q)z} - ab^\dagger e^{-j(k-q)z} + a^\dagger b^\dagger e^{j(k+q)z} \right] \\
&+ S_G S_G^* \frac{\omega_G}{16}\left[-bb e^{-j2qz} + b^\dagger b + bb^\dagger - b^\dagger b^\dagger e^{j2qz} \right] \\
&+ S_E S_E^* \omega_E \left[aa e^{-j2kz} + a^\dagger a + aa^\dagger + a^\dagger a^\dagger e^{j2kz} \right] \\
&+ S_G S_E^* \frac{\sqrt{\omega_E \omega_G}}{4}\left[-ba e^{-j(k+q)z} - b^\dagger a e^{-j(k-q)z} - ba^\dagger e^{j(k-q)z} - b^\dagger a^\dagger e^{j(k+q)z} \right] \\
&+ S_E S_G^* \frac{\sqrt{\omega_E \omega_G}}{4}\left[-ab e^{-j(k+q)z} - a^\dagger b e^{j(k-q)z} - ab^\dagger e^{-j(k-q)z} - a^\dagger b^\dagger e^{j(k+q)z} \right] \\
&+ S_G S_G^* \frac{\omega_G}{16}\left[bb e^{-j2qz} + b^\dagger b + bb^\dagger + b^\dagger b^\dagger e^{j2qz} \right] \Bigg\}
\end{aligned}
\tag{B2}
$$

Collecting terms.

$$
\begin{aligned}
\mathbf{H} = \frac{1}{2V}\int_{\text{Vol.}} dv \Bigg\{ & S_E S_E^* \hbar \omega_E \left[a^\dagger a + aa^\dagger \right] \\
&- \frac{S_G S_E^* + S_E S_G^*}{2}\frac{\hbar\sqrt{\omega_E \omega_G}}{2}\left[b^\dagger a e^{-j(k-q)z} + ba^\dagger e^{j(k-q)z} \right] \\
&+ S_G S_G^* \frac{\hbar \omega_G}{16}\left[b^\dagger b + bb^\dagger \right] \Bigg\}
\end{aligned}
\tag{B3}
$$

Glitching Pulsars: Unraveling the Interactions of General Relativistic and Quantum Fields in the Strong Field Regimes

Ahmad A. Hujeirat[1], Ravi Samtaney[2]

[1]IWR, Universität Heidelberg, Heidelberg, Germany
[2]Applied Mathematics and Computational Science, KAUST, Thuwal, Jeddah, KSA
Email: AHujeirat@uni-hd.de, ravi.samtaney@kaust.edu.sa

Abstract

In this article we modify our previous model for the mechanisms underlying the glitch phenomena in pulsars. Accordingly, pulsars are born with embryonic cores that are made of purely incompressible superconducting gluon-quark superfluid (henceforth SuSu-cores). As the ambient medium cools and spins down due to emission of magnetic dipole radiation, the mass and size of SuSu-cores must grow discretely with time, in accordance with the Onsager-Feynmann analysis of superfluidity. Here we argue that the spacetime embedding glitching pulsars is dynamical and of bimetric nature: inside SuSu-cores the spacetime must be flat, whereas the surrounding region, where the matter is compressible and dissipative, the spacetime is Schwarzschild. It is argued here that the topological change of spacetime is derived by the strong nuclear force, whose operating length scales are found to increase with time to reach $\mathcal{O}(1)$ cm at the end of the luminous lifetimes of pulsars. The here-presented model is in line with the recent radio- and gravitational wave observations of pulsars and merger of neutron stars.

1. Internal Structure of UCSs

Pulsars, neutron stars (NSs) and magnetars build the family of ultra-compact

stars (UCSs). This is a sub-class of the compact objects (COs), which, in addition, include white dwarfs (WDs) and black holes (BHs) as well. Unlike COs, the members of UCSs share the same evolution and may have the same cosmological fate. Our analysis here applies to UCSs but neither to WDs nor to BHs. The compactness parameter of UCSs, α_S, is generally larger than half (see [1] [2] [3] and the references therein). Recalling that the average density of matter in the interiors of UCSs is larger than the nuclear one, ρ_0, then these objects are well-suited for probing the interaction of general relativity with quantum fields in the strong field regime (Figure 1).

In fact pulsars and NSs have been successfully used for probing general relativity, such as the emission of gravitational waves (GWs) in binary pulsars and direct detection GWs through merger of neutrons stars and black holes (see [4] and [5] for detailed reviews). However, the internal structure of UCSs will continue to be a mystery and remain a challenge for astrophysicists not for a short time (see the review in [6] and the references therein). On the other hand, the glitch-phenomena observed to associate pulsars [7] [8] are events that may be considered to be connected to the dynamics of matter inside their interiors (see [6] [7] [9] [10] and the references therein). However, based on observations and theoretical arguments, one may try to constrain the nature of matter inside normal UCSs as follows:

1) The observed continuous spin-down of UCSs results from the combined loss of magnetic and rotational energies (see [6] and the references therein). These are estimated to fall in the range: $[10^{37}, 10^{40}]$ erg/s, depending on the nature and age of the concerned UCSs and specifically whether these concerned ones are magnetars, pulsars or neutron stars [9] [11]. This would imply complete exhaustion of the stored removable energies[1] inside pulsars within about ten million years, provided that the heat conductivity operates on length scales that are larger than the nuclear ones. Consequently, very old and isolated UCSs, including those formed through the collapse of the first generation of stars, must be dark by now and therefore excellent candidates for stellar black hole. This argument would explain why neither UCSs nor black holes have never been observed in the mass range $\left[2M_\odot \leq \mathcal{M} \leq 5M_\odot\right]$.

2) The rest of thermal, kinetic and magnetic energies that are left from the collapse of the progenitors of UCSs are transported outwards into the outer shells and subsequently liberated away. Due to the relatively small thermal energy content in UCSs and in the absence of nuclear energy generation, the Tolman-Oppenheimer-Volkoff equation (TOV-equation) may still accept a positive gradient of the thermal energy, turning the central core to the coldest region inside UCSs, thereby facilitating a phase transition of the compressible dissipative nuclear matter into incompressible superfluid (see [12] for further details on the properties of incompressible fluid flows). Such a phase transition may still occur even when the matter's temperature is still beyond several million degrees [11] (Figure 2).

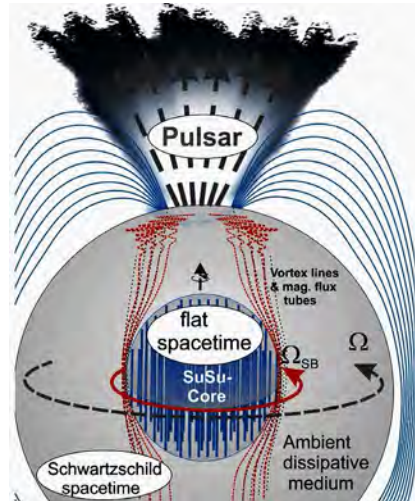[1]*i.e.* energies other than rest energy.

Figure 1. A schematic description of the internal structure of glitching pulsars. Pulsars are born with embryonic cores that are made of incompressible gluon-quark superfluids and embedded in flat spacetime. The overlying shells are made of dissipative and compressible quantum fluids, but embedded in Schwarzschild spacetime.
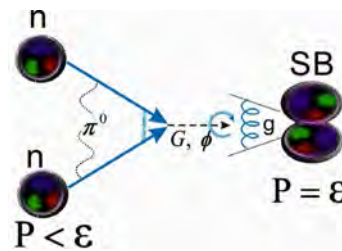

Figure 2. Neutron merger at the centers of pulsars. The compressible and dissipative neutron fluid is governed by EOSs in which $P < \varepsilon$. When the density approaches the critical density, ρ_c, then the EOS changes into $P = \varepsilon$, which corresponds to incompressible quantum fluid. At $\rho = \rho_c$, it is energetically favourable for neutrons to start deconfine the quarks and merge together to form an ocean of gluon-quark superfluid, though the resulting global gluon cloud must be much more energetic.

3) Theoretical studies show that in the regime of nuclear density and beyond, almost all EOSs used for modelling the state of matter in the interiors of UCSs tend to converge to the limiting case: $\varepsilon = P$ (see [9] and the references therein). However, this state corresponds to pure incompressible nuclear fluids [2]. Due to causality and stability reasons, incompressible nuclear fluids should be free of all other removable energies, such as thermal, kinetic and magnetic energies. Hence the core is expected to end up as a condensate with zero-entropy, whose constituents communicate with each other with the speed of light and therefore the momentum exchange between them must saturate around a universal maximum. In this case, the coupling constant in the context of asymptotic freedom in QCD would converge to its universal minimum value, where quarks inside merged-neutrons are allowed to oscillate locally [13] [14]. Such a zero-entropy superfluid[2] cannot accept spatial variations or stratification due to gravity and

---

[2]Vanishing energy loss due to acceleration/deceleration should be excluded.

therefore the embedding spacetime ought to be flat. This state may be maintainable, if involved quarks are attached to a spatially fixed lattice, where they may behave collectively as a single macroscopic quantum entity.

Indeed, although both entropy and energy states of colliding protons at the RHIC and LHC differ significantly from those at the centers of UCSs, these experiments have shown that the properties of the resulting fluids mimic those of perfect fluids (see [15] [16] for further details).

4) Based on astronomical observations, there appears to be a gab in the mass spectrum of compact objects: neither black holes nor NSs have never been observed in the mass range $\left[2\mathcal{M}_\odot < \mathcal{M} < 5\mathcal{M}_\odot\right]$. Moreover, intensive astronomical observations of the newly detected NS-merger GW170817 [1] failed to unambiguously classify the nature of the remnant object, though theoretically it must be a stellar black hole. These both facts are in line with our scenario which predicts that massive pulsars should evolve on the cosmological time scale toward forming massive dark energy objects that become indistinguishable from stellar black holes. A schematic description of the scenario is shown in **Figure 1 Figure 2** and **Figure 4**.

1.1. The Model and the Governing Equations

For modelling the internal structure of pulsars, the general relativistic field equations should be solved:

$$G_{\mu\nu} = \kappa T_{\mu\nu}, \quad \text{for } \mu, \nu : 0 \to 4, \tag{1}$$

where $G_{\mu\nu}, T_{\mu\nu}$ are the Einstein and the Stress-Energy tensors, respectively, and κ is a coefficient (see [17] [18] for further details). The rotational, magnetic, thermal and other energies in UCSs are generally about three orders of magnitude smaller than the rest energy and therefore they may be safely neglected. In this case, Schwarzschild spacetime is most suited for modelling their internal structures. Hence the corresponding metric reads:

$$\mathrm{d}s^2 = \mathrm{e}^{2\nu(r)}\mathrm{d}t^2 - \mathrm{e}^{2\lambda(r)}\mathrm{d}r^2 - r^2\mathrm{d}\Omega^2, \tag{2}$$

where $\mathrm{d}\Omega = \mathrm{d}\theta^2 + \sin^2\theta\mathrm{d}\varphi^2$ is a surface element on a sphere of radius "r".

The field equations can then be reduced to just one single equation, *i.e.* to the so-called Tolman-Oppenheimer-Volkoff (TOV) equation:

$$\frac{\mathrm{d}P}{\mathrm{d}r} = -\frac{G}{c^4 r^2} \frac{\left[\varepsilon + P\right]\left[m(r) + 4\pi r^3 P\right]}{1 - r_s/r}, \tag{3}$$

where $r, r_s, G, P, m(r)$ correspond to the radius, Schwarzschild radius, gravitational constant, pressure and the dynamical mass, respectively (see Sec. (4) in [2] for further details).

Recalling that GR is incapable of modelling gravitationally bound incompressible matter, then the spacetime embedding pulsars may be decomposed into two separate domains: a flat spacetime that embeds the SuSu-core and a surrounding Schwartzschild spacetime that embeds the ambient media as mentioned above. The decomposition of the domain is motivated by relativistic cau-

sality which prohibits fluid stratification or spatial variation of the density of purely incompressible fluids; hence why the spacetime embedding the core must have zero-curvature, *i.e.* purely flat.

Based thereupon the line element in the core is described by the metric in spherical polar coordinates (t, r, θ, φ):

$$\mathrm{d}s^2 = c^2\mathrm{d}t^2 - \mathrm{d}r^2 - r^2\mathrm{d}\Omega^2. \tag{4}$$

The physical properties of the SuSu-core are set to affect the structure of the ambient medium by allowing $m(r)$ and r_s in the TOV-equation to depend on the total enclosed mass, *i.e.* on $m(r) = M_{SuSu} + 4\pi\int_{r=r_{SuSu}}^{\infty} \rho r^2 \mathrm{d}r$.

On the other hand, as the matter in the rotating core is in incompressible superfluid state, it must contain a discrete array of vortices. Their total number, N, the mass and size growth of the core are determined through the Onsager-Feynmann equation for modelling quantized circulations:

$$\oint v \cdot \mathrm{d}\ell = \frac{2\pi\hbar}{m^*}N, \tag{5}$$

where $v, \ell, \hbar, m^*, N$ correspond to rotational velocity, line-element along the circular path, the reduced Planck constant, the mass of the superfluid particles and the enclosed number of vortices, respectively [19] [20]

Inside the core, the quantum fluid is assumed to have zero-entropy and has reached the critical supranuclear density, $\rho = 3\rho_0$, beyond which merger of individual gluon clouds into a global one becomes possible.

The effective energy of the latter cloud correlates linearly with the number of merged neutrons, *i.e.*

$$\sum_1^N E_n^0 \xrightarrow{\text{mergering process}} \sum_1^N E_n^0 + N \times \Delta E_{bag}, \tag{6}$$

where ΔE_{bag} is the bag energy enhancement needed to confine the quarks inside the super-baryon and N denotes the total number of merged neutrons to forming the super-baryon, E_n is the rest energy of a single neutron. In this case the energy and pressure of the incompressible gluon-quark superfluid inside the core read: $\varepsilon_{tot} = \varepsilon_0 + \varepsilon_\phi$, $P_{tot} = P_0 + P_\phi$, where ε_0 is the energy density of the baryonic matter and $\varepsilon_\phi = \frac{1}{2}\dot{\phi}^2 + V(\phi) + \frac{1}{2}(\nabla\phi)^2$ and

$P_\phi = \frac{1}{2}\dot{\phi}^2 - V(\phi) + \frac{1}{6}(\nabla\phi)^2$ are the energy density and pressure of the scalar field, which are assumed to be identical to ΔE_{bag}. As the matter inside the cores of pulsars is set to be incompressible and stationary, it is reasonable to assume $\phi = constant$. In this case, $\dot{\phi}$ and $\nabla\phi$ must vanish and $V(\phi)$ can be considered as the energy density required for deconfining the quarks inside the super-baryon, *i.e.*, the SuSu-core. Here we set $\varepsilon_{tot} = 2\varepsilon_0$, whereas the pressure $P_{tot} = P_0 - V(\phi) = \varepsilon_0 - V(\phi) = 0$. Thus the total local pressure of incompressible gluon-quark superfluid inside SuSu-cores vanishes completely. Exterior to the core, the matter is said to be baryonic, dissipative, compressible and embedded in a Schwarzschild spacetime.

1.1.1. Initial and Boundary Conditions

The present scenario is based on a previous model for the origin of glitches in pulsars. Accordingly, pulsars and young neutron stars are expected to undergo billions of glitch events during their luminous lifetimes before ending as ultra-compact and invisible dark energy objects.

In the present study, we select several epochs in the lifetimes of pulsars and the corresponding internal structures are calculated subject to the following conditions:

◆ The pulsar has the initial mass of $1.33\mathcal{M}_\odot$, which is made of a purely baryonic compressible matter.

◆ The pulsar is set to have initially the compactness parameter $\alpha_s = 1/2$.

◆ The central baryonic density is set to be equal to the critical $\rho_c = 3\rho_0$, at which a transition into quark-deconfinement occurs, and where the Gibbs function vanishes.

◆ The dissipative and compressible baryonic matter is set to obey the polytropic EOS: $P = \mathcal{K}\rho^\gamma$.

The selected models correspond to pulsar phases in which the enclosed SuSu-cores have reached the following radii: $R_{SuSu} = 0.333$, 0.525, 0.78525 and 0.8575 in units of $\left[\tilde{R}\left(= R_S/\alpha_s\right)\right]$, where R_S is the corresponding Schwarzschild radius. The total density inside SuSu-cores amounts to:

$$\rho_{tot} = \rho_b + \rho_\phi = 2\rho_c \approx 6\rho_0.$$

1) Model-0: The pulsar is made of purely baryonic matter. Here, the TOV-equation is solved for the pressure starting from a given $P(r=0) = P_0$ up to a radius, where the pressure vanishes.

2) Combined-models: The pulsar models are made both of SuSu-cores surrounded by dissipative and compressible quantum fluid. The radii of the cores here read: $R_{SuSu} = 0.333, 0.525, 0.78525, 0.8575$. The total mass of the core is calculated through the integration:

$$m_{tot}\left(r = R_{core}\right) = \int_0^{R_{core}} \left(\varepsilon_b + \varepsilon_\phi\right)\mathrm{d}r. \tag{7}$$

The solutions here are based on adapting the parameters $\mathcal{K}$ and γ of the EOS in such a manner so that the initial baryonic mass of $1.33\mathcal{M}_\odot$ the pulsar remain preserved.

3) The ultimate final phase: Here the radius and mass of the SuSu-core are roughly equal to the critical values: $R_{SuSu} = 0.859 \approx R_{Schw.}$ and $M_{SuSu} \approx M_{Schw.}$. Here the initial pulsar must have metamorphosed entirely into an invisible SuSu-object.

1.1.2. Results

For enhancing the spatial accuracy of the calculations, an explicit adaptive mesh refinement (EAMR) has been developed, in which the aspect ratio, $\mathrm{d}r_{max}/\mathrm{d}r_{min}$, may reach 100 million. Unlike self-adaptive mesh refinement (AMR), EAMR is based on a posteriori refining the grid distribution in certain locations of the domain, where the gradients of the physical variables are large. This may be

achieved by externally and manually manipulating the grid distribution and restarting the calculations anew. In the present case, for example, the location, where the pressure vanishes is vitally important and therefore the resolution should be maximally refined (**Figure 3**). Unlike AMR, solution methods based on EAMR generally converge much faster than their AMR-counterparts, hence contributing to the global efficiency and robustness of the numerical solution procedure (see [21] and the references therein).

Based on the previous study [22], five episodes in the cosmological evolution of pulsars have been selected (see **Figure 4**). For each episode, the TOV equation, modified to include dark energy input at the background of the here-presented bimetric scenario of spacetime, is solved.
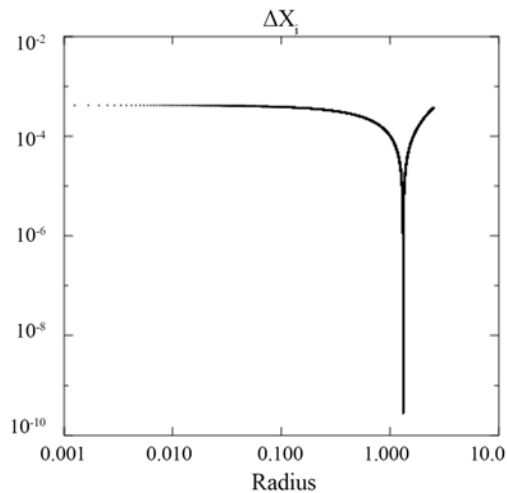

Figure 3. The distribution of the finite volume cells as function of radius. Here the explicit adaptive mesh refinement (EAMR) has been employed to increase the accuracy at both the interface between the core and the ambient medium as well as to outer radius of the object.
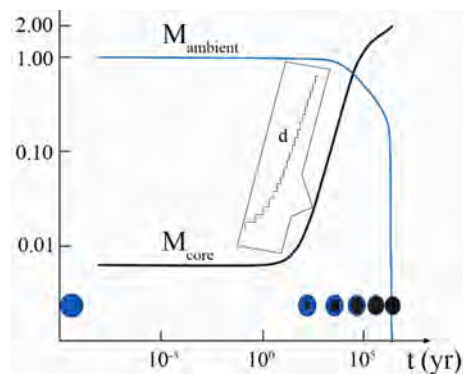

Figure 4. Based on the solution of the TOV equation in combination with Onsager-Feynmann equation, the size and mass of SuSu-cores grow with time following a well-defined mathematical sequence $\{\alpha_c^n\}$. The discrete increase of $\mathcal{M}_{core}$ is magnified and shown "d". To verify the bimetric model of pulsars, six epochs with different core-sizes have been selected: a newly born pulsar, four intermediate phases and the final massive state, where the whole object turns into an invisible dark energy object.

In **Figure 5** and **Figure 6** the profiled of the corresponding five runs are displayed. Profile (1) corresponds to the radial distribution of the pressure obtained by solving the TOV equation. The phase here corresponds to the moment of birth of the pulsar, when it is entirely embedded in a Schwartzschild spacetime.

Profiles (2, 3, 4 and 5) in **Figure 5** show the radial distributions of the pressure at different epochs, specifically when the SuSu-core has grown in mass and size to reach the radii values: $R_{SB} = 0.333$, 0.525, 0.78525 and 0.7875.

Note that as the SuSu-core becomes more massive, the curvature of spacetime embedding the ambient medium is enhanced, which, in turn, compresses the ambient medium even more, thereby reducing the effective radius of the pulsar. This would explain the mass-radius relations displayed in **Figure 7** and **Figure 8**. Here the corresponding Schwarzschild radius increases and propagates outwards to finally meet the decreasing radius of the contacting pulsar. The overlapping of both radii is expected to occur at the end of the pulsar's luminous lifetime (see **Figure 4** and Profile 5 of **Figure 5**).

As purely incompressible superfluids in flat spacetime have zero-spatial variations (**Figure 9**), then the gravitational potential inside SuSu-cores should attain a sequence of constant values. Their magnitudes correlate with the mass and size of the SuSu-core. Consequently, as the SuSu-core becomes more massive, the gravitational redshift of the pulsar increases to finally reach very large values at the end of the pulsar's luminous lifetime (Profile "6" in **Figure 10**). Here the Schwarzschild radius becomes almost equal to the effective radius of the object, enforcing the object to sink deeply in spacetime to become invisible.

Note that the profiles shown in **Figure 9** and **Figure 10** are not just schematic representations, but have been obtained using direct numerical computations.
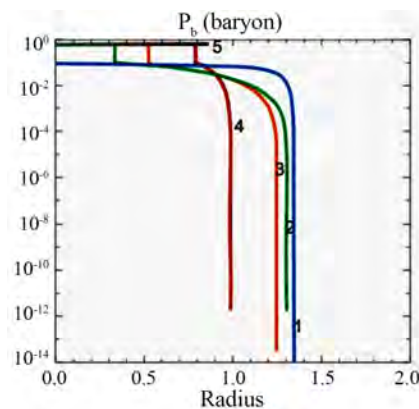

Figure 5. The distribution of the baryonic pressure inside an evolving pulsar after five selected glitch events at different epochs. Inside the core, in addition to the rest energy of the baryonic matter, there is an energy enhancement due to the scalar field, which is equivalent to the additional energy required for re-confining the sea of quarks. The transition between both regions is not smooth as the matter inside the core evolves quantum mechanically, whereas the ambient medium obeys the normal laws of continuum.
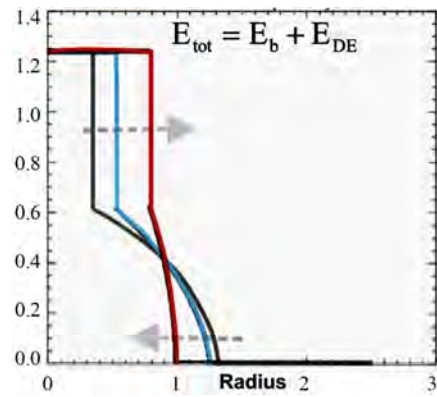
Figure 6. Similar to the previous figure: the distribution of the total energy density inside both the core and the ambient dissipative medium are shown.
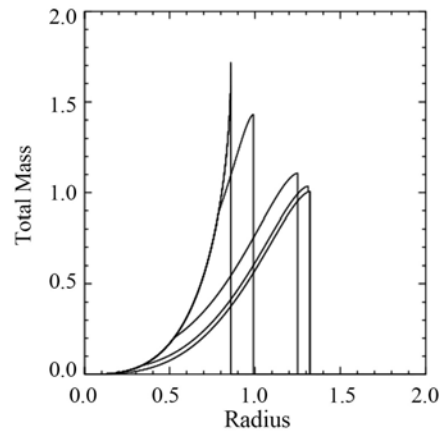

Figure 7. The total enclosed mass of the object versus radius after selected glitch events. As the mass of the SuSu-core increases, its compactness of the whole object increases as well to finally reach the critical Schwarzschild mass.
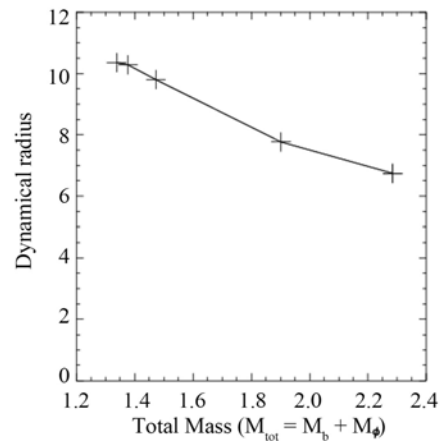

Figure 8. The mass-radius relation of an evolving pulsar after selected glitch events. As the core becomes more massive, the Schwarzschild radius grows and converges asymptotically to the effective radius of the entire contracting object.
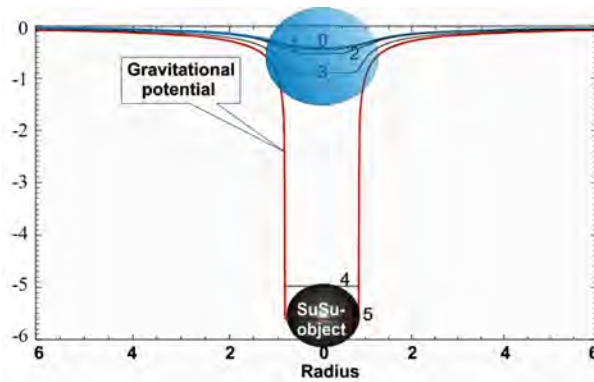
1704

Figure 9. The radial distribution of the gravitational potential shown for different epochs in the lifetime of the pulsar, which is equivalent to the radial projection of spacetime inside the SuSu-core governed by Minkowski spacetime, as well as in the surrounding region governed by the Schwarzschild metric. Obviously, as the object become more massive, it sinks deeper in spacetime, becomes gravitational redshifted to finally ends as an invisible dark energy object.
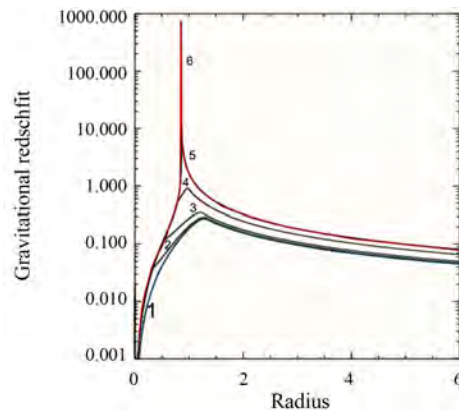

Figure 10. The radial distribution of the gravitational redshift (Z) of the pulsar at different evolutionary epochs. Profile "1" corresponds to the low "Z" immediately after the pulsar was born, whereas Profile "6" depicts the divergent limit of "Z" at the surface of the object when it becomes completely invisible.

2. Summary and Discussion

The here-presented pulsar model is analogous to the terrestrial rotating super-fluid Helium in a container. While the SuSu-matter inside the core corresponds to rotating superfluid Helium, the ambient dissipative medium would represent the solid container.

However, the pulsar model here is much more sophisticated, as quantum and general relativistic effects are taken into account. In the following, we discuss the main features of the model.

- For $\rho \geq \rho_{crit}$, neutrons at the center of pulsars are set to merge together to form an incompressible gluon-quark superfluid, governed by the critical EOS $P = \varepsilon$. This argument is supported by the following two observations:
- ✧ Theoretical studies of nuclear interactions in the regime $\rho \geq \rho_0$ show that almost all EOSs converge to the limiting case: $P = \varepsilon = a_0 n^2$, corresponding

to the pure incompressible state. However, once the matter is governed by $P = \varepsilon$, then the chemical potential μ must achieve a universal maximum, *i.e.* $\dfrac{\partial \mu}{\partial n} = 0$.

◇ Based on thermodynamical considerations, it was shown in [2] that at $\rho = \rho_{crit} \approx 3 \times \rho_0$, in combination with zero-entropy condition, the Gibbs function attains a global zero-minimum, thereby facilitating a crossover phase transition into a globally confined gluon-quark superfluid, where $\dfrac{\partial \mu}{\partial n} = 0$.

• The formation of incompressible gluon-quark superfluids is associated with energy enhancement of the gluon field at the surface of the core, which is needed for globally re-confining the enclosed quarks, thereby effectively enhancing the effective mass of the core.

• The phase transition of the quantum fluid in the BL from compressible-dissipative into incompressible superfluid states is associated with changes of the spacetime topology from a curved spacetime into a purely flat one. The latter reaction is due to causality, which prohibits incompressible superfluids to be embedded by a curved spacetime. Indeed, the topology change of spacetime is associated with the emission of gravitational waves. However, due to the tiny little volume of the BL, the detection of GW-emission during glitch-events would be much below the sensitivity of today GW-detectors.

• Both the phase transition of matter and the topological change of spacetime in the boundary layer can be provoked by the strong nuclear force (SNF) only, which appears to develop into a macroscopic force as the pulsars ages.

In fact, as the core is made of SuSu-matter, the core is equivalent to a super-baryon, in which the enclosed quarks are shielded by a gluon cloud [23]. As it will be shown later, the SNF transmitted by this cloud is found to correlate nicely with the size and mass of the core. The neutrons in the BL become increasingly locked to the core, thereby gradually adapting the physical conditions of the matter inside the core.

Following the scenario of [22], the occurrence of glitches in pulsars follows a well defined sequence, whose elements are $\{\alpha_c^n\}$ where $\alpha_c^n = \Omega_c^n / \Omega_c^{n+1} = 1 + (\Delta \Omega / \Omega)^n$, and $n : 0 \to \infty$. Here $n = 0$ corresponds to the first glitch event immediately after the pulsar's formation, whereas $n = \infty$ corresponds to the final glitch event at the end of the pulsar's luminous lifetime.

Thereupon, let R_n, Ω_n be respectively the radius and angular frequency of the SuSu-core at the verge of the glitch event number "n". The rotational energies of the SuSu-core at time t_n and t_{n+1} read:

$$E_{rot,SB}^n = \frac{4 \pi \rho_{crit}}{15} R_n^5 \Omega_n^2$$

$$E_{rot,SB}^{n+1} = \frac{4 \pi \rho_{crit}}{15} R_{n+1}^5 \Omega_{n+1}^2.$$

From the conservation of rotational energy: $E_{rot,SB}^n = E_{rot,SB}^{n+1}$, we obtain the relation:

$$\left(\frac{R_{n+1}}{R_n}\right)^5 = \left(\frac{\Omega_n}{\Omega_{n+1}}\right)^2. \tag{8}$$

Inserting $R_{n+1} = R_n + \delta R_n^{BL}$, $\Omega_n = \Omega_{n+1} + \delta\Omega_n$ and using Taylor-expansion, then the width of the boundary layer (BL) would correlate as follows:

$$\frac{\delta R_n^{BL}}{R_n} \approx \frac{2}{5}\frac{\delta\Omega_n}{\Omega_n}. \tag{9}$$

$\delta R_n^{BL}, \delta\Omega_n$ here denote the width of the boundary layer between the Su-Su-core and the ambient dissipative medium and the absolute difference between the rotational frequencies of the core before and after the glitch event, respectively.

Based thereon, the width of the BL during different evolutionary epochs of the pulsar may be estimated as follows:

$$\frac{\delta R_{BL}^n}{R_{SB}^n} \approx \begin{cases} \leq 1.4\times10^{-10} & \tau_{age} = 0 \\ 2.2\times10^{-8} & \tau_{age} = 1000 \text{ yrs/Crab} \\ 1.6\times10^{-6} & \tau_{age} = 10000 \text{ yrs/Vela} \\ 3.8\times10^{-6} & \tau_{age} = 10 \text{ Myr} \end{cases} \tag{10}$$

where τ_{age} stands for the age of the pulsar, provided the object is perfectly isolated and shielded from whatsoever external effects. In calculating the ratio at $\tau_{age} = 0$, the initial values $\alpha_c^{(n=0)} = 3.5\times10^{-10}$, $\Omega^{(n=0)} = 1400/s$ and $B^{(n=0)} = 10^{13}$ Gauss have been used (see [24] for further details). The values at $\tau_{age} = 1000, 10000$ yrs and $\tau_{age} = 10$ Myr are chosen to enable partial comparison with observations of the glitch events of the Vela and Crab pulsars. On the other hand the numerical values of $\alpha_c^{n,n+1}$ have been selected from the sequence $\{\alpha_c^n\}$ displayed in **Figure 8** of [22].

For determining R_{SB}^n we use the current glitch-observation of the Vela and Crab and try to extrapolate them to other epochs. Based on Equations (13, 14, 15) in [22], the correlation of the inertia of the ambient dissipative media, I_{AM}, of the Crab and Vela pulsars reads:

$$I_{AM}^{Vela} \approx 10^{-2} I_{AM}^{Crab}, \tag{11}$$

whereas the requirement that the ejected rotational energy off the core of the Vela pulsar in the form of vortices to be observationally noticeable, implies that $\delta R_{SB}^{now,Vela} \geq 10^{-2} R_\star^{Vela}$. This implies that $\delta R_{SB}^{now,Vela} \approx \frac{5}{2}\delta R_{SB}^{now,Crab}$. Consequently, the cosmic values of R_{SB}^n can be summarized as follows:

$$\delta R_{SB}^n = \begin{cases} \mathcal{O}\left(10^{-7} \text{cm}\right) & \tau_{age} = 0 \\ \mathcal{O}\left(10^{-4} \text{cm}\right) & \tau_{age} = 1000 \text{ yrs/Crab} \\ \mathcal{O}\left(10^{-2} \text{cm}\right) & \tau_{age} = 10000 \text{ yrs/Vela} \\ \mathcal{O}\left(1 \text{cm}\right) & \tau_{age} = 10 \text{ Myr} \end{cases} \tag{12}$$

An urgent question here is:

What is the nature of force in the boundary layer that is capable of triggering glitches?

Here we argue that the SNF is the deriving force that is capable of changing instantly both the physical properties of the quantum fluid as well as the topology of spacetime in the BL.

- Following [22], the core mimics a super-baryon (SB), in which the enclosed quarks are shielded by a gluon-cloud. The medium inside the SB interacts with overlaying supranuclear dense neutrons via vector mesons: the messengers of the SNF. In turn, the SNF locks the neutrons gradually to the core and enforces them to rotate rigidly with the core.

- The SNF generally operates effectively on nuclear length scales, *i.e.* when $\delta R_{BL}^n \approx R_{SB}^n = \mathcal{O}(1)\,\mathrm{fm}$. However, the inertia of a core having the neutron-size would be approximately 100 orders of magnitude smaller than that of the ambient medium. In this case, its rotational and thermal decoupling from the ambient medium would be almost impossible.

On the other hand, in order for a SuSu-core to survive and affect the dynamics of the ambient medium, its inertia must have a minimum critical value. Here we recall that the initial frequency of a newly born pulsar is approximately 1400/s [24]. In order for a SuSu-core to be able to eject one single vortex, its radius must be larger than 10^3 cm, hence its minimum mass: $\mathcal{M}_{SB}^{t=0} \geq 2.58 \times 10^{24}\,\mathrm{g}$.

Indeed, the above tabulated values of δR_{BL}^n show that δR_{BL}^n correlates nicely with the size of the enclosed SuSu-core and it may even become of macroscopic size at the end of pulsars luminous lifetime.

- The next related question reads: What keeps the core dynamically stable against the weight of the overlying massive shells, or equivalently to be stable against further compression by the surrounding curved spacetime?

As the gravitational potential inside the core is constant, then the medium has zero stratification due to gravity. In this case the only opposing force against gravitational collapse is the pressure due to the uncertainty principle as well as the pressure jump across the interface between SuSu-cores and the ambient compressible dissipative medium. The medium in the BL is still fermionic and the governing pressure is due to the Pauli exclusion principle. Moreover, similar to the bag energy confining the quarks inside individual baryons, the dynamics across the surface of the SuSu-core may be dominated by an extraordinary strong surface tension that is capable of confining the ocean of quarks quarks as well as opposing further compression.

- As the neutron's density in the BL approaches the critical value, ρ_{crit}, and as the chemical potential becoming closer to the upper-limit, μ_{cr}, the EOS should converge to $P \rightarrow \varepsilon = a_0 \bar{n}^2$, where $\bar{n}$ is the number density.

This limiting EOS corresponds to purely incompressible fluids and therefore the topology of the embedding spacetime ought to change into purely flat spacetime. In this case, two instantaneous reactions in the BL are expected to occur (see **Figure 11** detailed description):
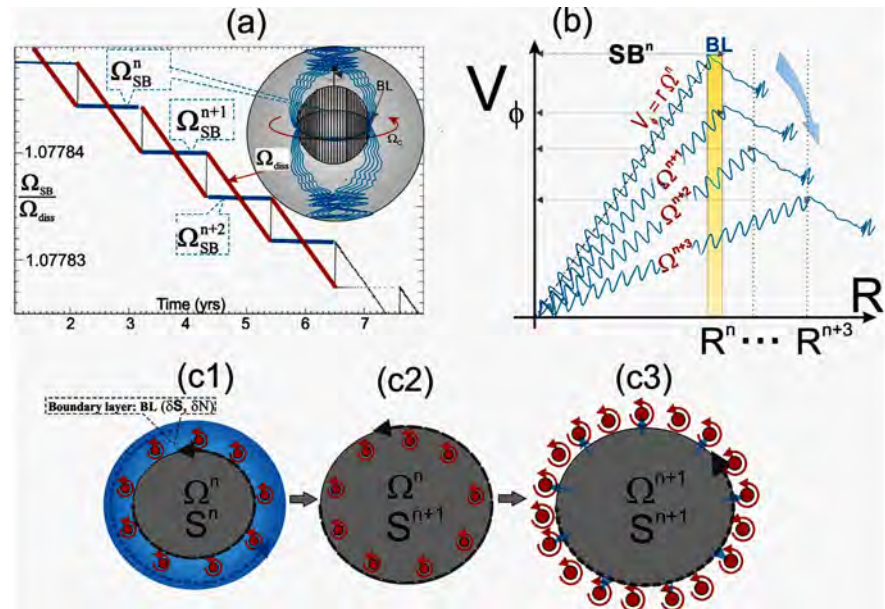
Figure 11. The three-stage glitch scenario. In (a) the time-development of both rotational frequencies of the SuSu-core (blue-color) and of the ambient medium (red-color) are shown, using GR-numerical calculations. In (b) the rigid-body rotation and increasing size of the SuSu-core for four successive glitch-events are shown. The boundary layer here has the width δR, area δS and contains δN vortices. In the lower panel we show the three-stage scenario of the glitch phenomena in pulsars. In (c1) the SuSu-core and boundary at the verge of a glitch event are shown. Once the SNF has locked the neutrons inside the BL, to the core and enforced them to adopt the same thermo- and hydrodynamical properties of the matter inside the core, then the spacetime embedding the BL undergoes a topological change into a flat spacetime and merges with that of the core (c2). However, once the resulting difference $\Delta\Omega$ between Ω_{SB}^n of the core and the ambient medium Ω_{AM}^n has surpassed a critical value, then the core must undergo a transition into the next lower energy state by expelling a certain number of vortices (c3). In turn, the ambient medium absorbs the vortices and re-distribute them viscously, thereby giving rise to the prompt spin-up observed in glitching pulsars.

1) As the supranuclear dense matter in the BL becomes increasingly colder and its thermodynamical state and dynamics become indifferent from those of the matter inside the core, then it merges instantly with the core, thereby increasing its size and effective mass.

2) However, when $\Delta\Omega = \Omega_n - \Omega_{n+1}$, which measures the difference between the rotational frequency of the modified core and that of the matter at the base of the ambient medium, has surpassed a critical quantum value, $\Delta\Omega_{cr}$, then the system undergoes a transition into the next lower energy state by promptly expelling a certain number of vortices into the ambient medium. The associated rotational energy will be absorbed and viscously re-distributed in the ambient medium. The corresponding time scale here is predicated to be of order:

$$\tau_{vis} = \frac{R_*^2}{\nu} = \mathcal{O}(1)\,\text{s}, \tag{13}$$

where we have optimistically assumed that the viscous length scale is of order

$10^{-4} R_*$ and that the viscous interaction occurs at the frequency $\Omega_{vis} = O(10^2)\,\mathrm{s}^{-1}$. This prediction agrees with observations of pulsars during glitch events [25].

- Based on the here-presented scenario, the mechanisms underlying the glitch phenomena in pulsars are due to dramatic changes of the physical conditions of the matter as well as of the topology of spacetime in the BL. Here the system operates on two different time scales: a relatively long times scale, $\tau_{spin\text{-}down}$ and on the very short time scale, $\tau_{quantum}$.

  During $\tau_{spin\text{-}down}$:

- The pulsar's crust spin-down due to the emission of magnetic dipole radiation almost in a continuous manner.

  However as the crust is viscously coupled to the ambient dissipative and compressible medium in the shell overlying the SuSu-core, the matter in the whole shell must spin down in a similar manner, *i.e.* $\dot{\Omega}_{AM} < 0$.

- Cooling and spinning down of the matter in the shell enforces the supranuclear dense fluid at its base, *i.e.* in the BL, to adopt the physical and dynamical conditions of the SuSu-core almost in a continuous manner from inside-to-outside, facilitating a phase transition of the EOS into $P = \varepsilon$, *i.e.* into purely incompressible whilst changing the topology of the embedding spacetime into a purely flat one. As a consequence, the rotational frequency difference $\delta\Omega^n = |\Omega_{BL} - \Omega_{AM}|$ becomes increasingly larger.

  The above process provokes an instantaneous reaction of the SuSu-core: similar to superfluid Helium in a container, once $\delta\Omega^n$ has surpassed the critical value $\delta\Omega^n_{cr}$, then the SuS-core reacts promptly: the BL then merges with the SuS-core, thereby triggering the core to make a transition into the next lower and quantum-mechanically permitted energy state by expelling a certain number of vortices.

  $\tau_{quantum}$ may be predicted to be order $\delta R_{BL}/V_s \leq 10^{-10}\,\mathrm{s}$.

- By the end of luminous lifetime of pulsars, the discrete repetition of mergers of the BL with SuSu-core should have metamorphosed the entire pulsars into a SuSu-object, thereby doubling its initial mass and reducing its radius to roughly coincide with the corresponding event horizon. For remote observers the object becomes practically invisible and therefore indistinguishable from stellar black holes.

The present evolutionary scenario may explain nicely, why neither black holes nor neutron stars have ever been observed in the mass range $\{2.5\mathcal{M}_\odot \leq \mathcal{M} \leq 5\mathcal{M}_\odot\}$ as well as why the NS-merger GW170817 [4] did not collapse to form a stellar BH. If nature indeed forbids the formation of BHs in this mass regime, then our understanding of the big bang, the nature of dark matter and dark energy in cosmology should be revised (see [3] [26] for further details).

Acknowledgements

University of Heidelberg. We also thank Dr. Al-Marouf for reading the manuscript.

Conflicts of Interest

The authors declare no conflicts of interest regarding the publication of this paper.

References

[1] Haensel, P., Potekhin, A.Y. and Yakovlev, D.G. (2007) Neutron Stars 1. Springer, Berlin. https://doi.org/10.1007/978-0-387-47301-7

[2] Hujeirat, A.A. (2018) *Journal of Modern Physics*, **9**, 51-69. https://doi.org/10.4236/jmp.2018.91004

[3] Hujeirat, A.A. (2018) *Journal of Modern Physics*, **9**, jmp.2018.94037.

[4] Abbott, B.P., *et al.* (2017) *Physical Review Letters*, **119**, Article ID: 161101.

[5] Miller, M.C. and Yunes, N. (2019) The New Frontier of Gravitational Waves. https://doi.org/10.1038/s41586-019-1129-z

[6] Ozel, F. and Freire, P. (2016) *Annual Review of Astronomy and Astrophysics*, **54**, 401-440. https://doi.org/10.1146/annurev-astro-081915-023322

[7] Espinoza, C.M., Lyne, A.G., Stappers, B.W. and Kramer, C. (2011) *Monthly Notices of the Royal Astronomical Society*, **414**, 1679-1704. https://doi.org/10.1111/j.1365-2966.2011.18503.x

[8] Eya, I.O. and Urama, J.O. (2014) *International Journal of Astrophysics and Space Science*, **2**, 16.

[9] Camenzind, M. (2007) Compact Objects in Astrophysics. Springer, Heidelberg.

[10] Cook, G.B., Shapiro, S.L. and Teukolsky, S.A. (1994) *ApJ Letters*, **423**, L117. https://doi.org/10.1086/187250

[11] Rajagopal, K. and Wilczek, F. (2000) *The Frontier of Particle Physics*, **3**, 2061-2151. https://doi.org/10.1142/9789812810458_0043

[12] Hujeirat, A.A. (2012) *Monthly Notices of the Royal Astronomical Society*, **423**, 2893-2900. https://doi.org/10.1111/j.1365-2966.2012.21102.x

[13] Bethke, S. (2007) *Progress in Particle and Nuclear Physics*, **351**, 58.

[14] Tanabashi, M., *et al.* (2018) *Physical Review D*, **98**, Article ID: 030001.

[15] LHCb Collaboration (2015) *Physical Review Letters*, **115**, Article ID: 072001.

[16] PHENIX Collaboration (2019) *Nature Physics*, **15**, 214-220. https://doi.org/10.1038/s41567-018-0360-0

[17] Glendenning, N. (2007) Special and General Relativity. Springer, Berlin. https://doi.org/10.1007/978-0-387-47109-9

[18] Hujeirat, A.A. and Thielemann, F.-K. (2009) *Monthly Notices of the Royal Astronomical Society*, **400**, 903-916. https://doi.org/10.1111/j.1365-2966.2009.15498.x

[19] Yarmchuk, E.J., Gordon, M.J.V. and Packard, R.E. (1979) *Physical Review Letters*, **43**, 214. https://doi.org/10.1103/PhysRevLett.43.214

[20] Walmsley, P.M., Golov, A.I., *et al.* (2007) *Physical Review Letters*, **99**, Article ID: 265302. https://doi.org/10.1103/PhysRevLett.99.265302

[21] Fischer, M. and Hujeirat, A.A. (2019) Preprint, in Preparation.

[22] Hujeirat, A.A. (2018) *Journal of Modern Physics*, **9**, jmp.2018.94038.

[23] Witten, E. (1984) *Physical Review D*, **30**, 272.
https://doi.org/10.1103/PhysRevD.30.272

[24] Haensel, P., Lasota, J.P. and Zdunik, J.L. (1999) *AandA*, **344**, 151.

[25] Ashton, G., Lasky, P.D., Graber, V. and Palfreyman, J. (2019) *Nature Astronomy*, **3**, 1143-1148. https://doi.org/10.1038/s41550-019-0844-6

[26] Hujeirat, A.A. (2018) *Journal of Modern Physics*, **9**, 70-83.
https://doi.org/10.4236/jmp.2018.91005

Call for Papers

Journal of Modern Physics

Journal of Modern Physics **(JMP)** is an international journal dedicated to the latest advancement of modern physics. The goal of this journal is to provide a platform for scientists and academicians all over the world to promote, share, and discuss various new issues and developments in different areas of modern physics.

Editor-in-Chief

Prof. Yang-Hui He   City University, UK

Subject Coverage

Journal of Modern Physics publishes original papers including but not limited to the following fields:

Biophysics and Medical Physics	New Materials: Micro and Nano-Mechanics and Homogeneization
Complex Systems Physics	Non-Equilibrium Thermodynamics and Statistical Mechanics
Computational Physics	Nuclear Science and Engineering
Condensed Matter Physics	Optics
Cosmology and Early Universe	Physics of Nanostructures
Earth and Planetary Sciences	Plasma Physics
General Relativity	Quantum Mechanical Developments
High Energy Astrophysics	Quantum Theory
High Energy/Accelerator Physics	Relativistic Astrophysics
Instrumentation and Measurement	String Theory
Interdisciplinary Physics	Superconducting Physics
Materials Sciences and Technology	Theoretical High Energy Physics
Mathematical Physics	Thermology
Mechanical Response of Solids and Structures	

We are also interested in: 1) Short Reports—2-5 page papers where an author can either present an idea with theoretical background but has not yet completed the research needed for a complete paper or preliminary data; 2) Book Reviews—Comments and critiques.

Notes for Intending Authors

Submitted papers should not have been previously published nor be currently under consideration for publication elsewhere. Paper submission will be handled electronically through the website. All papers are refereed through a peer review process. For more details about the submissions, please access the website.

Website and E-Mail

https://www.scirp.org/journal/jmp   E-mail: jmp@scirp.org

What is SCIRP?

Scientific Research Publishing (SCIRP) is one of the largest Open Access journal publishers. It is currently publishing more than 200 open access, online, peer-reviewed journals covering a wide range of academic disciplines. SCIRP serves the worldwide academic communities and contributes to the progress and application of science with its publication.

What is Open Access?

All original research papers published by SCIRP are made freely and permanently accessible online immediately upon publication. To be able to provide open access journals, SCIRP defrays operation costs from authors and subscription charges only for its printed version. Open access publishing allows an immediate, worldwide, barrier-free, open access to the full text of research papers, which is in the best interests of the scientific community.

- High visibility for maximum global exposure with open access publishing model
- Rigorous peer review of research papers
- Prompt faster publication with less cost
- Guaranteed targeted, multidisciplinary audience

Scientific Research Publishing

Website: https://www.scirp.org
Subscription: sub@scirp.org
Advertisement: service@scirp.org